SONOCHEMISTRY: THE MECHANISM AND THE APPLICATION

Thesis by

Hui-Ming Hung

In Partial Fulfillment of the Requirements

for the Degree of

Doctor of Philosophy

California Institute of Technology

Pasadena, CA

2000

(Submitted March 2, 2000)

Acknowledgments

First of all, I would like to thank my advisor, Michael R. Hoffmann, for his accepting me into his group and allowing me to choose a project which interested me. Mike's contagious enthusiasm and his broad understanding of environmental chemistry have been and continue to be a source of inspiration to me. I also wish to thank my Ph.D. examining committee: Professors Michael Hoffmann, Rudolph A. Marcus, John E. Bercaw, Robert H. Grubbs and Mitchio Okumura.

I am also grateful to my colleagues in Keck building, and especially to the other members of my research group. I was initiated into the sonochemistry project by Linda Weavers during my first year at Caltech. Wongyong Choi gave me my first GC-ECD lesson even though he had already graduated. Dr. A. J. Colussi helped me to recall all the thermochemical kinetics that I had learned but forgotten since I was a sophomore. I could not forget the other members of the group who have helped along the way including: Dean Willberg, Ralf Höechemer, Anne Johansen, Nicole Peil, Patrick Lang, Steve Szczepankiewicz, Hugo Destaillats, Nathan Dalleska, John Moss, Yael Dubowski, Yaniv Dubowski, Weng-Ki Ching, Catherine Cornu, Tim Lesko and Jiju Joseph.

Help from the undergraduate students should not be ignored. Frank Ling performed the majority of the experiments described in chapter 6. Angela Lin did a very good job with the GC analysis for MTBE and chlorinated hydrocarbons.

There are so many people working in Keck who have been helpful over the years. Many thanks to Bob Becker for his analytical support and shuttle service. Peter Green was always willing to offer advice about analytical approaches; Rich Eastvedt and Mike Vondrus provided invaluable assistance with building equipment. Linda Scott, Fran

Matzen, Irene Loera and Dian Buchness (chemistry department) made my life easier in a variety of ways as I went about the business of being a graduate student.

Most of all, I deeply appreciated constant and unlimited love, support and encouragement from my parents from the very beginning. Finally, I cannot thank Hung-Wen enough for his support both intellectually and emotionally.

Abstract

The ultrasonic irradiation of chlorinated hydrocarbon and iodide in aqueous solution is studied under various physical conditions. The observed sonochemical rate constants can be analyzed to yield information about the nature of the bubbles which exist during acoustic cavitation and to determine which parameters are significant for enhancing cavitation chemistry.

A significant feature of the sonolytic decomposition of chlorinated hydrocarbon is the dependence on Henry's law constant, H_X. First-order degradation rate constants, k_X, for a series of chlorinated hydrocarbons vary as $k_X \sim H_X^{0.30\pm0.03}$ at all frequencies(f), change with f by less than a factor of two in this range, and peak near 600 kHz for all species. The non-linear dependence of the observed rate constants on H_X indicates that rate constants are not solely determined by equilibrium parameters. Rectified diffusion contributes significantly to the composition of the vapor phase of a cavitation bubble before collapse, particularly for the less volatile substrates.

The maximum •OH production rates measured by iodine dosimetry depend on frequency, f, and acoustic intensity in a concerted manner, e.g., the optimal frequency is 358 kHz at 83 W/L, and 205 kHz at 33 W/L. The zero-order production rate of •OH radical increases with acoustic intensity up to 248 W/L before leveling off. A temperature range of 3900 to 4300 K inside the cavitation bubble is estimated from the power dependence data at 205 and 358 kHz.

The combination of ultrasound and iron metal was used to study the degradation of carbon tetrachloride and nitrobenzene. In the coupled ultrasound and iron system, the contribution to the overall degradation rate of carbon tetrachloride by direct reaction with

Fe^0 results in an apparent rate enhancement by a factor of 40. A comparison of the first order degradation rate constants for carbon tetrachloride and nitrobenzene by Fe^0 reduction with/without sonication revealed that the observed enhancement upon the combination of ultrasound and Fe^0 is attributed 1) to the continuous cleaning and chemical activation of the Fe^0 surface by the combined chemical and physical effects of acoustic cavitation, and 2) to accelerated mass transport rates of reactants to the Fe^0 surfaces.

In addition, a new advanced oxidation process, combination of ultrasound and ozone, was developed to investigate the decomposition of methyl tert-butyl ether (MTBE). The faster rates of MTBE degradation in actual groundwaters by ultrasound/O_3 systems are most likely due to the fact that ozone is more effectively converted to hydroxyl radical in high alkalinity groundwater, and that the carbonate radical anion, which is formed from the oxidation of bicarbonate by hydroxyl radical, reacts further with MTBE by a hydrogen-atom abstraction pathway.

Table of Contents

Chapter 1

Introduction

After Loomis *et al.* reported the acceleration of chemical reactions by ultrasound in 1927 (*1*), ultrasound has been widely used for medical imaging, emulsification, and plastic welding (*2*). In chemistry, ultrasound is applied for a wide variety of synthetic applications (*3*). Recently, ultrasonic irradiation has been applied to problems associated with water pollution (i.e., the removal of toxic and hazardous organic compounds from contaminated water (*4-6*)). For aqueous contaminants such as chlorinated hydrocarbons, which are widely used in industrial processes, but are persistent in the environment, the ultrasonic process has the advantage of completely destroying or converting these organics to inorganic products, instead of simply transferring them to another phase (*6*).

The chemical effects of ultrasound are due to the phenomenon of acoustic cavitation, which is the production of microbubbles in a liquid when a large local negative pressure is applied (*2,7*). Sound travels through a fluid as a wave consisting of alternating compression and rarefaction cycles. If the sound wave has a sufficiently high amplitude, it can overcome the intermolecular forces bonding the fluid. As a result, the liquid will break down and voids will be created, *i.e.*, cavitation bubbles will be formed. In most liquids, cavitation is initiated with pre-existing microbubbles or weak spots which are any type of inhomogeneity in the fluid. The inhomogeneity can be anything from particles to gas nuclei. These microbubbles gradually grow during the compression and rarefaction cycles until they reach a critical size, then in the succeeding compression cycles, these cavities can collapse violently releasing a large amount of energy. This rapid implosion is accompanied by an adiabatic heating of the vapor phase of the bubbles, which yields localized and transient high temperatures and pressures. Temperatures of the order of 5000 K have been experimentally obtained (*8*), and pressures of the order of 1000 bar have been calculated (*9*).

Upon ultrasonic irradiation, organic compounds in water are degraded via several mechanisms, due to the extreme transient conditions. Three main pathways involving

hydroxyl radical oxidation, pyrolytic degradation, and the existence of supercritical water have been proposed. In the case of an aqueous solution, water vapor present in the bubble is homolytically split to yield H• and •OH radicals. Chemical substrates present within or in the vicinity of the collapsing bubbles are subject to direct attack by •OH (*10,11*). Volatile compounds such as H_2S and CCl_4 partition into the gas phase (i.e., into the gaseous bubbles within the aqueous solution) and undergo direct pyrolysis (*2,12-16*). Furthermore, it has been found that hydrolysis reactions are accelerated by several orders of magnitude in the presence of ultrasound. These accelerated reaction rates have been attributed to the existence of transient supercritical water during ultrasonic irradiation (*17*).

Background

Ultrasound

Ultrasound, a longitudinal wave, has frequencies ranging from 16 kHz to 5 MHz for gases and up to 500 MHz for liquids and solids (*2*). The wave traveling in one-dimension in a fluid medium can be described through the following equation:

$$\frac{\partial^2 q}{\partial t^2} = v^2 \frac{\partial^2 q}{\partial x^2} \tag{1}$$

where q represents the instantaneous displacement of a volume element in one-dimension and v is the speed of the wave traveling through the medium. In eq. 1, the medium is assumed to be perfectly elastic. The solution to the eq. 1 expresses how the physical variables change as the wave propagates:

$$q = Q\cos\omega(t - x/v) \tag{2}$$

where ω is the angular frequency, t and x are time and space coordinates, and Q is the amplitude of cyclic change for the variable q. During the propagation of a plane wave

through a medium the intensity decreases as the distance from the radiation source increases. The intensity, *I*, at distance *d*, from the source is given by (*2*):

$$I = I_0 \exp(-2\alpha\, d) \qquad (3)$$

where α is the absorption coefficient. This attenuation may arise as a result of reflection, refraction, diffraction or scattering of the wave or it may be the result of converting some of the mechanical energy of the wave into heat. According to Stokes, the absorption coefficient, α, due to frictional losses in the liquid is proportional to the square of the ultrasonic frequency (*2*):

$$\alpha = k\, f^2 \qquad (4)$$

where *k* is a constant. Therefore, any increase in sound frequency, *f*, would result in a compensatory increase in α and thus a more rapid attenuation of the sound intensity with distance.

Reactions due to ultrasound are not the result of direct interaction between the molecule and the energy of the wave as in photochemistry. Rather, the rarefaction and compression cycles of the wave create cavitation in the fluid, and the sudden collapsing of such cavitation creates local extreme conditions for chemical reactions.

Bubble Dynamics

Ultrasonic waves traveling through a solution impose upon the liquid a sinusoidal pressure variation, alternately compressing the liquid molecules and pulling them apart by overcoming the intermolecular forces. At an ultrasonic frequency of 20 kHz, the liquid will be compressed and rarefied 2×10^4 times each second. As a result of alternating compression and rarefaction cycles, bubbles can be produced from the "weak spots" in the fluid. Weak spots are any types of inhomogeneity in the fluid, for example, small particles and pre-existing gas bubble nuclei. If a bubble is mechanically excited by a pressure impulse, it will oscillate.

For a spherical bubble containing gas and vapor, in an infinite liquid, the equations of motion can be determined by solving the equations of mass, momentum and energy conservation for the gas and liquid. The dynamics of bubbles, in terms of their radii, can be expressed by the Rayleigh-Plesset Equation (Appendix) (*2,18,19*):

$$R\ddot{R} + \frac{3}{2}\dot{R}^2 = \frac{1}{\rho}\left[\left(P_0 + \frac{2\sigma}{R_0} - P_v\right)\left(\frac{R_0}{R}\right)^{3\kappa} + P_v - \frac{2\sigma}{R} - P_0 - P_a(t)\right] \tag{5}$$

where R is bubble radius, $\dot{R} = {}^{dR}/_{dt}$ = velocity of the cavity wall, $\ddot{R}$ is the acceleration of the cavity wall, P_0 is the hydrostatic pressure, P_v is the vapor pressure, $P_a(t)$ is the acoustic pressure, R_0 is the initial bubble radius, κ is the polytropic index, ρ is the density of water and σ is the surface tension of the liquid.

Let us assume the time-varying pressure has the form of a sinusoidal sound wave of amplitude P_A and angular frequency ω, i.e., $P_a(t) = -P_A \sin\omega t$. Also assume that vapor pressure and viscosity are negligible, and there are small-amplitude variations in bubble radius about the limiting value. The bubble radius at any time is given by $R(t) = R_0 + R_\varepsilon(t)$. If $R_\varepsilon << R_0$, substitution into eq. 5, followed by expanding in powers of R_0^{-1} to first order gives (*2,18*):

$$\ddot{R}_\varepsilon + \omega_0^{\,2} R_\varepsilon = \frac{P_A}{\rho R_0}\sin\omega t \tag{6}$$

where ω_0 is the resonant angular frequency, and is given by

$$\omega_0^{\,2} = \frac{1}{\rho R_0^{\,2}}\left\{3\kappa\left(P_0 + \frac{2\sigma}{R_0}\right) - \frac{2\sigma}{R_0}\right\} \tag{7}$$

If the surface tension terms are assumed to be negligible, then we obtain

$$\omega_0^{\,2} = \frac{3\kappa P_0}{\rho R_0^{\,2}} \tag{8}$$

For an air bubble in water at atmospheric pressure the product of the resonance radius and resonance frequency (ρ = 10^3 kg m^{-1}, P_0 = 1 atm = 10 N m^{-2} and κ = 1.33) is given by the following approximation:

$$f_0 R_0 = {\omega_0 R_0}/{2\pi} \approx 3 \text{ m} \cdot \text{s}^{-1} \tag{9}$$

where $f_0 = {\omega_0}/{2\pi}$ is the resonance frequency for bubble pulsation.

It follows that the solution to eq. 6 is:

$$R_\varepsilon(t) = \frac{P_A}{\rho R_0(\omega^2 - \omega_0^{\,2})}\left[\sin\omega t - \frac{\omega}{\omega_0}\sin\omega_0 t\right] \tag{10}$$

The greatest coupling of the ultrasonic energy occurs when the natural resonance frequency of the bubble is equal to the applied ultrasonic frequency, i.e., when $\omega = \omega_0$. Under such conditions, eq. 10 predicts a large oscillation with a high probability of bubble collapse. As a result, this approximation is suitable in predicting stable cavitation but fails in the description of transient cavitation.

A plot of bubble radius versus time for different frequencies, using eq. 10, is shown in Figure 1 (*2*). A bubble shown with an initial radius of 0.8 μm oscillates in a stable but complex manner for several cycles under an applied acoustic frequency of 15 MHz, but it collapses in less than one cycle if the acoustic frequency is 5 MHz. In other words, the tendency of a bubble to collapse is frequency dependent and is more likely to occur at the lower frequencies where the time available in the compression cycle is longer in this case. The actual optimized frequency is dependent on the applied power density as discussed in Chapter 3.

As the small bubbles are excited by acoustic pressure, they can either grow into stable bubbles or into much larger bubbles which then collapse violently. These are called stable cavities and transient cavities, respectively. Stable cavities oscillate many times as small bubbles and then grow in a sound field by rectified diffusion (discussed in

the following section), often to many times their original size, and become transient cavities.

Rectified Diffusion (*18,19*)

In liquids with high levels of dissolved gases, stable bubbles grow significantly as they oscillate due to the diffusion of gas molecules. This phenomenon is called "rectified diffusion." The rectified diffusion consists of two parts, which are nonlinear effects involving the mass transfer between the bubble and liquid. They are known as the 'area' and 'shell' effects and are described, respectively, as follows.

- During the compression cycle, the bubble is compressed and the gas diffuses outwards from the bubble into the liquid. In the rarefaction cycle, the bubble is expanded, so that gas diffuses inwards from the liquid into the bubble. Since the surface area of the bubble is greater in the rarefaction cycle, over a period of time, there is a net influx of gas to the bubble interior.
- We next consider a shell of fluid surrounding the bubble. As the bubble expands, the shell starts to become thinner, so that the gradient across the shell is higher. Because the diffusion rate of gas in a liquid is proportional to the gradient of the concentration of dissolved gas (Fick's law), the rate of inward diffusion is high for bubble expansion (*18*). When the bubble is contracted, the liquid shell surrounding the bubble is expanded. Though the concentration of gas near the bubble is higher now than when the bubble is expanded, the increased thickness of the shell means that the concentration gradient is not as great as when the bubble is expanded. The gas transfer influx is enhanced more than the flux out in the compression cycle.

Overall, both effects promote bubble growth.

Transient Cavitation

Transient bubbles exist for one, or at most a few acoustic cycles, or about a few μs. During the lifetime of a transient bubble, it is assumed that there is no time for mass transfer by diffusion of gas, into or out of the bubble. Rayleigh proposed that the gas cavity would rebound, and then oscillate between a maximum and a minimum value, $R = R_{max}$ and $R = R_{min}$, respectively, with an initial radius R_m. The wall speed being zero ($\dot{R} = 0$) at the two extremes. If there is no heat flow across the bubble wall, then the theoretical collapsing temperature (T_{max}) and pressure (P_{max}) inside the bubble is treated as an adiabatic process. The following expressions are obtained (*2,18*):

$$T_{max} = T_0 \left\{ \frac{P_m(\kappa - 1)}{P} \right\} \tag{11}$$

$$P_{max} = P \left\{ \frac{P_m(\kappa - 1)}{P} \right\}^{\kappa/(\kappa-1)} \tag{12}$$

where T_0 is the ambient (experimental) temperature; P, which usually assumed to be equal to the vapor pressure of the liquid, is the pressure in the bubble at its maximum size; and P_m, the summation of P_0 and P_a, is the pressure in the liquid at the moment of transient collapse (P_0 is the hydrostatic pressure, and P_a is the acoustic pressure). For example, for a bubble containing nitrogen ($\kappa = 1.33$) in water at an ambient temperature of 20 °C (T_0) and an ambient pressure of 1 atm (P_m), then T_{max} is about 4200 K and P_{max} is 1056 atm.

Stable Cavitation

For stable cavitation bubbles, the time scale over which the bubble exists is sufficiently long so that mass diffusion of gas, as well as thermal diffusion, with consequent evaporation and condensation of the vapor, can occur. It results in significant long-term effects. As the bubble grows, the acoustic and environmental conditions of the medium will change and the bubble may be transformed into a transient bubble and undergo collapse.

With the energy release from the collapsing of bubbles, local temperatures and pressures are elevated substantially. Therefore, chemical substances surrounding the bubbles are exposed to extreme conditions of temperature and pressure as the bubble collapses. As a result, chemical bonds are broken and reactions are accelerated.

Chemical Reactions

Sonochemistry is mainly concerned with reactions which involve a liquid component in which cavitation can be induced. Two typical classes of chemical reactions affected by ultrasonic irradiation are described below (*20*).

— Homogeneous reactions

A schematic representation of the three regions of homogeneous sonochemical reactions is given in Figure 2.

(a) Gas cavitation bubble: The bubble is formed during the rarefaction cycle and contains vapor from the solvent (or any volatile compound present) which enters as the bubble is being formed. Upon collapse, the vapor is subjected to the enormous increase in temperature and pressure as described above. Under such extreme conditions the solvent or reagent suffers homolytic bond cleavage to generate reactive species, e.g., radicals. The following reaction scheme shows the principle reactions that appear to be involved in water sonolysis in the presence of Ar (*13*).

$$H_2O \rightarrow H\bullet + \bullet OH$$

$$H\bullet + \bullet OH \rightarrow H_2O$$

$$H\bullet + \bullet H \rightarrow H_2$$

$$\bullet OH + \bullet OH \rightarrow O + H_2O$$

$$\bullet OH + \bullet OH \rightarrow H_2O_2$$

$$O + O \rightarrow O_2$$

$$H\bullet + O_2 \rightarrow HO_2\bullet$$

$$HO_2\bullet + HO_2\bullet \rightarrow H_2O_2 + O_2$$

$$H\bullet + HO_2\bullet \rightarrow H_2O_2$$

$$H_2O + \bullet OH \rightarrow H_2O_2 + H\bullet$$

(b) Gas-Liquid interface: The interface between the bubble and the bulk liquid is the region where surface-active reagents may accumulate or where species produced in the bubble will first react with chemicals in the bulk liquid.

(c) Bulk aqueous phase: In the liquid immediately surrounding the bubble, an intense shock wave is produced as liquid rapidly rushes into the volume previously occupied by the bubble (*21*). The shock wave creates enormous shear forces which have been shown to be sufficient to fragment polymer chains.

— Heterogeneous reactions

For heterogeneous reactions involving solid/liquid interfaces, there are two modes of cavitational bubble collapse that can affect the surface of solids (*20*):

(a) Cavitational collapse on the surface itself which causes direct damage by the shock waves produced on implosion. These bubbles are formed on nuclei such as surface defects, entrapped gases or impurities on the surface of the material (*22,23*).

(b) Cavitational collapse near solid surface in the liquid phase which causes microjets to hit the surface and produce a non-symmetrical shock wave. This is a well known cleaning action of ultrasound. As a result, more reactant surface area is ready for further reaction. For example, the combination of iron metal with ultrasound has been shown to undergo enhancements due to the increases in reactive iron surfaces (*22,23*).

Chapter 1 - Appendix:

The general form of the Rayleigh-Plesset equation (*2,18,19*) is derived in the following way.

Consider a spherical bubble of radius R_0 in a time-varying pressure field $P_a(t)$. The hydrostatic pressure, P_0, is a constant. At time $t > 0$, a pressure $P_a(t)$ is superimposed on P_0, so the liquid pressure at a point remote from the bubble is $P_\infty = P_0 + P_a(t)$. As a consequence its radius will change to some new value $R(t)$ (Figure 3). During this process, the liquid will acquire a kinetic energy of

$$\frac{1}{2}\rho\int_R^\infty \dot{r}^2 4\pi r^2 dr \qquad \text{(eq. 13)}$$

where ρ is the liquid density, r is the general radius outside the bubble and $\dot{r}$ is equal to dr/dt, the velocity of the liquid. If we assume the liquid is incompressible, then the volume lost by the bubble ($4\pi R^2 dR$) is equal to that filled by the liquid ($4\pi r^2 dr$).

$$R^2 dR = r^2 dr$$
$$\frac{\dot{r}}{\dot{R}} = \frac{R^2}{r^2} \qquad \text{(eq. 14)}$$

The kinetic energy of the liquid is $2\pi\rho R^3 \dot{R}^2$. This value is equal to the difference between the work done far from the bubble by P_∞ and the work done by the pressure P_L in the liquid just outside the bubble wall. It gives

$$\int_{R_0}^{R}(P_L - P_\infty)4\pi R^2 dR = 2\pi R^3 \dot{R}^2 \rho \qquad \text{(eq. 15)}$$

Differentiation of eq. 15 with respect to R gives

$$\frac{P_L - P_\infty}{\rho} = \frac{3\dot{R}^2}{2} + R\ddot{R} \qquad \text{(eq. 16)}$$

Since P_L is the pressure in the liquid immediately beyond the bubble wall (radius R), the gas pressure inside the bubble at radius R is $(P_L - P_v + \frac{2\sigma}{R})$ and $(P_0 - P_v + \frac{2\sigma}{R_0})$ is the gas pressure inside the bubble at radius R_0.

According to the adiabatic law, PV^{κ} = constant, we obtain

$$P_L = \left(P_0 + \frac{2\sigma}{R_0} - P_v \right) \left(\frac{R_0}{R} \right)^{3\kappa} + P_v - \frac{2\sigma}{R} \qquad \text{(eq. 17)}$$

where P_0 is the hydrostatic pressure, σ is the surface tension of the liquid, P_v is the vapor pressure and κ is the polytropic index.

Substituting eq. 17 and P_∞ into eq. 16, we obtain the following equation:

$$R\ddot{R} + \frac{3\dot{R}^2}{2} = \frac{1}{\rho} \left\{ \left(P_0 + \frac{2\sigma}{R_0} - P_v \right) \left(\frac{R_0}{R} \right)^{3\kappa} + P_v - \frac{2\sigma}{R} - P_0 - P_a(t) \right\} \qquad \text{(eq. 18)}$$

which is generally-known as the Rayleigh-Plesset equation (*19*).

References

1. Richards, W. T.; Loomis, A. L. *J. Am. Chem. Soc.* **1927**, *49*, 3086.
2. Mason, T. J.; Lorimer, J. P. *"Sonochemistry: Theory, Application and Uses of Ultrasound in Chemistry"* John Wiley & Sons, New York, **1988.**
3. Weissler, A.; Cooper, H. W.; Snyder, S. *J. Am. Chem. Soc.* **1950**, *72*, 1976.
4. Agranonik, Ya. R.; Karpukhin, V. F.; Fayngold, Z. L, *"Antibiotikii Khimioterapiya," Russ.* **1986**, *35*, 48-51.
5. Cheung, H. M.; Bhatnagar, A.; Jansen, G. *Environ. Sci. Technol.* **1991**, *25(8),* 1510.
6. Hua, I.; Hoffmann, M. R. *Environ. Sci. Technol.* **1996**, *30*, 864-861.
7. Mason, T. J., "Chemistry with ultrasound," published for the Society of Chemical Industry, Elsevisier Science Publishers Ltd., London, England, **1990**.
8. Suslick, K. S.; Hammerton, D. A.; Cline, D. E., Jr. *J. Am. Chem. Soc.* **1991**, *108*, 5614.
9. Shutilov, V. A. " *Fundamental Physics of Ultrasound*," Gordon & Breach Science Publishers, New York, **1988**.
10. Kotronarou, A.; Mills, G., Hoffmann, M. R. *J. Phys. Chem.* **1991**, *95*, 3630-3638.
11. Kotronarou, A.; Mills, G.; Hoffmann, M. R. *Environ. Sci. Technol.* **1992**, *26*, 1460-1462.
12. Kotronarou, A.; Mills, G.; Hoffmann, M. R. *Environ. Sci. Technol.* **1992**, *26*, 2420-2428.
13. Kotronarou, A., Ph.D. Thesis; California Institute of Technology, Pasadena, **1991**.
14. Wu, J. M.; Huang, H. S.; Livengood, C. D. *Environ. Prog.* **1992**, *11*, 195-201.
15. Bhatnagar, A.; Cheung, H. M. *Environ. Sci. Technol.* **1994**, *28*, 1481-1486.
16. Francony, A; Petrier, C. *Ultrasonics Sonochemistry* **1996**, *3*, S77-S82.
17. Hua, I.; Höchemer, R. H.; Hoffmann, M. R. *J. Phys. Chem.* **1995**, *99*, 2335-2342.

18. Leighton, T. G. *"The Acoustic Bubble"* Academic Press, Harcourt Brace & Company, London, **1994.**

19. Young, F. R. *"Cavitation"* McGRAW-HILL, London; New York, **1989.**

20. Mason, T. J. *"Practical Sonochemistry: User's Guide to Application in Chemistry and Chemical Engineering"* E. Horwood, New York, **1991.**

21. Weninger, K. R.; Barber, B. P.; Putterman, S. J. *Phys.Rew. Lett.* **1997**, *78*, 1799-1802.

22. Hung, H.-M.; Hoffmann, M. R. *Environ. Sci. Technol.* **1998**, *32*, 3011-3016.

23. Hung, H.-M.; Ling F. H.; Hoffmann, M. R. "Kinetics and Mechanism of the Enhanced Reductive Degradation of Nitrobenzene by Elemental Iron in the Presence of Ultrasound" in press, *Environ. Sci. Technol.* **2000**.

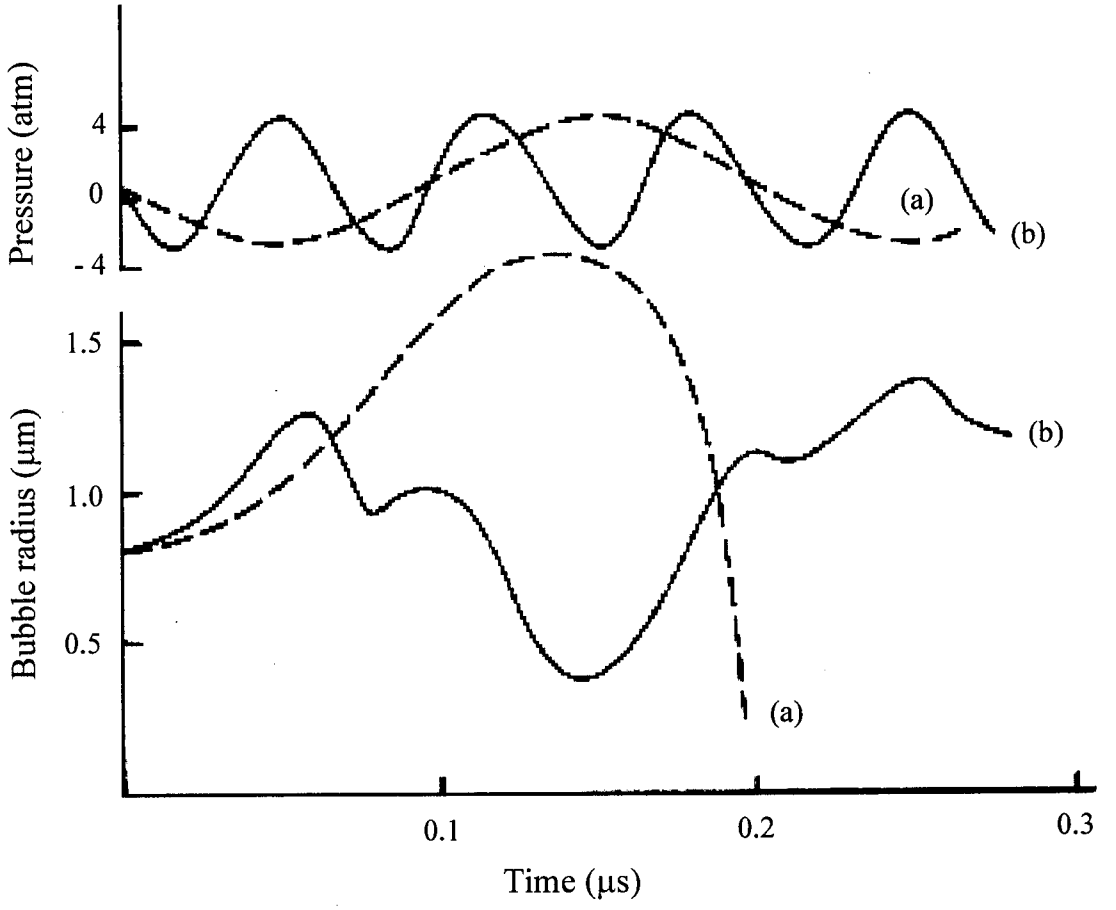

Figure 1. Radius vs. time curves for an air bubble in water subjected to ultrasonic irradiation at (a) 5 MHz; (b) 15 MHz; R_0 = 0.8 μm; P_a = 4 atm; P_0 = 1 atm. (Ref. 2).

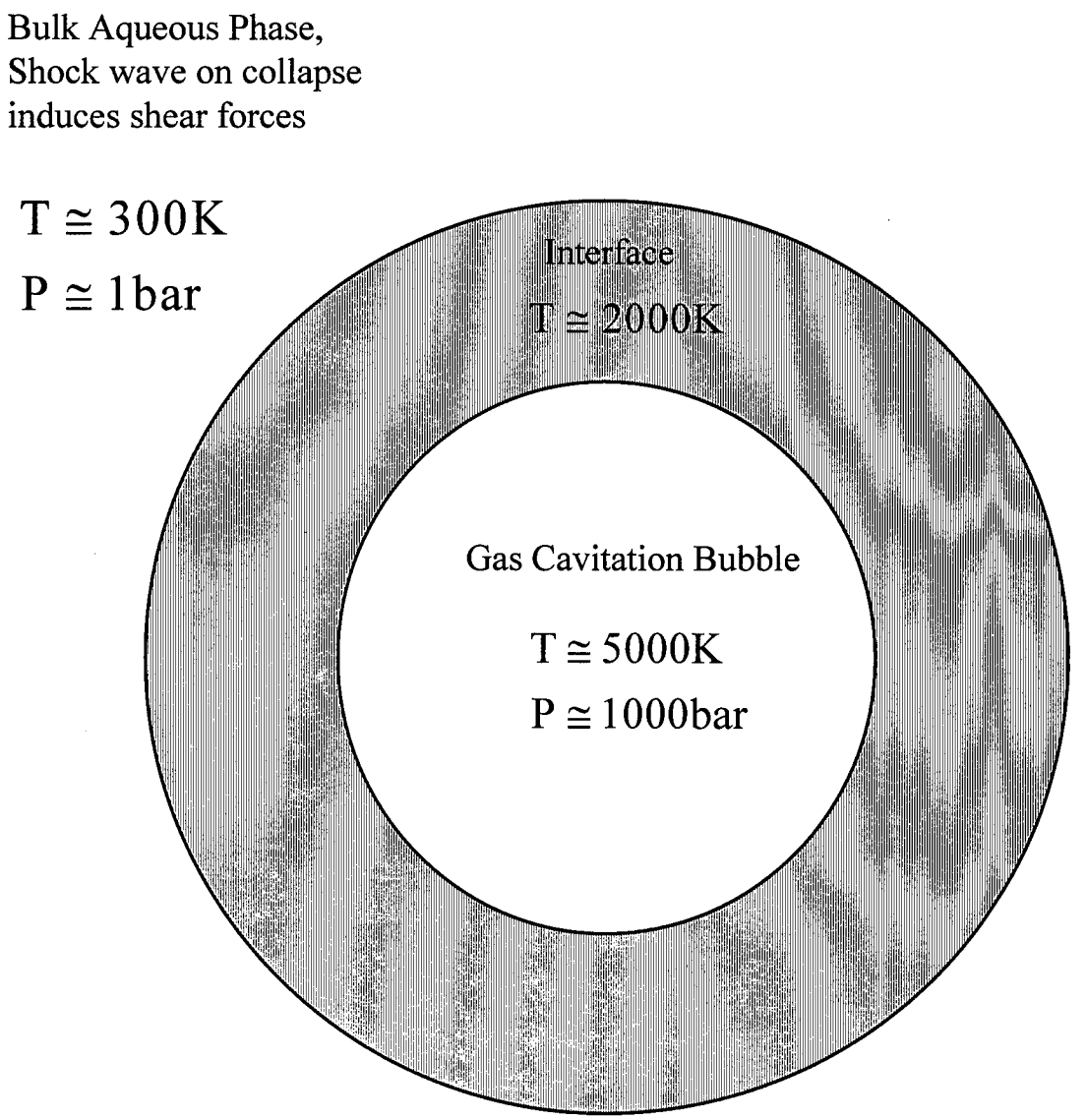

Figure 2. For a bubble formed by ultrasound, schematic representation of the regions of sonochemical reaction in aqueous sonochemistry.

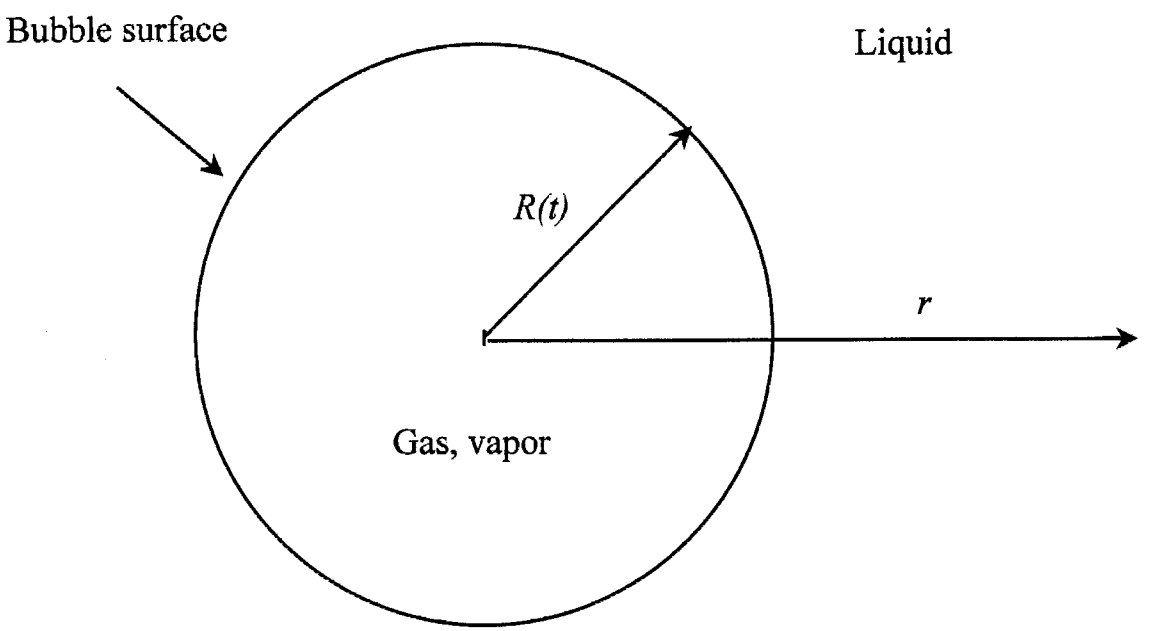

Figure 3. Schematic of a spherical bubble in an infinite liquid.

Chapter 2

Sonochemical Degradation Rates of Volatile Solutes

(*Journal of Physical Chemistry A*, **1999**, 103: (15) 2696-2699)

Abstract

We report degradation rates of chlorinated methanes, ethanes and ethenes —spanning the range of Henry's law constants $0.9 \leq H/(\text{atm } M^{-1}) \leq 24.5$ — in water solutions sonicated at f = 205, 358, 618 and 1078 kHz. First-order degradation rate constants, k_X, vary as $k_X \sim H_X^{0.30\pm0.03}$ at all frequencies, change with f by less than a factor of two in this range, and peak at about 600 kHz for all species. We show that experimental rates are consistent with: 1) complete decomposition of the solute contained in collapsing bubbles, 2) about 15% ultrasound power efficiency for transient cavitation and, 3) a rather flat $N(R_o) \propto R_o^n$, $n \simeq 0$, initial radius bubble distribution under continuous sonication. The solute content of collapsing bubbles is composed of the equilibrated vapor at R_o, plus the amount incorporated by diffusion from the surrounding solution during the acoustically driven expansion from R_o to R_{max}, the maximum radius attained prior to collapse. The finding that k_X's decline above 600 kHz is ascribed to the fact that increasingly smaller bubbles collapse at rates reaching a limiting value at sufficiently high frequencies.

Introduction

Ultrasound induces chemical reactions via acoustic cavitation (*1-6*). This phenomenon entails the sudden collapse of microbubbles of critical size generated by expansion of preexisting nuclei during the rarefaction cycle of acoustic waves. Although the chemical effects of ultrasound have been intensively investigated, the complex series of events preceding and following cavitation still defies a coherent description in terms of fundamental physical and chemical processes (*7*). From a practical point of view it would be useful, for example, to estimate the energy efficiency of sonochemical action under given conditions and, ultimately, to improve it. This consideration is particularly relevant to the possible use of ultrasonic degradation of persistent water contaminants in aquifers and potable water supplies (*8*). In this context it is of interest to understand the physical basis of the dependence of sonochemical rates on molecular and acoustical field parameters (*7*).

In this paper, we report experimental degradation rates for a series of chlorinated hydrocarbons —a pervasive class of water pollutants— as function of ultrasound frequency, in an attempt to provide a stringent test of current sonochemical models and gain new insights into the mechanism of sonication. Crucial to this analysis is the realization that most organic vapors fully decompose under the extreme conditions prevalent in collapsing bubbles (*7*). The discussion leads us to deal with several fundamental issues such as the dynamics of bubble expansion and collapse, the extent of mass transfer across the bubble surface prior to collapse, and the distribution of bubble sizes in liquids continuously exposed to ultrasound (*5b,6a,9,10*). As it emerges, sonochemical degradation rates of volatile solutes can be actually estimated within experimental error from generally available information.

Experimental Section

Sonications were performed on Ar-purged, aqueous solutions (V = 605 mL) contained in a covered, jacketed cylindrical reactor coupled to an ultrasound generator (Allied ELAC Nautik) through an emitting flange (A = 23.6 cm^2). The actual ultrasound power Π delivered to the reactor was determined by in-situ calorimetry. Reaction temperature was maintained at 283 K throughout by means of a refrigerated circulating bath (Haake A80). In the case of CH_2Cl_2, $CHCl_3$ and CCl_4 solutions sample aliquots (1 mL) were withdrawn at given intervals, and extracted with 0.5 mL pentane in capped vials. 0.5 μL of the pentane extracts were analyzed with a HP 5880A gas-chromatograph (HP-5 column) operated in the splitless mode, and equipped with electron capture detector. The analysis of other organic products was carried out with a HP 7694 headspace sampler injector in tandem with a HP 5890 Series II GC-FID gas-chromatograph equipped with a HP-624 capillary column (30 m x 0.32 mm x 1.8 um). Commercial chlorinated organic compounds: CCl_4 (99.9%, J. T. Baker reagent), $CHCl_3$ (LC grade), CH_2Cl_2 (EM Science HPLC grade), C_2Cl_4 (99.9%, Sigma-Aldrich), C_2Cl_6, (98%, Aldrich), CH_3CCl_3 (98%, Aldrich), and $CH_2ClCHCl_2$ (98%, Aldrich) were used without further purification. Aqueous solutions were prepared with water purified with a MilliQ UV Plus system (18.2 mΩ-cm resistivity).

Results and Discussion

Experimental Results

Experiments were routinely performed on solutions (initial concentrations for CH_2Cl_2, $CHCl_3$ and CCl_4 were about 0.15 mM, and ca. 1 μM for the other compounds) sonicated at Π = 50 W. All solutes decay with first-order kinetics over three half-lives

under present experimental conditions. Decay rate constants k_X (s^{-1}) measured for the different solutes at f = 205, 358, 618 and 1078 kHz as function of the corresponding Henry's constants H_X are shown in Table 1 and Fig. 1. The non-linear k_X vs. H_X^m dependences found over a 25-fold variation of H values at constant f are conveniently displayed in a scaled log-log plot. Linear regressions yield a mean $m = 0.33 \pm 0.03$ value at the four frequencies. Rate constants are not very sensitive to, but increase with f up to ca. 600 kHz and then decline.

Decomposition Rates of Volatile Solutes in Cavitated Liquids

Microbubbles present in media steadily exposed to ultrasound can either: 1) undergo periodic size oscillations, 2) expand during the rarefaction cycle of acoustic waves and then collapse violently, 3) slowly dissolve or, 4) escape from the liquid due to the combined effects of mass convection and buoyancy (*7*). The relative probabilities of the four processes are a function of bubble size and applied power. For example, bubbles smaller than the Blake radius R_B (μm):

$$R_B = \frac{0.77\sigma}{P_A - P_H} \tag{1}$$

will dissolve (*4a*); P_A is the acoustic pressure amplitude, P_H the hydrostatic pressure, and σ = 0.072 N m^{-1} is the surface tension of water at room temperature. Under present conditions, $I_A = \Pi/A$ = 2.12 W cm^{-2}, $P_A = (2\rho c I_A)^{1/2}$ = 2.5 atm (ρ = 1000 Kg m^{-3} is water density and c = 1500 m s^{-1} is the speed of sound in water), P_H = 1 atm (1 atm = 10^5 Pa), we get minimum bubble sizes of about $R_B \simeq 0.36$ μm (*4a*). On the other hand, very large bubbles will move upwardly under buoyancy forces and eventually escape from the liquid. It can be shown that bubbles larger than R_E:

$$R_E = \sqrt{\frac{9\eta v_b}{2\rho g}} \qquad (2)$$

where $\eta = 8.9 \times 10^{-4}$ Kg m^{-1} s^{-1} is the water viscosity and $g = 9.8$ m s^{-2}, will rise faster than v_b. The stationary density of bubbles expelled by buoyancy from a stirred medium at speeds larger than, say, $v_b = 0.1$ cm s^{-1}, will be small under mild insonation. Hence, we will assume that $R_E \leq 30$ μm, which is more than twice as large as resonance radii under present conditions (*4a*).

The bubble population in a liquid under continuous sonication is actually maintained by a cycle involving bubble expansion, collapse and fragmentation stages (*6, 7*). Near the end of collapse, the radial acceleration of the bubble shell vanishes and its motion becomes unstable (*6b*). Spherical bubbles are easily distorted and break up, dispersing their contents into the solution. The resulting fragments provide the nuclei for the development of new bubbles. If all fragment sizes were produced with the same probability, as it would be expected for a mechanism of random bubble fragmentation, and considering that the coalescence of any but the smallest fragments may be slower than re-expansion in an intense sonic field, a steady-state regime would attain characterized by a bubble size distribution function, $dN_o/dR_o = A\ R_o^n$, with $n \simeq 0$. This dependence must be contrasted with the *equilibrium* distribution in quiescent liquids, for which $n = -3$, or -4 applies (*6a, 9, 10*).

Besides dynamic restrictions, energetic considerations may limit the maximum bubble number density N_B in a sonicated liquid. Restrictions arise from the fact that the surface energy density E_S associated with the bubble cloud cannot exceed the energy

density $E_D = I_A/c$ (E_D = 14.1 μJ cm^{-3} in present experiments) of the sonic field. In terms of the average bubble area $\langle S_B \rangle$:

$$\langle S_B \rangle = \frac{4\pi \int_{R_B}^{R_E} R_o^{2+n} dR_o}{\int_{R_B}^{R_E} R_o^n dR_o} \qquad (3)$$

the surface energy density is given by: $E_S = N_B \sigma \langle S_B \rangle$. Therefore, the condition $E_S = \beta E_D$, with $\beta \leq 1$, links n and N_B. The bubble volume fraction F_B —an experimentally accessible parameter related to the effective mass density of a sonicated liquid— that could be sustained in sonochemical experiments can be evaluated from the expression: $F_B = N_B \langle V_B \rangle$, where $\langle V_B \rangle$ is the average bubble volume. The latter can be calculated once n is known. There is evidence that F_B generally increases with E_D (*10*).

It has been shown that the maximum radius a bubble can attain by acoustic expansion prior to cavitating collapse can be estimated from (*4a*):

$$R_{max} \approx (3000/f)(P_A - P_H)(P_A)^{-0.5}[1 + 0.67(P_A - P_H)]^{0.33} \qquad (4)$$

or $R_{max}(\mu m) = 3589/f(kHz)$ under present conditions. However, not all bubbles can grow up to R_{max} and undergo violent collapses because of the existence of a dynamic threshold: only bubbles with initial radii $R_o \leq R_{max}/3$ can reach R_{max} (*5a*). Thus, the bubble sub-population $\{R_o; R_B \leq R_o \leq R_{max}/3\}$ that is actually able to undergo cavitation and lead to chemical effects becomes increasingly sparser at higher frequencies (cf. the $R_{max} \propto 1/f$

dependence in Eq. 4). Therefore, the density of bubbles that can potentially undergo transient cavitation $N_{B,CAV}$:

$$N_{B,CAV} = N_B \frac{\int_{R_E}^{R_{max}/3} R_o^n dR_o}{\int_{R_B}^{} R_o^n dR_o} \quad (5)$$

is necessarily smaller than N_B. On the other hand, the maximum *rate* r_{CAV} (bubbles cm^3 s^{-1}) at which bubbles can be expanded to R_{max} also depends on ultrasound power Π according to (*7*):

$$r_{CAV} = (\Pi / V) / \varepsilon_B \quad (6)$$

where ε_B is the energy required to expand potentially cavitating bubbles (i.e., those having $R_o \leq R_{max}/3$) (*5a, 7*):

$$\varepsilon_B = (4\pi/3)(P_A + P_H)(R_{max}^3 - R_o^3) + 4\pi\sigma(R_{max}^2 - R_o^2) \approx (4\pi/3)(P_A + P_H)R_{max}^3 + 4\pi\sigma R_{max}^2 \quad (7)$$

As a consequence, the average frequency k_E at which bubbles are excited: $k_E(s^{-1}) = r_{CAV}/N_{B,CAV}$, is a strongly increasing function of f, because: 1) $r_{CAV} \propto (1/\varepsilon_B) \propto (1/R_{max}^3) \propto f^3$ (cf. Eqs. 3, 6 and 7) and, 2) $N_{B,CAV}$ decreases with f on account of the narrowing of the subpopulation of cavitating bubbles (cf. the upper integration limit in the numerator of Eq. 5). Notice that k_E cannot obviously exceed f and, therefore, the efficiency of cavitation becomes limited by this factor at high frequencies.

Recent calculations on the fate of volatile species in cavitating bubbles indicate that they are completely decomposed at the high temperatures attained at the end of collapse (*7,11*). Hence, solute decomposition rates r_{-X} can be evaluated as the product of the rate of generation of cavitating bubbles r_{CAV} (Eq. 6), times the total amount of solute $N_T(R_o)$ contained in such bubbles. The total number of solute molecules consists of those present within initial nuclei, N_m, plus those admitted during the expansion stage ΔN_m. Assuming liquid-vapor equilibrium, the former is given by (*7*):

$$N_m = \frac{4\pi R_o^3 H C_\infty}{3RT} \tag{8}$$

where H is the solute Henry's constant, C_∞ is the solute bulk concentration, and R is the gas constant. During expansion, an additional mass of solute enters from the initially saturated solution into the rarefied bubble. We evaluated ΔN_m using the high-frequency form of the first-order approximation to dynamic rectified diffusion derived by Eller and Flynn (*5a,12*):

$$\Delta N_m = C_{R_i}\left(\frac{C_\infty}{C_{R_o}} - \frac{\langle (R/R_o)\rangle}{\langle (R/R_o)^4\rangle}\right)\times\left[8\sqrt{\pi Dt\langle (R/R_o)^4\rangle}R_o^2 + 4\pi DtR_o\langle (R/R_o)\rangle\right] \tag{9}$$

where $C_{Ro} = C_\infty\,[1+2\sigma/(P_H R_o)]$, and $D \sim 2 \times 10^{-5}$ cm^2 s^{-1} is the assumed common value of solute diffusion coefficients in water at 300 K. Lower, approximate bounds to the required time averages of R were estimated for bubbles expanding at constant velocity, i.e.: $\langle (R/R_o)\rangle \sim 1 + 0.5\,[(R_{max}/R_o)\text{-}1]$, $\langle (R/R_o)^4\rangle \sim (1/5)\,[(R_{max}/R_o)^5 - 1]/[(R_{max}/R_o)\text{-}1]$. Therefore, first-order decay rate constants k_{-X} for solute decomposition in bubbles of radius R_o can be calculated from:

$$k_{-X} = \varphi r_{CAV}(N_m + \Delta N_m)/C_\infty \tag{10}$$

where φ is the energy efficiency of cavitation, i.e., the fraction of ultrasound energy actually utilized in bubble cavitation. It is assumed that φ is independent of f. Average values $\langle k_{-X} \rangle$, i.e., those to be compared with experimental data, involve averaging k_{-X} over the bubble size distribution:

$$\langle k_{-X} \rangle = \frac{\int_{R_B}^{R_{max}/3} k_{-X} R_o^n dR_o}{\int_{R_B}^{R_{max}/3} R_o^n dR_o} \qquad (11)$$

Trial fits of $\langle k_{-X} \rangle$, calculated by means of Eq. 11 at f = 205, 358, 618 and 1078 kHz, to the experimental data for the chlorocarbons of Table 1, were performed using n (the exponent in R_o^n of the bubble radii distribution), φ (the energy efficiency of transient cavitation) and β (the fraction of the acoustic field energy stored as surface energy of the bubble cloud) as adjustable parameters. The results of calculations are shown in Fig. 1. Typical sets of parameters reproducing experimental data are, e.g.: $\{n = 0.5, \varphi = 0.15, \beta = 1\}$, or $\{n = 0, \varphi = 0.15, \beta = 0.1\}$. The latter set implies a volume fraction of $F_B \sim 1 \times 10^{-4}$, i.e., close to the upper limit of the range suggested for water in cavitation tubes (*10*). We found that the onset of the k_{-X} fall-off as a function of f remains at about 600 kHz largely through the interplay of n and β. The non-linear k_{-X} vs. H dependence at all frequencies, as well as the peak efficiencies at $f \sim 600$ kHz for all substrates, are well accounted for by the model. We also found that in order to reach peak efficiencies at ~ 600 kHz with $n \leq 0$, it is necessary to invoke much larger R_E values. For example, n = -1 requires $R_E \geq 250$ μm, which is considered implausible. By setting R_E = 30 μm, calculations with n = -3 result in a monotonous, fourfold increase of $\langle k_{-X} \rangle$ between 205 and 1078 kHz. The n = -3 equilibrium distribution is so slanted toward small sizes that

nearly the same bubble pool is excited at all frequencies, despite the fact that the condition $R_o \leq R_{MAX}/3$ would allow for transient cavitation of larger bubbles at lower frequencies.

To summarize, the physical reasons underlying the observed behaviors are related to the fact that degradation rates are actually proportional to the density of bubbles excited per unit time —which increases with frequency as f^3 because much less work is required to expand bubbles to smaller $R_{max} \sim 1/f$ values— times the amount of solute accumulated within bubbles at the time of their collapse. Such amount is generally dominated by a leading term ΔN_m (the amount of solute incorporated into the bubble *during* expansion, Eq. 9) that roughly decreases as $\sim 1/f^2$. The breakdown of the expected $\langle k_X \rangle \propto f$ dependence at high frequencies is a consequence of the fact that the intermittence at which individual bubbles are excited cannot exceed f. As a result the $1/f^2$ dependence gradually takes over with the consequent slowdown of decomposition rates. The non-linear k_X vs. H_X dependence directly reveals that rate constants are not solely determined by equilibrium parameters. Rectified diffusion contributes significantly to the composition of the bubble vapor prior to collapse, particularly for the less volatile substrates. Further work is underway.

Acknowledgments

Financial support for this research was provided by the U. S. Department of Energy (DOE 1 963772 402).

References

1. Suslick, K. J., Ed., *Ultrasound, Its Chemical, Physical and Biological Effects.* VCH; Weinheim, Germany. 1988.
2. Margulis, M. A., Ed., *Sonochemistry and Cavitation*, Gordon and Breach, Newark, N.J., 1995.
3. Henglein, A. *Ultrasonics*, **1987**, *25*, 6.
4. a) Mason, T. J.; Lorimer, J. P., *Sonochemistry. Theory, Applications and Uses of Ultrasound in Chemistry*, Wiley, New York, 1988, chapter 2. b) Mason, T. J., Ed. *Advances in Sonochemistry*; JAI Press: New York, 1990-1994; Vols. 1-3.
5. a) Leighton, T. G., *The Acoustic Bubble,* Academic Press, London, 1994, chapter 4, section 4.4.3. b) Leighton, T. G., *Ultrasonics Sonochemistry,* **1995**, *2,* S123.
6. a) Brennen, C. E., *Cavitation and Bubble Dynamics,* Oxford University Press, New York, 1995, section 1.11. b) *ibid.,* section 2.12.
7. Colussi, A. J.; Weavers, L. K.; Hoffmann, M. R., *J. Phys. Chem. A,* **1998**, *102,* 6927.
8. a) Graham, J. L.; Hall, D. L.; Dellinger, B., *Environ. Sci. Technol.* **1986**, *20*, 703. b) Hua, I.; Hoffmann, M. R., *Environ. Sci. Technol.* **1997**, *31*, 2237.
9. Gavrilov, L. R. in *Physical Principles of Ultrasonic Technology*, vol 2. Part VI, Plenum Press, New York, 1973.
10. Gavrilov, L. R., *Soviet Physics-Acoustics,* **1970**, *15*, 285.
11. a) NIST Chemical Kinetics Database 17, Version 5.0, Westley, F.; Frizzell, D. H.; Herron, J. T.; Hampson, R. F.; Mallard, W. G. National Institute of Standards and Technology, Gaithersburg, MD, 1993. b) Baulch, D. L.; Cobos, C. J.; Frank, P.; Hayman, G.; Just, Th.;

Murrells, T.; Pilling, M. J.; Troe, J.; Walker, R. W.; Warnatz, J., *J. Phys. Chem. Ref. Data,* **1994**, 23, 847.

12. Eller, A. I.; Flynn, H. G., *J. Acoust. Soc. Am.* **1965**, *37*, 493.

13. Mackay, D.; Shiu, W. Y.; Ma, K. C., *Illustrated Handbook of Physical-Chemical Properties and Environmental Fate of Organic Chemicals, vol. III,* Lewis Publishers, Boca Raton, Fl., 1993.

Table 1. Sonochemical Degradation Rate Constants (in s^{-1}) at Different Frequencies, and Solubility Parameters for Various Chlorocarbons.

Species	205 kHz	358 kHz	618 kHz	1078 kHz	Henry's Constants* H (Pa m^3 mol^{-1})
CCl_4	7.3e-4	8.2e-4	9.2e-4	6.5e-4	2454
CCl_3CH_3	5.4e-4	8.8e-4	9.7e-4	6.3e-4	2025
C_2Cl_4	6.2e-4	8.1e-4	9.9e-4	6.5e-4	1621
$CHCl_3$	4.7e-4	-	-	-	537
C_2Cl_6	4.1e-4	6.3e-4	7.3e-4	4.5e-4	250
CH_2Cl_2	2.7e-4	-	-	-	200
CCl_2HCClH_2	2.1e-4	3.2e-4	3.2e-4	1.9e-4	90

* Taken from Ref. 13.

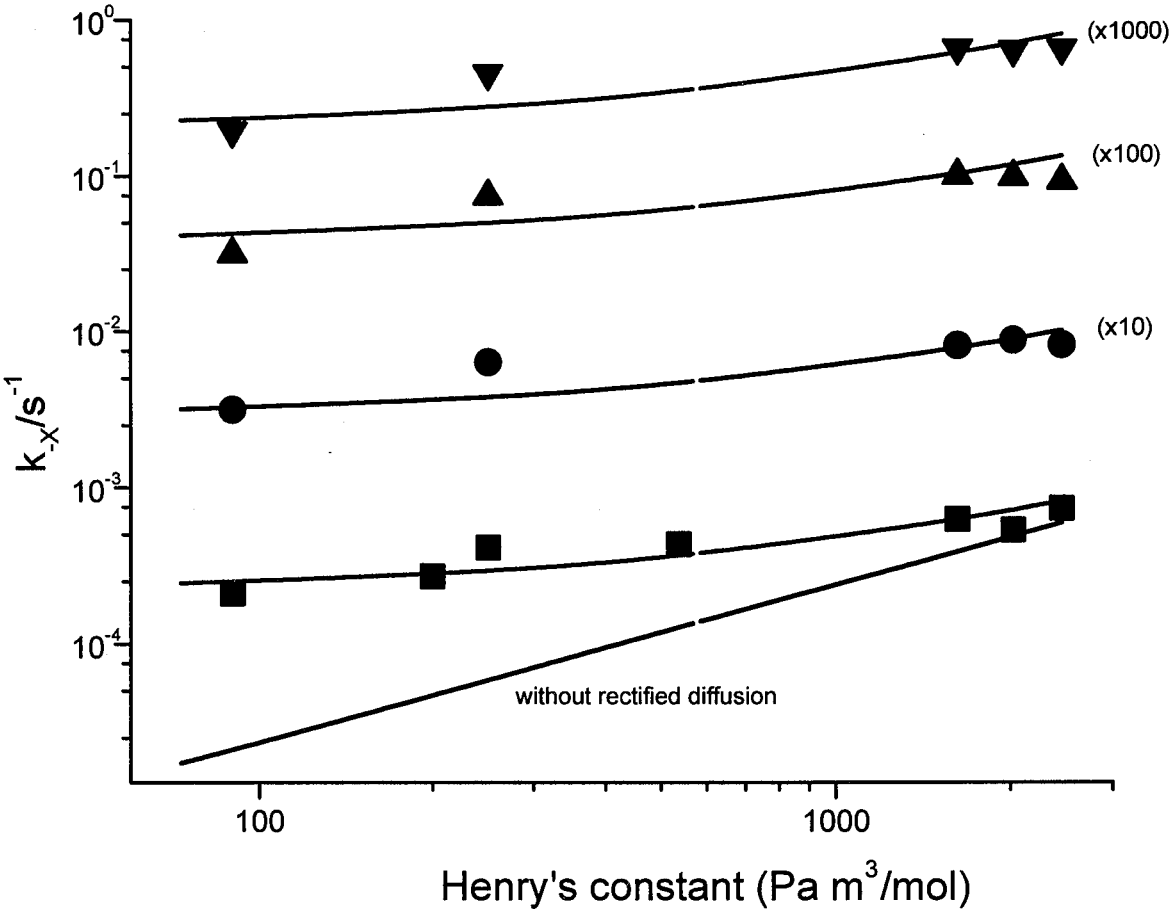

Figure 1. First order rate constants k_{-X} for the decomposition of volatile solutes. Experimental data from Table 1: ■ (205 kHz), ● (×10, 358 kHz), ▲ (×100, 618 kHz), ▼ (×1000, 1078 kHz). Solid lines calculated with Eq. 11 (see text). The straight line for the 205 kHz data was calculated by neglecting the ΔN_m term in Eq. 10.

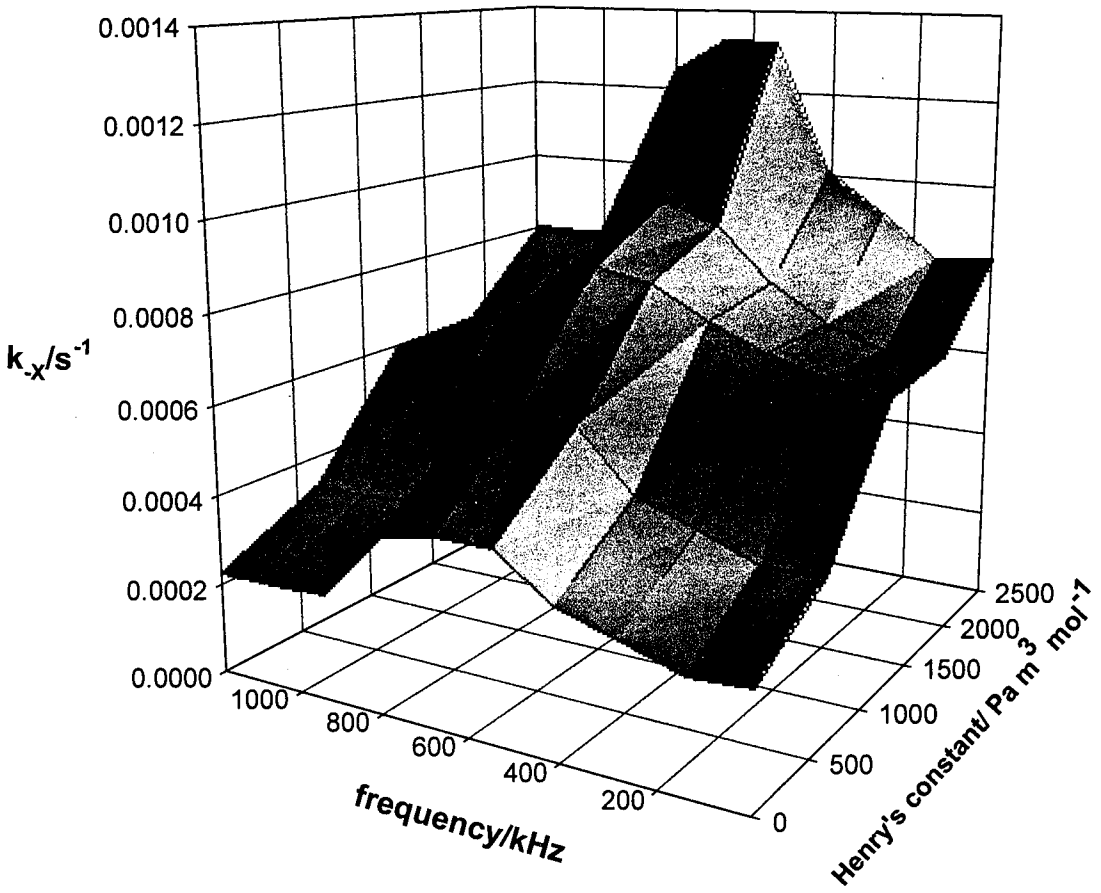

Figure 2. The landscape of k_{-X} as a function of f and H, calculated from Eq. 11 (see text).

Chapter 3

Sonochemical Reaction Rates: Effects of Frequency and Applied Power Density

(Submitted to *Journal of Physical Chemistry A*, **2000**)

Abstract

The oxidation of iodide is used to quantify the relative rate of production of •OH radical in sonicated Ar-saturated water as function of ultrasound frequency (f = 205, 358, 618 and 1078 kHz) and acoustic power density (Π_v = 33 - 290 W/L) at 283 K. The maximum production rates depend on f and Π_v in a concerted manner, e.g., the optimal frequencies at Π_v = 83 and 33 W/L are 358 and 205 kHz, respectively. The rate of production of •OH increases with acoustic intensity up to about 250 W/L before leveling off. Furthermore, we show that the power dependence data can be used to estimate effective temperatures inside the cavitation bubbles, which are of the order of 4100 ± 200 K at f = 205 and 358 kHz.

Introduction

The chemical effects of ultrasound are due to the phenomenon of acoustic cavitation, which involves the sudden collapse of critically expanded microbubbles occurring after a transient positive pressure is applied to the liquid (*1*). Sound travels through a fluid as a wave consisting of alternating compression and rarefaction cycles. If the sound wave has a sufficiently high amplitude, it can overcome the intermolecular bonding forces in the fluid. As a result, the liquid breaks down and voids are created. However, in most liquids, this process is initiated on pre-existing microbubbles or other inhomogeneities in the fluid such as suspended particles or gas bubble nuclei. The bubble nuclei grow gradually during successive compression and rarefaction cycles by rectified diffusion until they reach a critical size. In the following compression cycle, these cavities may collapse capturing the elastic energy stored in the liquid in a fraction of a microsecond. This rapid implosion is accompanied by the adiabatic heating of the gases and vapors contained within bubbles, which results in localized but transient high temperatures and pressures. Under such conditions, chemical reactions can be initiated or enhanced. By considering the energy associated with chemical reactions inside cavitating bubbles, Colussi *et al.* estimated maximum temperatures $T_{max} < 8000$ K, depending on the experimental condition (*2*). Suslick et al. (*3,4*) found effective emission temperatures in multi-bubble sonoluminescence from 5100 to 2300 K, depending on the properties of the gas-vapor mixture.

The effects of ultrasonic frequency have been explored previously, but the results are open to interpretation since the apparent optima are dependent on the specific physical

configuration of the transducers and on the size and shape of the reactors (*5-8*). For example, the maximum rate for the oxidation of I^- to I_3^- was observed at 59 kHz over the frequency range of 20 - 80 kHz by Cum *et. al.* (*5*). However, for the same chemical system faster reaction rates were observed at 900 kHz than at 20 kHz (*6*).

In this paper, we study the effects of frequency and sonication power on the oxidation rates of iodide solutions using the same reactor cell and the physical configuration at two different power densities. From the analysis of the power dependence data, we are able to estimate maximum temperatures inside cavitation bubbles.

Experimental Methods

Commercially available high-purity reagents (KI, and NaH_2PO_4, EM Science) were used without further purification. Aqueous solutions were made with deionized water (MilliQ UV Plus water, 18.2 MΩ-cm resistivity).

Sonolyses were performed in the same sonochemical reactor irradiated at 205, 358, 618 or 1078 kHz (Allied ELAC Nautik). The physical dimensions and the reactor configurations are shown in Figure 1. The transducer emitted between 20 and 175 W of acoustic power across an area of 23.6 cm^2 into a 605 mL iodide solution. The variation of I_3^- concentrations were followed by absorption spectrophotometer at $\lambda = 350$ nm ($\varepsilon = 2.6 \times 10^4\ M^{-1}\ cm^{-1}$) (*9*). The reactor temperature was maintained at 10 °C by means of a Haake A80 Refrigerated Bath.

The reaction solutions consisted of 0.1 M potassium iodide buffered with sodium phosphate, NaH_2PO_4, at pH = 4.5. At this pH, the sonochemical reaction products, H_2O_2 and I_3^-, are unable to react with each other via the following stoichiometry (*10*):

$$H_2O_2 + I_3^- \rightarrow 3I^- + O_2 + 2H^+ \quad (1)$$

The reaction solution was thermally equilibrated at 10 °C for 30 min before sonication was initiated. Samples were circulated between the reactor cell and a flow-through cuvette using a Cole-Parmer peristaltic pump. Absorbances were measured every 30 s and the data were stored for subsequent kinetics calculations. Under these operating conditions, iodide is oxidized by hydroxyl radical as follows:

$$2\ \bullet OH + 3\ I^- \rightarrow\ 2\ OH^-\ + I_3^- \quad (2)$$

The reaction system was covered by aluminum foil to prevent any photolytic reactions.

Results and Discussion

The primary reactive species formed during the ultrasonic irradiation of water saturated with Ar are H• and •OH (*10*). The •OH radicals formed inside the cavitation bubble may self-react to form H_2O_2 or diffuse into the interfacial region; then react with other species. The iodine dosimeter provides a convenient way to quantify •OH radical yields. One mole of I_3^- is produced for every two moles of •OH consumed. The sonochemical formation of iodine follows zero-order kinetics. However, the rate constant for I_3^- formation was determined from the data obtained in the first 5 min of reaction.

Frequency Dependence

Figure 2 shows the experimental results for different frequencies for different values of Π_v. For Π_v = 33 W L^{-1} (0.85 W/cm^2), the production rate of I_3^- decreases with increasing ultrasonic frequency, *f*. This phenomenon may be due to the fact that fewer nuclei are excited to form cavitation bubbles at higher frequencies. The minimum radius for a bubble nucleus, which is known as the Blake radius R_B, is given by (*11-13*):

$$R_B \approx \frac{0.77\sigma}{P_A - P_H} \quad (\mu m) \tag{3}$$

where P_A is the acoustic pressure amplitude, P_H is the hydrostatic pressure, and σ = 0.074 N m^{-1} is the surface tension of water at 10 °C. With P_A = 1.58 atm (for 0.85 W cm^{-2}), P_H = 1 atm, we predict minimum bubble nuclei sizes of about R_B > 1 μm. On the other hand, the maximum radius a bubble can attain during acoustic expansion before cavitational collapse can be estimated as follows (*1,12,13*):

$$R_{max} \approx (3000/f)(P_A - P_H)(P_A)^{-0.5}[1 + 0.67(P_A - P_H)]^{0.33} \tag{4}$$

or R_{max} (μm) = 1542/*f* (kHz) at P_A = 1.58 atm and P_H = 1 atm. However, not all bubbles can expand to R_{max} and undergo violent collapses because of the existence of a limiting dynamic threshold. In this case, only bubbles with initial radii $R_o \leq R_{max}/3$ can reach R_{max}. At *f* = 618 and 1078 kHz, $R_{max}/3 \leq R_B$, which means that almost no bubbles can be excited to form cavitation bubbles. At *f* = 358 kHz, the radius of cavitation nuclei range from 1 μm ≤ R_o ≤ 1.4 μm. Within such a narrow radius range, most of this input energy may be consumed by stable oscillating bubbles under present conditions. The optimal frequency for these experimental conditions is 205 kHz.

At Π_v = 83 W L^{-1} (2.1 W/cm^2), the production rate of I_3^- first increases with *f* and then declines as *f* > 358 kHz. The maximum observed rate constant occurs between 358 and 618 kHz. Since the resonant radius of the bubble is smaller at higher frequency, the surface area-volume ratio is correspondingly larger at higher frequencies (*8,14*). The larger values of surface area-volume ratio leads to an enhanced rectified diffusion rate at higher frequencies. For this the reason, the observed rate constant is faster at 358 kHz than at 205

kHz.

Power Dependence

As the bubbles collapse, H_2O will decompose to form •H and •OH radicals under the extremely high temperature and high pressures that are achieved. The rate constant for the dissociation of H_2O inside the bubble with k_A (s^{-1}) = [M] k_A', where $k_A' = 5.8 \times 10^{-9}$ exp(-52900/T) cm^3/molecules-sec (*13*), and [M] is the concentration of the vapor-phase third body. As T increases from 4000 K to 5000 K, k_A will increase ten times at a constant [M]. As shown in Figure 3, as power increases from 80 to 250 W L^{-1} there is a threefold enhancement in reaction rate.

If we assume that the bubble will be in thermal equilibrium during the expansion cycle and then collapse adiabatically, the concentration of H_2O inside the bubble at radius R without reaction could be expressed as follows:

$$[H_2O]_R = [H_2O]_0 \left(\frac{R_{max}}{R} \right)^3 \qquad (5)$$

where $[H_2O]_0$ is the concentration of H_2O at $R = R_{max}$. Consider the equilibrium relationship among H_2O, •H and •OH that occurs inside the bubble during collapse:

$$H_2O \xleftrightarrow{K} H\bullet + \bullet OH \qquad (6)$$

Let the degree of water decomposition be r. Then: $P_{OH} = P_H = r\, P_{H2O}'$ and $P_{H2O} = (1 - r)\, P_{H2O}'$ (P_{H2O}' is the water pressure before dissociation), and the equilibrium constant:

$$K = \frac{r^2 P_{H_2O}'}{(1-r)} = \exp(-\Delta G/RT) \qquad (7)$$

The equilibrium constant K can be evaluated as a function of temperature, T (kK), based

on the following thermochemical data (*15*):

$$\Delta H \text{ (kJ/mole)} = 7.57\ T - 1.95T^2 + 0.23\ T^3 - 0.011\ T^4 - 8.4/T + 510.4 \quad (8)$$

$$\Delta S \text{ (J/mole-K)} = 7.57\ln(T) - 3.91\ T + 0.34\ T^2 - 0.01\ T^3 - 4.2\ /\ T^2 + 134 \quad (9)$$

$$\Delta G \text{ (kJ/mole)} = \Delta H - T\Delta S$$

$$= -7.57\ T\ \ln(T) - 126.43\ T + 1.95\ T^2 - 0.11\ T^3 + 0.0036\ T^4 - 4.2/T + 510.4 \quad (10)$$

Consider the adiabatic compression process for the cavitation bubble where the following relationships hold:

$$PV^{\gamma} = \text{constant} \quad (11)$$

$$TV^{\gamma-1} = \text{constant} \quad (12)$$

$$PT^{\gamma/(1-\gamma)} = \text{constant} \quad (13)$$

If we assume a negligible phase transfer of water vapor during cavitation, the water vapor pressure before dissociation can be estimated as:

$$P_{H_2O}{}' = P_{H_2O_0}\left(\frac{T}{T_0}\right)^{\frac{\gamma}{\gamma-1}} \quad (14)$$

Where $P_{H_2O_0} = 0.0123$ atm, $T_0 = 283$ K and $\gamma = 1.33$ for water vapor. From Eqs. 7 and 14, we calculate the degree of decomposition ratio *r* as a function of temperature shown in Figure 4.

With the high temperature (> 1 kK) inside the cavitation bubble, the chemical reactions may be able to reach an equilibrium state very quickly inside the bubble. If we assume that there is a dynamic equilibrium state during bubble collapse, then the production of •OH, $N_{\cdot OH}$ (mole) in one bubble can be expressed as

$$N_{\cdot OH} = r[H_2O]_{R_{min}} V_{bubble} = r[H_2O]_0 \frac{4\pi}{3} R_{max}{}^3 \quad (15)$$

The maximum rate r_{CAV} (bubbles L^{-1} s^{-1}) at which bubbles can be expanded to R_{max} depends on the applied ultrasonic power density Π_v according to

$$r_{CAV} = \Pi_v / \varepsilon_B \quad (16)$$

where ε_B is the energy required to expand potential cavitating bubbles (i.e., those having $R_0 \leq R_{max}/3$) (*12,13*).

$$\begin{aligned} \varepsilon_B &= (4\pi/3)(P_A + P_H)(R_{max}^3 - R_o^3) + 4\pi\sigma(R_{max}^2 - R_o^2) \\ &\approx (4\pi/3)(P_A + P_H)R_{max}^3 + 4\pi\sigma R_{max}^2 \approx (4\pi/3)(P_A + P_H)R_{max}^3 \end{aligned} \quad (17)$$

The production rate of •OH radicals (mole s^{-1}) in the solution can be expressed as follows:

$$R_{\cdot OH, production} = \varphi\, r_{CAV} \times r[H_2O]_0 \frac{4\pi}{3} R_{max}{}^3 \quad (18)$$

where φ is the energy efficiency of cavitation, *i.e.*, the fraction of ultrasonic energy actually utilized in bubble cavitation. Since not all of •OH will react with iodide to form iodine, we assume the formation of iodine by •OH oxidation with an efficiency of ϕ; then the production rate of I_3^- (M s^{-1}) can be expressed as follows:

$$\begin{aligned} R_{I_3^-, production} &= \frac{R_{OH, production}}{2}\phi = \frac{1}{2}\varphi' r_{CAV} \times r[H_2O]_0 \frac{4\pi}{3} R_{max}{}^3 \\ &= \frac{\Pi_v}{2(P_A + P_H)(4\pi/3)R_{max}{}^3 \times 0.001} \times \varphi' r[H_2O]_0 \frac{4\pi}{3} R_{max}{}^3 \\ &= \frac{\Pi_v}{0.002(P_A + P_H)} \times \varphi' r[H_2O]_0 \end{aligned} \quad (19)$$

where $\varphi' = \phi\varphi$ is the energy efficiency of cavitation times the efficiency of •OH reacting with I^-. If we assume that the values of "φ' r" for the same frequency at a small power

range are the same, the production of I_3^- as a function of power density should be expressed in the following equation ($P_A = 0.35\ (\Pi_v\ V)^{0.5}$ atm and $P_H = 1$ atm):

$$R_{I_3^-,\,production}(\mathrm{M\,s^{-1}}) = \frac{\Pi_v}{0.002(0.35(\Pi_v V)^{0.5}+1)\times 10^5}\times \varphi' r[\mathrm{H_2O}]_0 = \frac{\Pi_v}{(0.35(\Pi_v V)^{0.5}+1)\times 200}\times A \qquad (20)$$

where $A = \varphi' r[\mathrm{H_2O}]_0$, is assumed to be a constant at the same frequency for a small power range.

Results of this analysis show that an increase in applied sonication power results in a corresponding increase in the sonochemical rates of reaction as illustrated in Fig. 3. In this case, there is a clear increase in $d[I_3^-]/dt$ with increasing power density. The experimental measurement of $d[I_3^-]/dt$ (i.e., the solid data points of Fig. 3) compare well with the predicted results obtained from eq. 20. The value of A in eq. 20 was determined to be 3.34×10^{-7} M L^{-1} at 358 kHz for low power densities. With $[H_2O]_0 = 5.3 \times 10^{-4}$ M, we obtain a value of $\varphi' r = 6.3 \times 10^{-4}$. In a previous study (*12*) we reported a value of $\varphi = 15\%$.

For the formation of I_3^-, we also have to consider the efficiency of diffusion of •OH radicals inside the vapor phase of bubble to the interfacial region. If we assume $\varphi' \sim 1\%$, then $r = 0.063$ at lower power densities, which translates to $T \approx 4100$ K. At higher power densities, the value of A is 3.8×10^{-7} M L^{-1}. With $\varphi' \sim 1\%$, we obtain $r = 0.072$, which translates to $T \approx 4250$ K. With a constant efficiency, $\varphi' = 1\%$, the temperature estimated by iodine dosimetry is approximately 4100 to 4300 K for power densities in the range of 80 to 250 W L^{-1} at 358 kHz and 3900 to 4100 K at 205 kHz. If $\varphi' = 5\%$, the estimated T is

reduced to 3000 K. The temperatures obtained here (~ 4 kK) are less than the calculated maximum temperatures (5 - 10 kK) attainable in a real bubble from the energy available for heating the vapor in the adiabatic stage (*12*).

With an increase in the acoustic amplitude, the cavitation bubble may grow so large on rarefaction (R_{max}) that the time available for collapse is insufficient. Deviations at high power densities are due to the limited time available for completion of the bubble collapse event. The time to achieve bubble collapse as a function of acoustic pressure is as follows (*1*):

$$\tau = 0.915 R_{max} [\rho/(P_A + P_H)]^{0.5} [1 + P_v/(P_A + P_H)] \quad (21)$$

where ρ is the density of solution and P_v is the vapor pressure of the solvent. In Figure 5, we show that R_{max} and τ increase with P_A at a sonication frequency of 205 kHz. The pressure wave period at 205 kHz is 4.8 μs. The time available for bubble collapse estimated from the numerical solution of the RP equation (*1*) is approximately 1/3 of the cycle time, then the actual time available for collapse at 205 kHz is ~ 4.8/3 = 1.6 μs. If τ is greater than 1.6 μs, the bubble cannot be completely compressed to produce higher temperatures and higher pressures that will lead to additional chemical reactions. Our experimental data shows that the •OH yield levels off at a power density = 290 W L^{-1}, where P_A = 4.7 atm and τ ~ 1.5 μs. This latter value is close to the upper limit of 1.6 μs.

In summary, an equilibrium temperature ~ 4000 K inside the cavitation bubble was estimated from the analysis of the power dependence data for I_3^- production with an assumption of 1% efficiency. At higher power densities, the •OH yield plateaus due to the insufficient compression cycle times.

Acknowledgments

Financial support from the Office of Naval Research and the Department of Energy (via Argonne National Laboratory) is gratefully acknowledged.

Definition of Symbols:

Symbol	Parameter	Units
Π_v	Applied power density	$W\ L^{-1}$
f	Ultrasonic frequency	kHz
P_A	Acoustic pressure	atm
P_H	Hydrostatic pressure	atm
σ	Surface tension	$N\ m^{-1}$
R_B	Blake radius	μm
R_{max}	The maximum bubble radius during expansion cycle	μm
K	The equilibrium constant among H_2O, ·H and ·OH	atm
r	The degree of water decomposition	
r_{CAV}	The maximum expanded bubble rate	Bubbles $L^{-1}\ s^{-1}$
ε_B	The energy required to expand a cavitating bubble	J
φ	Energy efficiency of cavitation	
ϕ	Efficiency of OH reacting with I^-	
ϕ'	Product of $\phi\varphi$	
τ	The time to achieve bubble collapse	sec

References

1. Mason, T. J.; Lorimer, J. P. *Sonochemistry: Theory, Application and Uses of Ultrasound in Chemistry*; John Wiley & Sons: New York, 1988.
2. Colussi, A. J.; Hoffmann, M. R. *J. Phys. Chem. A* **1999**, *103*, 11336-11339.
3. Suslick, K. S.; Choe, S. B.; Cichowlas, A. A.; Grinstaff, M. W. *Nature* **1991**, *353*, 414-416.
4. McNamara III, W. B.; Didenko, Y. T.; Suslick, K. S. *Nature* **1999**, *401*, 772-775.
5. Henglein, A.; Gutierrez, M. *J. Phys. Chem.* **1993**, *97*, 158-62.
6. Gutierrez, M.; Henglein, A.; Ibanez, F. *J. Phys. Chem.* **1991**, *95*, 6044-7.
7. Leighton, T. G. *The Acoustic Bubble*; Harcourt Brace & Company, 1994.
8. Colussi, A. J.; Hung, H. M.; Hoffmann, M. R. *J. Phys. Chem. A* **1999**, *103*, 2696-2699.
9. Colussi, A. J.; Weavers, L. K.; Hoffmann, M. R. *J. Phys. Chem. A* **1998**, *102*, 6927-6934.
10. Hua, I.; Hoffmann, M. R. *Environ. Sci. Technol.* **1997**, *31*, 2237-2243.
11. Hung, H. M.; Hoffmann, M. R. *J. Phys. Chem. A* **1999**, *103*, 2734-2739.
12. NIST Chemisty WebBook, NIST Standard Reference Database Number 69 - November 1998 Release.

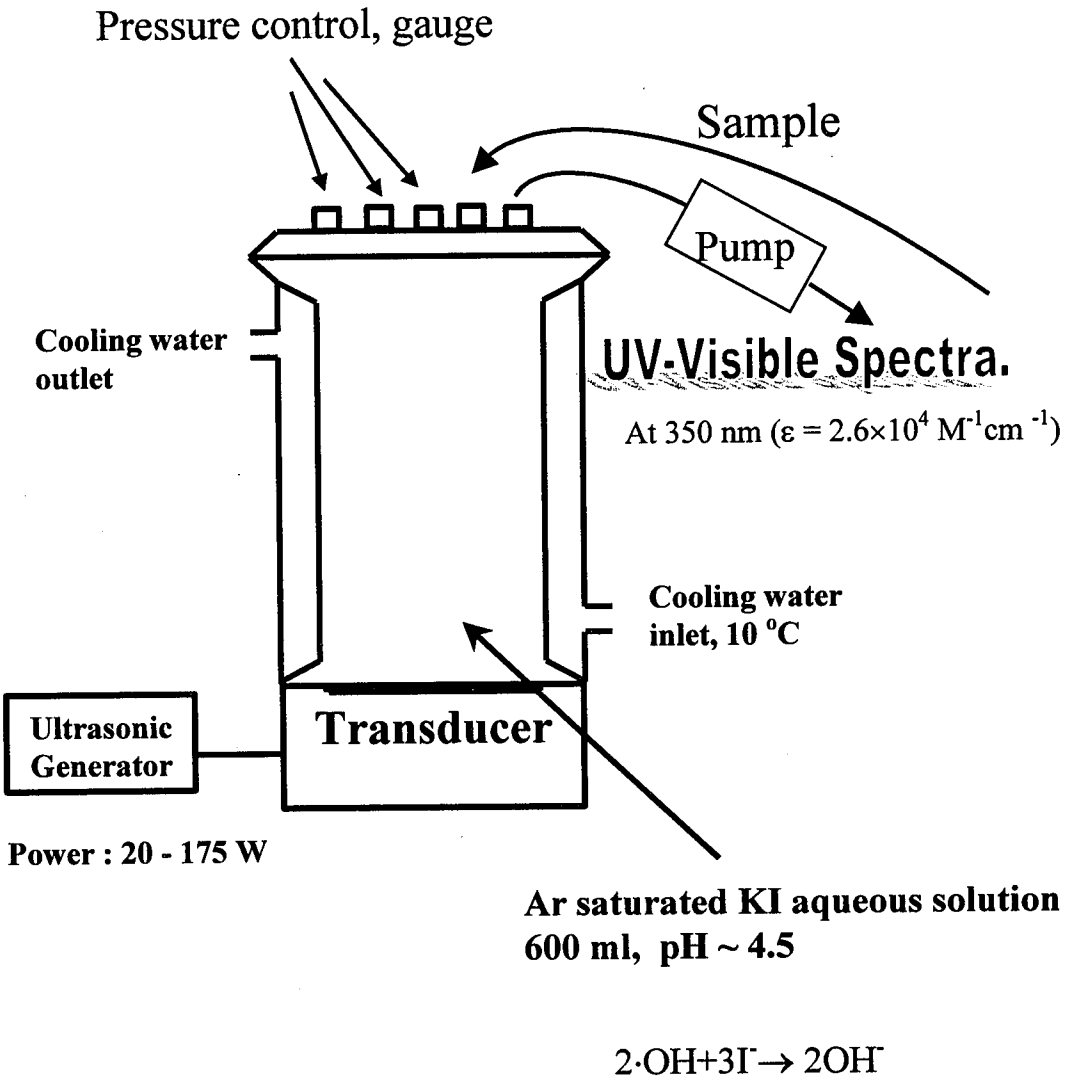

Figure 1. Schematic representation of the instrument set-up.

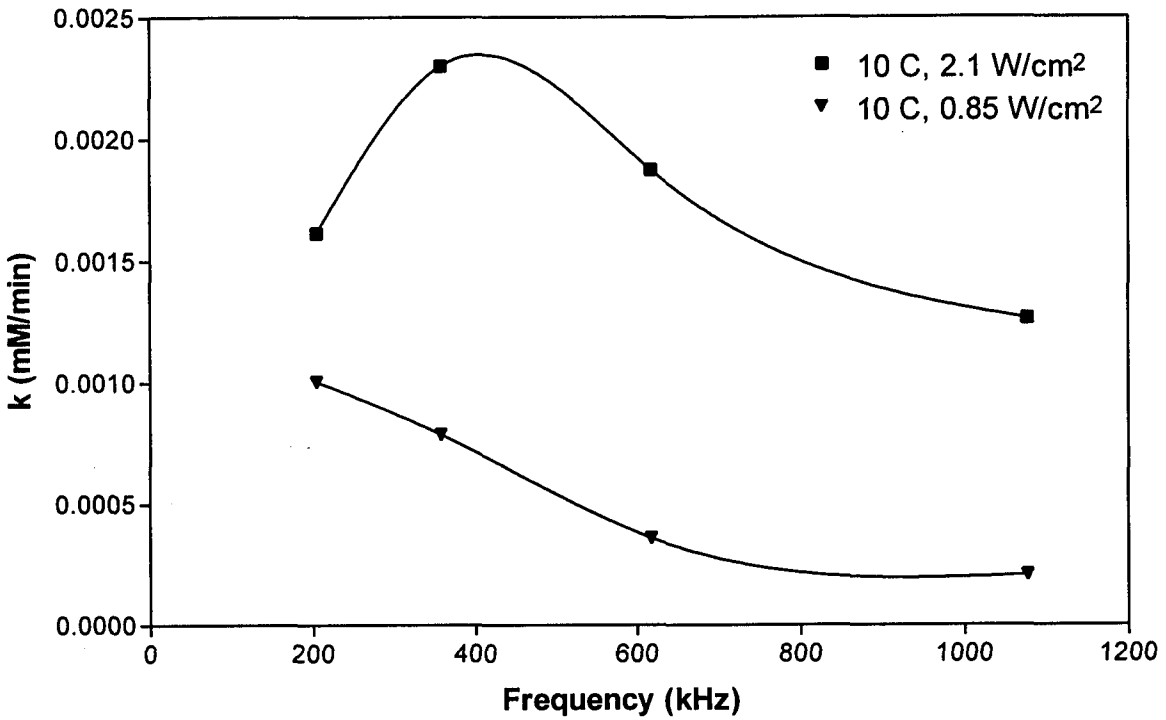

Figure 2. Variation of the I_3^- production rate constant vs. frequency at power densities = 2.1 W/cm^2 and 0.84 W/cm^2.

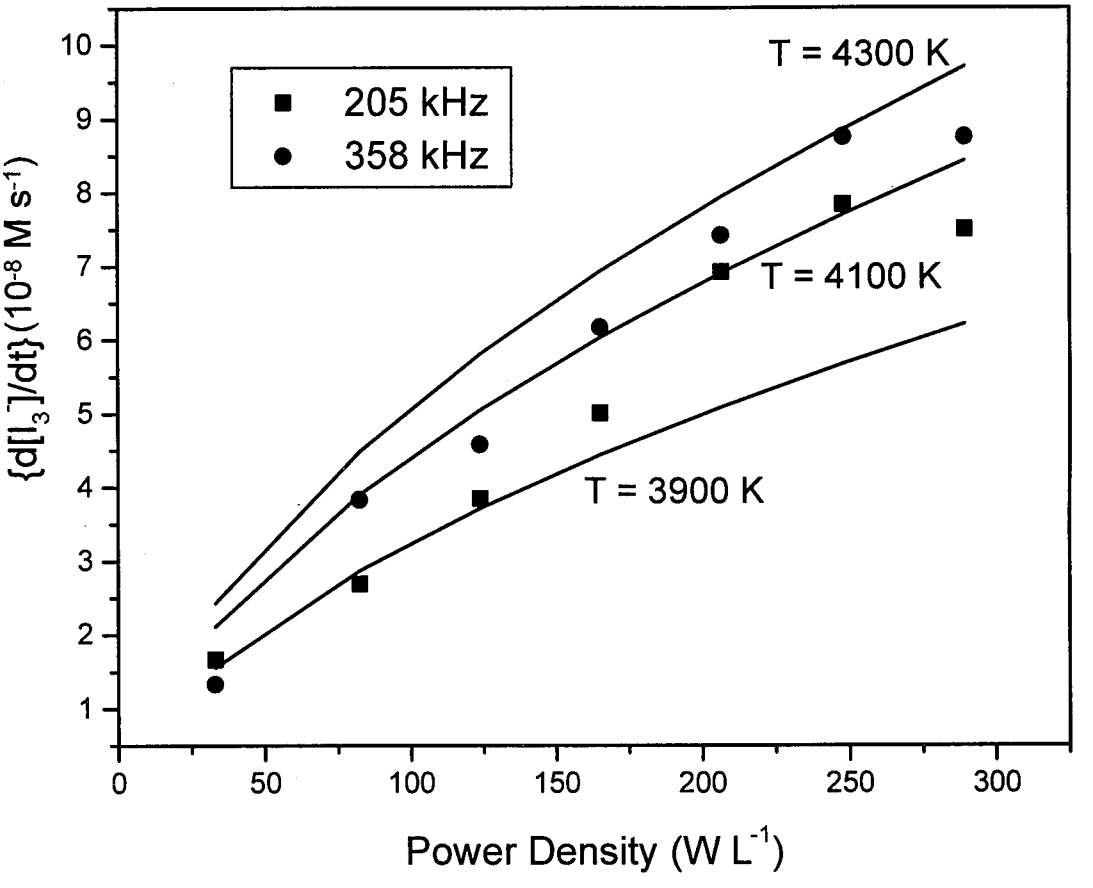

Figure 3. The rate of I_3^- production as a function of power density and the solid fitting lines determined at different temperatures according to eq. 20.

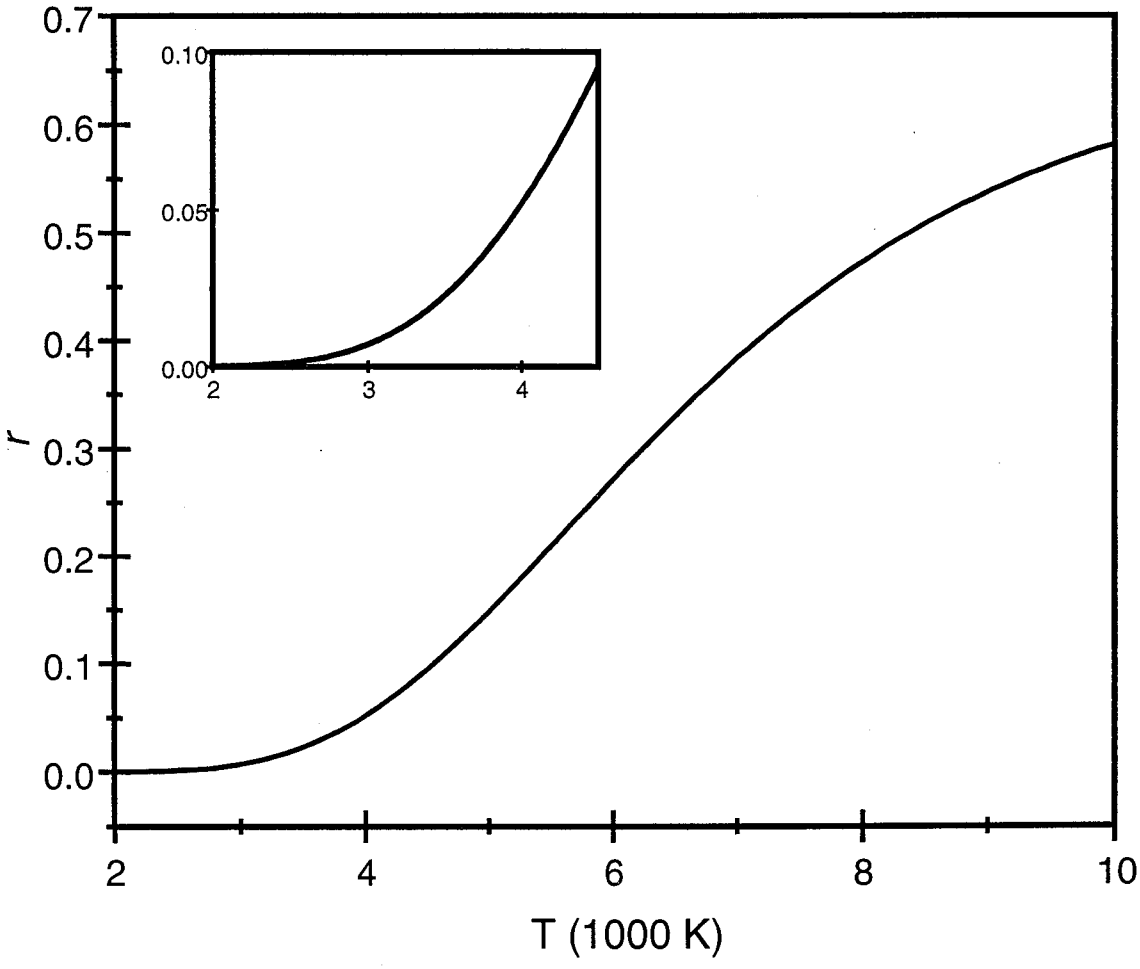

Figure 4. The decomposition ratio r as a function of temperature with $\gamma = 1.33$.

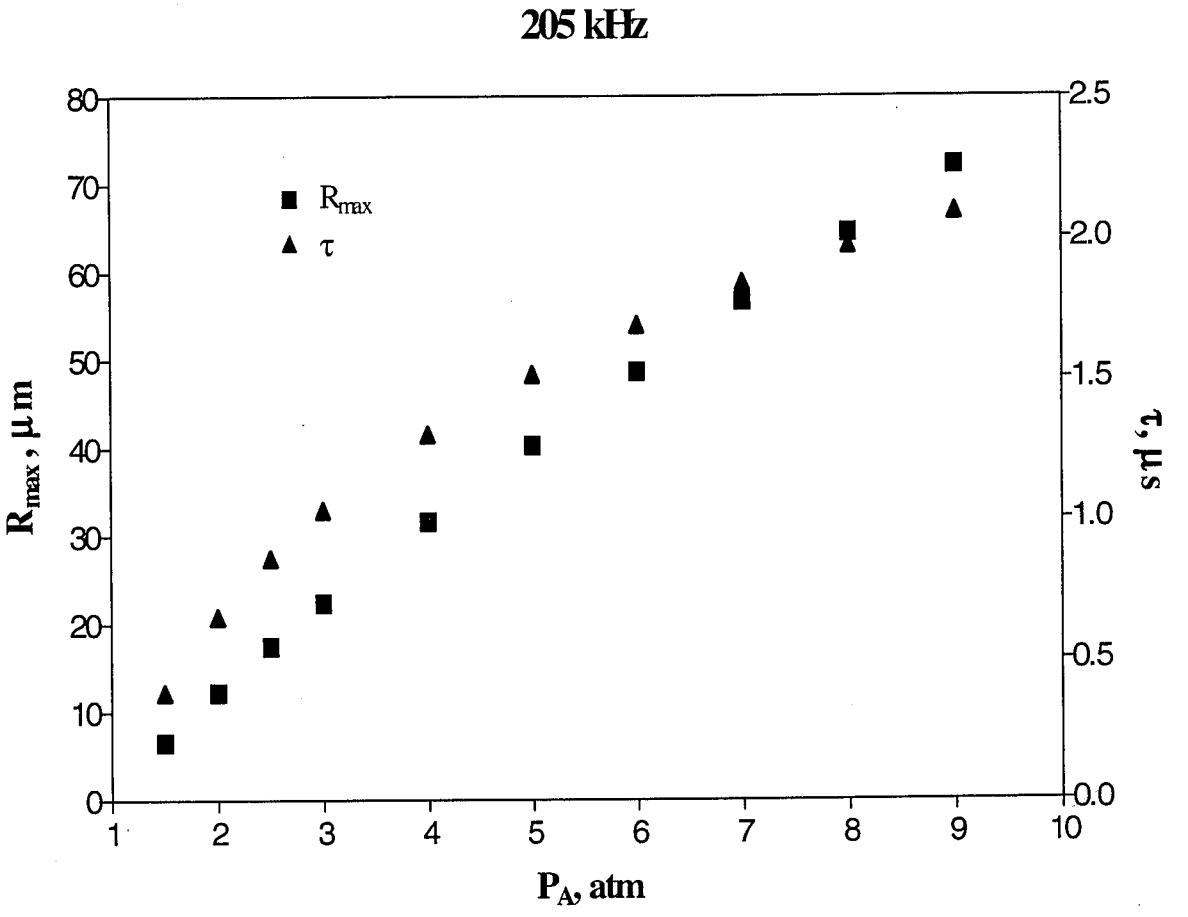

Figure 5. The time, τ, required to bubble collapse and R_{max} as functions of power density according to eq. 4 and 21.

Chapter 4

Kinetics and Mechanism of the Sonolytic Degradation of Chlorinated Hydrocarbons: Frequency Effects

(*Journal of Phsical Chemistry A*, **1999,** 103: (15) 2734-2739)

Abstract

The kinetics of the sonolytic degradation of aqueous solutions of carbon tetrachloride and hexachloroethane (C_2Cl_6) were investigated at six different frequencies over the range from 20 to 1078 kHz. The rates of degradation of CCl_4 and C_2Cl_6 were shown to increase with increasing frequency with optimal degradation rates at 500 kHz. At 205 kHz, the relative rates of sonolytic degradation of the three chlorinated methanes followed the order of $CCl_4 > CHCl_3 > CH_2Cl_2$. Hexachloroethane, which was formed as the primary intermediate in the degradation of CCl_4, was degraded at a rate comparable to that of CCl_4 at all six frequencies.

Introduction

Ultrasound has been used for a wide variety of biological, physical and chemical applications (*1-6*). For example, chlorinated hydrocarbons, which are often used as industrial degreasing agents, are readily degraded to inorganic products during aqueous-phase ultrasonic irradiation (*3,6-9*).

The chemical consequences of the ultrasonic irradiation of liquids are due to the phenomenon of acoustic cavitation (*10*). In most liquids, cavitation is initiated by excitation of pre-existing microbubbles or other inhomogeneities in the fluid such as suspended particles or gas-bubble nuclei. The theoretical maximum temperature (T_{max}) and pressure (P_{max}) obtained inside a collapsed cavitation bubble can be calculated from eqs. 1 and 2, if the bubble collapse is assumed to be an adiabatic process (*11*).

$$T_{max} = T_0\left\{\frac{P_m(\kappa-1)}{P}\right\} \tag{1}$$

$$P_{max} = P\left\{\frac{P_m(\kappa-1)}{P}\right\}^{\kappa/(\kappa-1)} \tag{2}$$

Temperatures near 5000 K have been observed experimentally, while pressures on the order of 1000 bar have been calculated (*12*). From the measurement of sonoluminescence during the cavitational collapse of single, isolated bubbles, extreme temperatures (e.g., > 10^3 K) and pressures (e.g., > 10^3 atmospheres) have been reported (*13-15*).

Dissolved organic compounds are chemically degraded during the sonolysis of aqueous solutions as a direct consequence of the extreme transient conditions of elevated temperature and pressure obtained during cavitational bubble collapse. The three main chemical pathways for compound degradation include 1) hydroxyl radical oxidation, 2)

direct pyrolytic degradation, and 3) supercritical water reactions (*16-18*). In aqueous solution, water vapor present in the bubble is homolytically split during bubble collapse to yield H· and ·OH radicals, while chemical substrates present either within or near the gas-liquid interface of the collapsing bubble are subject to direct attack by ·OH (*16,17*). Volatile compounds such as H_2S and CCl_4 readily partition into the vapor of the growing cavitation bubbles and then undergo direct pyrolysis during transient collapse (*3,17,19*). In addition, hydrolysis reactions have been observed to be accelerated by several orders of magnitude in the presence of ultrasound. For example, the acceleration in the observed rate of the hydrolysis of p-nitrophenyl acetate has been attributed to the existence of transient supercritical water during ultrasonic irradiation (*20*).

Carbon tetrachloride (CCl_4), which is one of the most widespread chemical contaminants in the subsurface aquatic environment, is difficult to treat with conventional technologies (*21-30*). However, the sonolytic degradation of CCl_4 in water has been shown to be an effective means for its elimination from contaminated water (*3,7-9*). In this regard, Hua and Hoffmann (*3*) have proposed the following mechanism for the sonolytic degradation of CCl_4 in water (where '))))' is sonilysis):

$$CCl_4 \xrightarrow{))))} Cl\cdot + \cdot CCl_3 \qquad (3)$$

$$CCl_4 \xrightarrow{))))} Cl_2 + :CCl_2 \qquad (4)$$

$$\cdot CCl_3 \rightarrow \cdot Cl + :CCl_2 \qquad (5)$$

$$\cdot CCl_3 + \cdot CCl_3 \rightarrow CCl_4 + :CCl_2 \qquad (6)$$

$$\cdot CCl_3 + \cdot CCl_3 \rightarrow C_2Cl_6 \qquad (7)$$

Dichlorocarbene formed in eq. 5 self-reacts to form tetrachloroethylene:

$$:CCl_2 + :CCl_2 \rightarrow C_2Cl_4 \qquad (8)$$

or it reacts with water to form carbon monoxide and hydrochloric acid:

$$:CCl_2 + H_2O \rightarrow 2\,HCl + CO \qquad (9)$$

C_2Cl_6 and C_2Cl_4, which are produced as intermediates during the sonolytic degradation of CCl_4, are also readily degraded during aqueous-phase sonication. Chlorine atoms produced in eq. 3 rapidly self-react to form molecular chlorine, which hydrolyzes readily to yield hypochlorous, HOCl, and hydrochloric acids:

$$2\,Cl^{\cdot} \rightarrow Cl_2 \xrightarrow{+H_2O} HOCl + HCl \qquad (10)$$

In this paper, we present the experimental results of a detailed investigation of the sonolytic degradations of $CHCl_3$, CH_2Cl_2 and CCl_4 in aqueous solutions as a function of ultrasonic frequency.

Experimental Procedures

The chlorinated hydrocarbons ($CHCl_3$, CH_2Cl_2, CCl_4) were obtained in high purity and used without further purification. The reagents were obtained from several sources: carbon tetrachloride, CCl_4, 99.9% (J. T. Baker); chloroform, $CHCl_3$, LC grade; dichloromethane, CH_2Cl_2, HPLC grade (EM Science); hexachloroethane, C_2Cl_6, 98% (Aldrich); and tetrachloroethene, C_2Cl_4, 99.9% (Sigma-Aldrich). Pentane (Omnisolv grade, EM Science) was used as the analytical solvent for extraction and GC analysis. Aqueous solutions were prepared with purified water obtained from a Milli-Q UV Plus system (18.2 mΩ-cm resistivity).

Sonications at frequencies of 205, 358, 618 and 1078 kHz were performed in glass reactor using an Allied ELAC Nautik ultrasound generator. At 20 kHz ultrasound was generated with a Branson 200 sonifier, and at 500 kHz with an Undatim power generator and transducer. Temperature was maintained constant at 10 °C with a Haake A80 Refrigerated Bath and Circulator. The initial solution temperature is about 13 ± 3 °C. Replaceable titanium tips on the 20 kHz transducers were polished and the transducer was tuned before each experiment in order to give a minimum power output when vibrating in air. The tuning process is a standard procedure to bring the transducer into resonance as part of the complete probe assembly (*31*). Ultrasonic irradiations at 205, 358, 618 and 1078 kHz were carried out in a 605 mL reactor cell, while those at 20 kHz were performed in a 95 mL reactor and those 500 kHz were carried out in a 483 mL reactor. The physical dimensions and characteristics of each transducer and the corresponding reactor configurations are summarized in Table I and shown schematically in Fig 1.

Sample aliquots were withdrawn from each respective reactor with a 1 mL Hamilton syringe, filtered through a 0.45 μm nylon filter into a 2.5 mL glass vial containing 0.5 mL of pentane. The glass vials were sealed with a PTFE/silicone septum-lined threaded cap. A 0.5 μL sample of the pentane extract was injected into a HP 5880A gas chromatograph equipped with an electron capture detector (GC-ECD) and operated in the splitless mode using a HP-5 column for the analysis of CCl_4, $CHCl_3$, $H_2C_2Cl_2$, C_2Cl_4 and C_2Cl_6. The GC-ECD was calibrated with chromatographic standards. Duplicate measurements were made for each sample. All sample aliquots were analyzed immediately after collection. The residual aqueous phase in the extraction vials was analyzed by ion-

exchange chromatography (IC) for Cl^- using a Dionex Bio-LC system equipped with a conductivity detector and a Dionex OmniPac AS-11 Column.

The ultrasonic power output was measured using standard calorimetric procedures (*31*). The measured power densities given in Table II were used to normalize the observed reaction rate constants (*vide infra*).

Results and Discussion

- ***Frequency Effects***

Experiments were performed with initial H_xCCl_{4-x} concentrations set at 0.20 ± 0.05 mM. Under these conditions, the extent degradation of CCl_4 was found to be greater than 99% after 90 min of sonolysis. Loss of CCl_4 due to vapor stripping was found to be less than 2% in separately run control experiments in the absences of ultrasonic irradiation. pH values after complete sonolytic degradation of CCl_4 were near 3.5, while the principle products were found to be OCl^-, Cl^-, C_2Cl_4 and C_2Cl_6. The final concentrations of HOCl were in the μM range at all frequencies.

The sonication of CCl_4 followed simple pseudo first-order reaction kinetics, in which the slopes of standard linear regressions of the observed $\ln [CCl_4]_t/[CCl_4]_o$ vs. time data corresponded to the observed first-order rate constants. In order to determine the effects of frequency on the observed reaction rates, the observed first-order rate constants at different frequencies were normalized for differences in acoustic energy densities as follows (*32*):

$$k_{corr,f} = k_{obs,f}\left(\frac{P_{f_S}}{P_f}\right) \qquad (11)$$

where $k_{corr,\ f}$ and $k_{obs,\ f}$ are the corrected and the observed rate constants at a given irradiation frequency, f. P_f is the power density, in watts per unit volume at that frequency and P_{fs} is the power density at the reference-state ultrasonic frequency, f_s (i.e., 205 kHz). Using the measured power densities as given in Table II, the rate constants for CCl_4 degradation were corrected relative to the reference standard. These values are listed in Table III.

As shown in Fig 2, the rate of CCl_4 degradation appears to increase from 205 kHz to 618 kHz and then decreases slightly at 1078 kHz for the same reactor system. Furthermore, the measured reaction rate in the 500 kHz reactor was found to be substantially larger than in the 20 kHz reactor. These trends are comparable with those reported previously by Francony et al. (*9*) (i.e., an increase in observed degradation rate with an increase in ultrasonic frequency). Since the geometry of the reactor and the corresponding transducer may affect the observed reaction rate, the following discussion will focus only on the data obtained for the same reactor and transducer configuration as a function of frequency, where f = 205, 358, 618 or 1078 kHz.

The higher degradation rate observed at 618 kHz may be the result of differences in the relative lifetimes and the surface area-to-volume ratios of the cavitation bubbles at this frequency relative to the other frequencies. At 618 kHz, a stable cavitation bubble will oscillate more frequently per unit time, and thus result in more extensive mass transfer of volatile solute (e.g., CCl_4) between the vapor phase of the bubble and the bulk liquid solution. As a result, the CCl_4 degradation rate should be enhanced due to a greater number of bubble events per unit time and due to a more efficient mass transfer of reactive solute from the liquid phase to the vapor phase. Once gas transfer has taken place, CCl_4 is

subjected to pyrolytic reactions within the vapor phase of the collapsing bubbles or within the hot interfacial region of bubbles. As shown in eq. 12, the resonant radius of an acoustically-cavitating bubble is inversely correlated with the ultrasonic frequency (*11,32*).

$$R_r^2 = \frac{3\kappa P_0}{\rho \omega_r^2} \qquad (12)$$

where ρ is the density of the solution, ω_r is the resonant frequency, R_r is the resonant radius, P_0 is the hydrostatic pressure, and κ ($\kappa = C_p/C_v$) is the polytropic index. The relative differences in the surface area-to-volume ratios as a function of ultrasonic frequency are illustrated in Table IV. As a consequence, the higher frequencies produce smaller cavitation bubbles with higher surface area-to-volume ratios. Therefore, the net diffusion of semivolatile reactants between the bubble and the liquid is enhanced (*32*). At higher frequencies, more CCl_4 vapor diffuses into the vapor phase of the bubble and into the interfacial region, where it is likely to undergo pyrolytic decomposition. In addition, smaller bubbles produced at higher frequencies require fewer acoustic cycles before they reach the requisite resonant size. Given the greater number of acoustic cycles per unit time at higher frequencies, rectified diffusion occurs more rapidly before transient bubble collapse. Thus, a greater number of gas nuclei can reach the resonance size more quickly than at lower frequencies. The net effect is to produce a greater enhancement of sonochemical reactions at frequencies up to 700 kHz (*32*). However, at 1078 kHz, the cavitation bubbles undergo a stable mode of oscillation for longer times without transient collapse. This results in decreased overall reaction rates as reflected in the data shown in Fig 2 and Table IV.

- ***Sonolysis of Chlorinated Methanes at 205 kHz***

The observed rates of sonolytic degradation of CCl_4, $CHCl_3$ and CH_2Cl_2 at 205 kHz at an applied power of 50 W in water are shown in Fig 3. In this series, the rate of CCl_4 degradation was found to be the fastest while CH_2Cl_2 was the slowest. Due to a higher Henry's Law Constant or larger vapor pressure, more CCl_4 should diffuse into the bubbles and undergo pyrolytic decomposition as the bubbles collapse than will $CHCl_3$ and CH_2Cl_2. For our particular case, $K_H = \gamma_w V_w P^o$ with units of Pa m^3 mol^{-1} where γ_w is the activity coefficient of the chlorinated hydrocarbon in water, V_w is the partial molar volume of water, P^o is the vapor pressure of the pure organic liquid. A clear relationship between the observed reaction rate constants and the corresponding Henry's Law Constants is apparent from the data compiled in Table V (*33*). Since the rates of pyrolysis for the chlorinated methanes are rapid, we assume that molecules diffusing into a bubble during a rarefaction cycle will be totally degraded during the corresponding compression cycle. The observed rate constants in this study are given for the following generalized pyrolytic decomposition:

$$CH_xCl_{4-x} \xrightarrow{)))} \cdot CH_xCl_{3-x} + \cdot Cl \qquad (13)$$

while the final observed reaction products for the decomposition of CCl_4, $CHCl_3$ and CH_2Cl_2 were HCl and CO_2. The growth and disappearance of principal intermediates, C_2Cl_4 and C_2Cl_6, obtained during the degradation of CCl_4 and $CHCl_3$ are shown in Fig 4. The primary intermediate observed during $CHCl_3$ sonolysis was C_2Cl_4, while in the case of CCl_4 sonolysis, C_2Cl_6 was found to be the principal intermediate. The difference in the relative behavior of these intermediates, depending on the specific nature of the solute, suggests that somewhat different mechanisms are operative. In the case of $CHCl_3$ sonolysis, the following mechanism is probable (*34*):

$$H_2O \xrightarrow{)))} \cdot H + \cdot OH \quad (14)$$

$$CHCl_3 \xrightarrow{)))} \cdot H + \cdot CCl_3 \quad (15)$$

$$CHCl_3 \xrightarrow{)))} \cdot Cl + \cdot CHCl_2 \quad (16)$$

$$\cdot H + CHCl_3 \rightarrow H_2 + \cdot CCl_3 \quad (17)$$

$$\cdot H + CHCl_3 \rightarrow HCl + \cdot CHCl_2 \quad (18)$$

$$\cdot Cl + CHCl_3 \rightarrow HCl + \cdot CCl_3 \quad (19)$$

$$\cdot OH + CHCl_3 \rightarrow H_2O + \cdot CCl_3 \quad (20)$$

In an alternative pathway, the pyrolytic decomposition of $CHCl_3$ may proceed via a molecular elimination reaction to form dichlorocarbene (*35*):

$$CHCl_3 \xrightarrow{)))} :CCl_2 + HCl \quad (21)$$

Dichlorocarbenes may then self-react to give C_2Cl_4 as observed by Hua and Hoffmann (3).

$$:CCl_2 + :CCl_2 \longrightarrow C_2Cl_4 \quad (22)$$

Since very small concentrations of C_2Cl_6 (i.e., < 2 nM) were found during the sonication of $CHCl_3$ compared to that formed during CCl_4 sonication, $CHCl_3$ sonication appears to proceed preferentially via eqs. 21 and 22. On the other hand, the sonolytic degradation of CCl_4 has been shown to form the trichloromethyl radical via the direct pyrolysis of a C-Cl bond (*3*). After formation, the trichloromethyl radical self-reacts to give C_2Cl_6 or decomposes to form dichlorocarbene according to the reactions of eqs. 23 - 25:

$$CCl_4 \xrightarrow{)))\ k_1} \cdot CCl_3 + \cdot Cl \quad (23)$$

$$2\ \cdot CCl_3 \xrightarrow{k_2} C_2Cl_6 \xrightarrow{))) k_3} \text{products} \qquad (24)$$

$$\cdot CCl_3 \xrightarrow{))) k_4'} :CCl_2 + \cdot Cl \qquad (25)$$

$$2:CCl_2 \xrightarrow{k_5} C_2Cl_4 \xrightarrow{))) k_6} \text{products} \qquad (26)$$

If most of $\cdot CCl_3$ were decomposed to $:CCl_2$ during CCl_4 sonolysis, then the concentration of C_2Cl_4 should have been higher than C_2Cl_6 as was observed for $CHCl_3$. However, C_2Cl_6 is the principal intermediate observed during CCl_4 sonolysis. In this latter case, the concentration of C_2Cl_6 is approximately 5 times greater than that of C_2Cl_4. This result indicates that the rate of the trichloromethyl radical self-reaction is clearly faster than the rate of $\cdot CCl_3$ decomposition. Consistent with this argument is the fact that the rate constant for the self-reaction of the trichloromethyl radicals is to be 10^{10} M^{-1} sec^{-1} (36).

In a recent study, Kruus et al. (6) reported on their observations of the reaction intermediates produced during the sonication of aqueous chloroform solutions at 900 kHz at an acoustic power of 25 W and an applied power density of 0.17 W cm^{-3}. With an initial concentration of $[CHCl_3]_o$ = 4.2 mM, Kruus et al. observed the formation of carbon tetrachloride (18 μM), tetrachloroethene (43 μM) hexachloroethane (32 μM), pentachloroethane (17 μM), trichloroethene (10 μM), 1,1,2,2-tetrachloroethane (3 μM), and hexachlorobutadiene (4 μM) after 10 min of sonication. In contrast, in our system hexachloroethane and tetrachloroethene were observed as the most substantial reaction intermediates even though chromatographic evidence for the occurrence of CCl_4 and the other intermediates observed by Kruus et al. was obtained. However, the concentrations of these intermediates were barely above the detection limits of the GC-ECD (e.g., ≤ 1 nM). In addition, we observed the attainment of maximum steady-state concentrations of C_2Cl_6

(1.5 nM) and C_2Cl_4 (130 nM) after 25 minutes of continuous irradiation of a 0.2 mM chloroform solution at 205 kHz with an applied power of 50 W and an absorbed power density = 0.06 W cm^{-3}. For comparison, Kruus et al. (6) reported that the attainment of the maximum concentrations (vide supra) of all intermediates occurred within the timeframe of the first sample aliquot (i.e., collected after 10 min. of irradiation).

Kinetic Analysis

A simple kinetic model can be used to describe the rate of production and subsequent degradation of C_2Cl_6 for the sonolyses of CCl_4. Since the degradation of CCl_4 was observed to be a pseudo first-order reaction, the reverse reaction of $\cdot CCl_3$ and $\cdot Cl$ radicals can be ignored. Furthermore, we assume that all of the $\cdot CCl_3$ radicals yield C_2Cl_6. The mechanism of eqs. 23-24 yield the corresponding kinetic expressions:

$$\frac{d[CCl_4]}{dt} = -k_1[CCl_4] \tag{27}$$

$$\frac{d[\cdot CCl_3]}{dt} = k_1[CCl_4] - 2k_2[\cdot CCl_3]^2 \tag{28}$$

$$\frac{d[C_2Cl_6]}{dt} = k_2[\cdot CCl_3]^2 - k_3[C_2Cl_6] \tag{29}$$

Integration of eq. 27 yields

$$[CCl_4] = [CCl_4]_0 e^{-k_1 t} \tag{30}$$

Assuming a steady state for $\cdot CCl_3$ (37),

$$\frac{d[\cdot CCl_3]}{dt} = k_1[CCl_4] - 2k_2[\cdot CCl_3]^2 = 0 \tag{31}$$

we obtain

$$[\cdot CCl_3]_{ss} = \sqrt{\frac{k_1}{2k_2}}[CCl_4]^{\frac{1}{2}} \quad (32)$$

Substitution of $[\cdot CCl_3]_{ss}$ into eq. 29 following by integration under the boundary condition of $[C_2Cl_6]_{t=0} = [C_2Cl_6]_{t=\infty} = 0$ yields

$$[C_2Cl_6] = \frac{k_1}{2(k_1 - k_3)}[CCl_4]_o(e^{-k_3t} - e^{-k_1t}) \quad (33)$$

The concentration versus time data for the appearance and disappearance of C_2Cl_6 compared to the numerical prediction based on eq. 33 is shown in Fig 5. The corresponding observed and normalized rate constants (k_1 and k_3) for C_2Cl_6 as a function of frequency are given in Table VI. As expected, the rate constants, k_1, for all frequencies are very close to those given in Table III (which characterizes the total degradation rate of CCl_4). These kinetic results are consistent with a mechanism involving CCl_4 pyrolysis into $\cdot CCl_3$ and $\cdot Cl$ as the rate-limiting step in CCl_4 sonolysis. The degradation rate constant for C_2Cl_6, k_3, is also larger at the higher frequencies and decreases again at 1078 kHz. The calculated degradation rates for C_2Cl_6 in CCl_4 solutions are faster than in the absence of CCl_4. This may be due to the attack on C_2Cl_6 by the chlorine radicals produced during CCl_4 sonolysis other than $\cdot OH$ only (*3*) or the assumption of all $\cdot CCl_3$ self-reactions to give C_2Cl_6.

Since the final stable Cl-containing product of CCl_4 sonolysis is Cl^-, we can simplify the overall reaction mechanism in the following way:

$$CCl_4 \xrightarrow{)))\ k_1} \cdot CCl_3 + \cdot Cl \quad (34)$$

$$2 \cdot CCl_3 \xrightarrow{k_2} C_2Cl_6 \quad (35)$$

$$C_2Cl_6 \xrightarrow{))) k_3} aCl^- + \text{other products.} \quad (36)$$

$$\cdot Cl + H_2O \xrightarrow{k_4} HCl + \cdot OH \quad (37)$$

The mechanisms yields the following kinetic equations:

$$\frac{d[\cdot Cl]}{dt} = k_1[CCl_4] - k_4[\cdot Cl] \quad (38)$$

$$\frac{d[Cl^-]}{dt} = k_4[\cdot Cl] + ak_3[C_2Cl_6] \quad (39)$$

Assuming a steady state for ·Cl,

$$\frac{d[\cdot Cl]}{dt} = k_1[CCl_4] - k_4[\cdot Cl] = 0 \quad (40)$$

we obtain

$$[\cdot Cl]_{ss} = \frac{k_1}{k_4}[CCl_4] \quad (41)$$

Substitution of $[Cl]_{ss}$ along with eqs. 30 and 33 into eq. 39, followed by integration under the boundary condition of $[Cl^-]_{t=0} = 0$, yields

$$[Cl^-] = [CCl_4]_0\left[1 - e^{-k_1 t} + \frac{ak_1}{2(k_1 - k_3)}(1 - e^{-k_3 t}) - \frac{ak_3}{2(k_1 - k_3)}(1 - e^{-k_1 t})\right] \quad (42)$$

From the data presented in Table VI, we know that k_1 and k_3 are nearly identical. If we assume $k_3 = k_1 + \delta$ and take the limit of $\delta \rightarrow 0$, we can simplify eq. 42 to yield

$$[Cl^-] = [CCl_4]_0\left[(1 + \frac{a}{2})(1 - e^{-k_1 t}) - \frac{ak_1 t}{2} e^{-k_1 t}\right] \quad (43)$$

If we further assume that the effect of the second term is small, we can use the following equation as our fitting function for the $[Cl^-]$ vs. time data.

$$[Cl^-] = [Cl^-]_\infty(1 - e^{-k_{Cl^-} t}) \quad (44)$$

Based on the curve fitting of our data with eq. 44, we obtained the rate constants, k_{Cl^-}, for Cl^- formation as shown in Table VII for all frequencies. As expected, k_{Cl^-} is very similar to the rate constant, k_1 (Table VII). The experimental and predicted $[Cl^-]$ vs. time profiles are shown in Fig 6, while a direct comparison of the specific values for k_{Cl^-} and k_{CCl_4} is given in Table VII.

The total measured Cl^- accounts for only 75% of the total chlorine initially present in the CCl_4. Weissler et al. (*2*) reported that Cl_2 was produced during the sonolyis of CCl_4 solutions. The total oxidizing chlorine capacity of the released chlorine corresponded closely to four Cl atoms per carbon tetrachloride molecule. However, sonication reactions at higher initial concentrations of carbon tetrachloride, $[CCl_4]_0$, are clearly more complicated. For example, at higher initial concentrations of CCl_4, the initial pyrolysis product, $\cdot CCl_3$, will self-react to give C_2Cl_6, instead of decomposing further via an additional C-Cl bond breaking to produce $:CCl_2$.

In this study, we have demonstrated that the rate of CCl_4 sonolysis increases with increasing frequencies up to 618 kHz and that the principal intermediate product, C_2Cl_6, shows a similar frequency dependence. These results are consistent with general predictions based on underlying physics of acoustic bubble dynamics. At higher frequencies, stable cavitation bubbles oscillate more frequently per second, which leads to enhanced CCl_4 degradation rates. If the cavitation bubbles were to oscillate only in the stable mode without undergoing transient collapse, the net observed reaction rate should be lower as observed at 1078 kHz.

The sonolytic degradation rate constants for the chlorinated methanes were found to increase with a corresponding increase in their respective Henry's Law Constants (i.e.,

$K_{H,CCl_4} > K_{H,CHCl_3} > K_{H,CH_2Cl_2}$) in the order $k_{CCl_4} > k_{CHCl_3} > k_{CH_2Cl_2}$. This relative order is consistent with the argument that the driving force for diffusion into the bubbles is increased as the value of K_H is increased.

Acknowledgments

The authors wish to thank Linda Weavers, Ralf H. Höchemer, Chao-Ping Hsu and Christian Schiller for their helpful discussions. Financial support from the Office of Naval Research, ONR, and the Department of Energy is gratefully acknowledged.

References

1. Mason, T. J.; Lorimer, J. P. *Sonochemistry: Theory, Application and Uses of Ultrasound in Chemistry*; John Wiley &Sons: New York, 1988.
2. Weissler, A.; Cooper, H. W.; Snyder, S. *J. Am. Chem. Soc.* **1950**, *72*, 1769-1775.
3. Hua, I.; Hoffmann, M. R. *Environ. Sci. Technol.* **1996**, *30*, 864-71.
4. Petrier, C.; Micolle, M.; Merlin, G.; Luche, J. L.; Reverdy, G. *Environ. Sci. Technol.* **1992**, *26*, 1639-42.
5. Cheung, H. M.; Bhatnagar, A.; Jansen, G. *Environ. Sci. Technol.* **1991**, *25*, 1510-12.
6. Kruus, P.; Beutel, L.; Aranda, R.; Penchuk, J.; Otson, R. *Chemosphere* **1998**, *36*, 1811-1824..
7. Bhatnagar, A.; Cheung, H. M. *Environ. Sci. Technol.* **1994**, *28*, 1481-6.
8. Wu, J. M.; Huang, H. S.; Livengood, C. D. *Environ. Prog.* **1992**, *11*, 195-201.
9. Francony, A.; Petrier, C. *Ultrasonic Sonochemistry* **1996**, *3*, S77-S82.
10. Mason, T. J. *Chemistry with Ultrasound*; Elsevisier Applied Science: London, 1990.
11. Leighton, T. G. *The Acoustic Bubble*; Harcourt Brace & Company, 1994.
12. Shutilov, V. A. *Fundamental Physics of Ultrasound*; Gordon & Breach Science: New York, 1988.
13. Moss, W. C.; Clarke, D. B.; White, J. W.; Young, D. A. *Phys. Fluids* **1994**, *6*, 2979-2985.
14. Hiller, R.; Putterman, S. J.; Barber, B. P. *Phys. Rev. Lett.* **1992**, *69*, 1182-1184.
15. Putterman, S. J. *Scientific Am.* **1995**, *272*, 46-51.

16. Kotronarou, A.; Mills, G.; Hoffmann, M. R. *J. Phys. Chem.* **1991**, *95*, 3630-8.

17. Kotronarou, A.; Mills, G.; Hoffmann, M. R. *Environ. Sci. Technol.* **1992**, *26*, 1460-2.

18. Hua, I.; Hochemer, R. H.; Hoffmann, M. R. *Environ. Sci. Technol.* **1995**, *29*, 2790-6.

19. Entezari, M. H.; Kruus, P. *Ultrasonic Sonochemistry* **1994**, *1*, S75-S79.

20. Hua, I.; Hochemer, R.; Hoffmann, M. R. *J. Phys. Chem.* **1995**, *99*, 2335-2342.

21. Petrosius, S. C.; Drago, R. S.; Young, V.; Grunewald, G. C. *J. Am. Chem. Soc.* **1993**, *115*, 6131-6137.

22. Taylor, P. H.; Dellinger, B.; Tirey, D. A. *Int. J. Chem. Kinet.* **1991**, *23*, 1051-1074.

23. Matheson, L. J.; Tratnyek, P. G. *Environ. Sci. Technol.* **1994**, *28*, 2045-2053.

24. Johnson, T. L.; Scherer, M. M.; Tratnyek, P. G. *Environ. Sci. Technol.* **1996**, *30*, 2634-2640.

25. Choi, W. Y.; Hoffmann, M. R. *J. Phys. Chem.* **1996**, *100*, 2161-2169.

26. Bromberg, L.; Cohn, D. R.; Koch, M.; Patrick, R. M.; Thomas, P. *Phys. Lett. A* **1993**, *173*, 293-299.

27. Narayanan, B.; Suidan, M. T.; Gelderloos, A. B.; Brenner, R. C. *Water Res.* **1993**, *27*, 181-194.

28. Loraine, G. A. *Hazard. Waste Hazard. Mater.* **1993**, *10*, 185-194.

29. Elliott, D. C.; Phelps, M. R.; Sealock, L. J.; Baker, E. G. *Ind. Eng. Chem. Res.* **1994**, *33*, 566-574.

30. Elliott, D. C.; Sealock, L. J.; Baker, E. G. *Ind. Eng. Chem. Res.* **1994**, *33*, 558-565.

31. Mason, T. J. *Practical Sonochemistry: User's Guide to Application in Chemistry and Chemical Engineering*; Ellis Horwood, 1991.

32. Hua, I.; Hoffmann, M. R. *Environ. Sci. Technol.* **1997**, *31*, 2237-2243.

33. Mackay, D.; Shiu, W. Y.; Ma, K. C. *Illustrated Handbook of Physical-Chemical Properties and Environmental Fate for Organic Chemicals*; Lewis:, 1993; Vol. III.

34. Jennings, B. H.; Townsend, S. N. *J. Phys. Chem.* **1961**, *65*, 1574-1579.

35. Henglein, A.; Fischer, C. H. *Ber. Bunsen Ges.* **1984**, *88*, 1196-1199.

36. Matheson, I. A.; Sidebottom, H. W.; Tedder, J. M. *Int. J. Chem. Kinet.* **1974**, *VI*, 493-506.

37. Eyring, H.; Lin, S. H.; Lin, S. M. *Basic Chemical Kinetics*; John Wiley & Sons: New York, 1980.

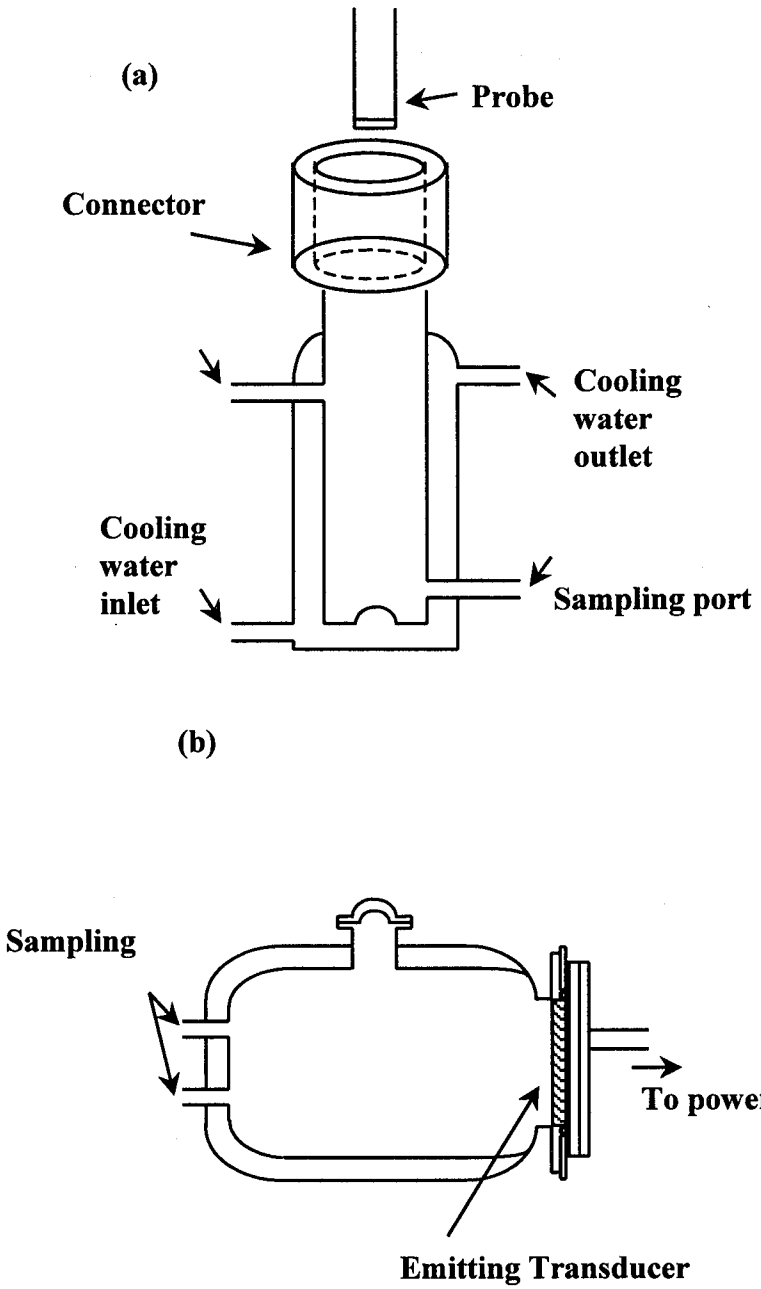
(a)
Probe
Connector
Cooling
water
outlet
Cooling
water
inlet
Sampling port
(b)
Sampling
To power generator
Emitting Transducer

Figure 1.

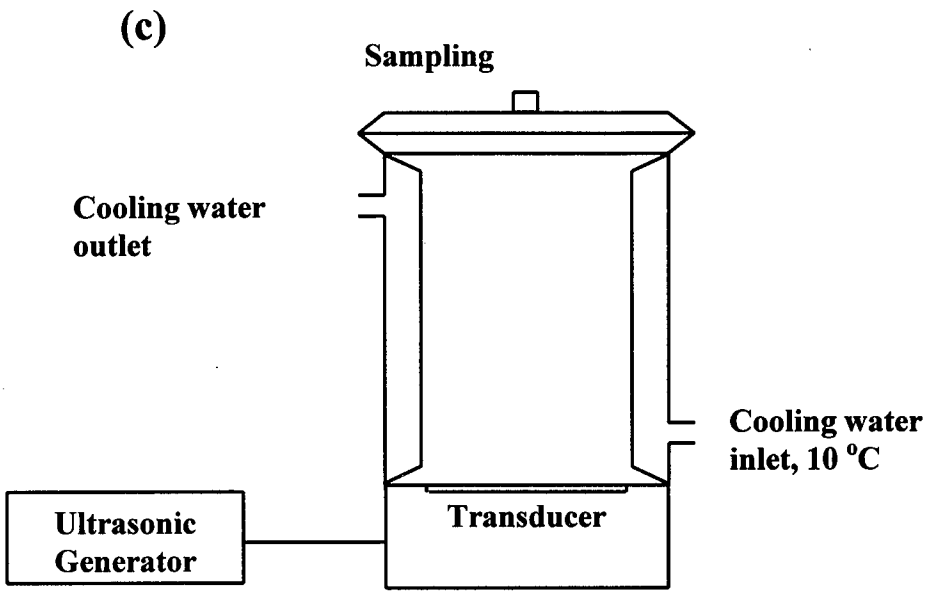

Figure 1. Schematic representation of the reactor cells used in this study. (a) for 20 kHz, (b) for 500 kHz and (c) for 205, 358, 618 and 1078 kHz.

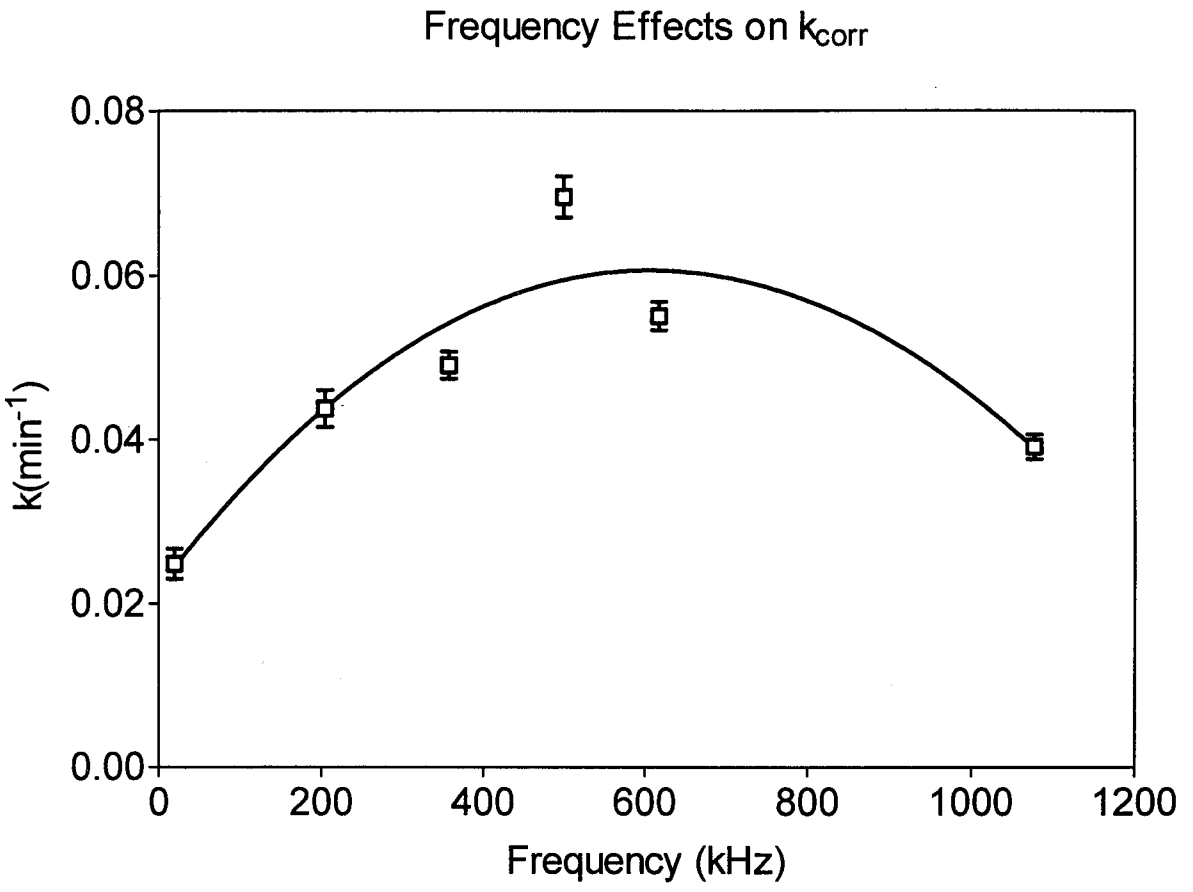

Figure 2. Variation of the CCl_4 degradation rate constant with ultrasonic frequency. Data points are the mean values obtained from multiple experiments.

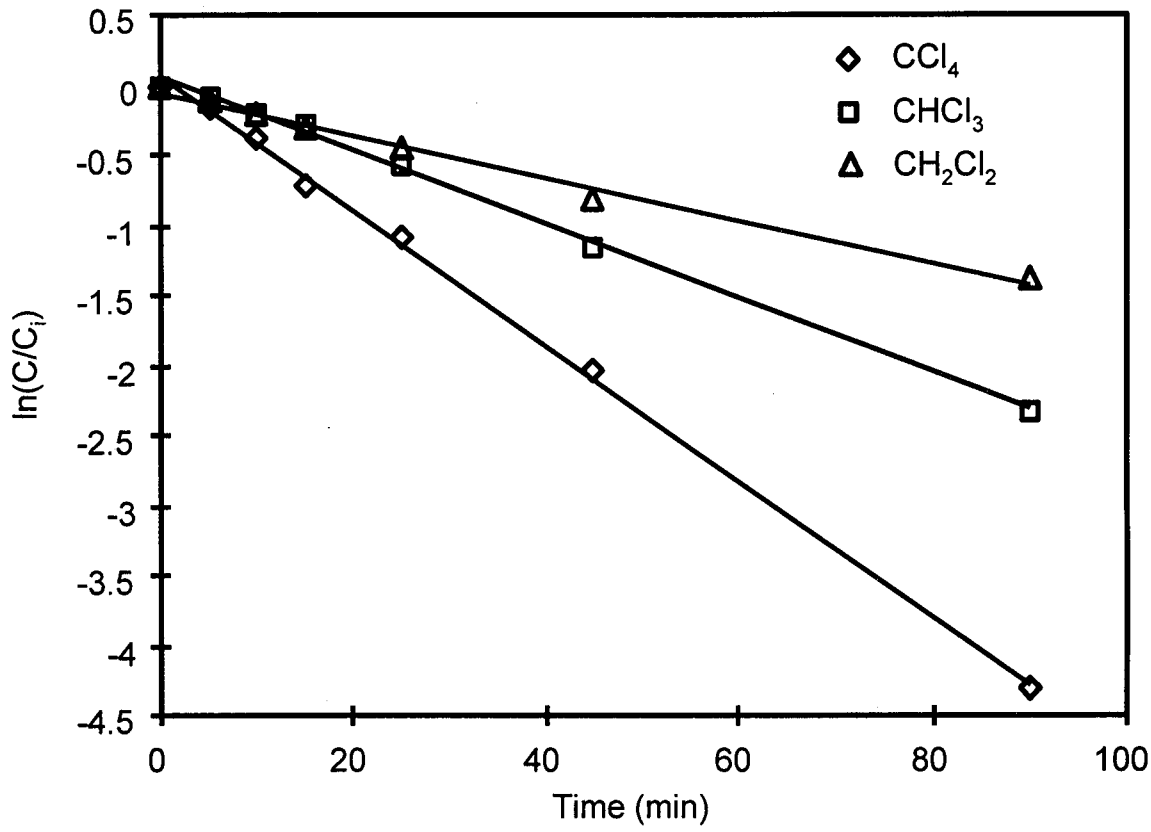

Figure 3. Observed first-order kinetic plots for the degradation of CCl_4, $CHCl_3$ and CH_2Cl_2 at 205 kHz.

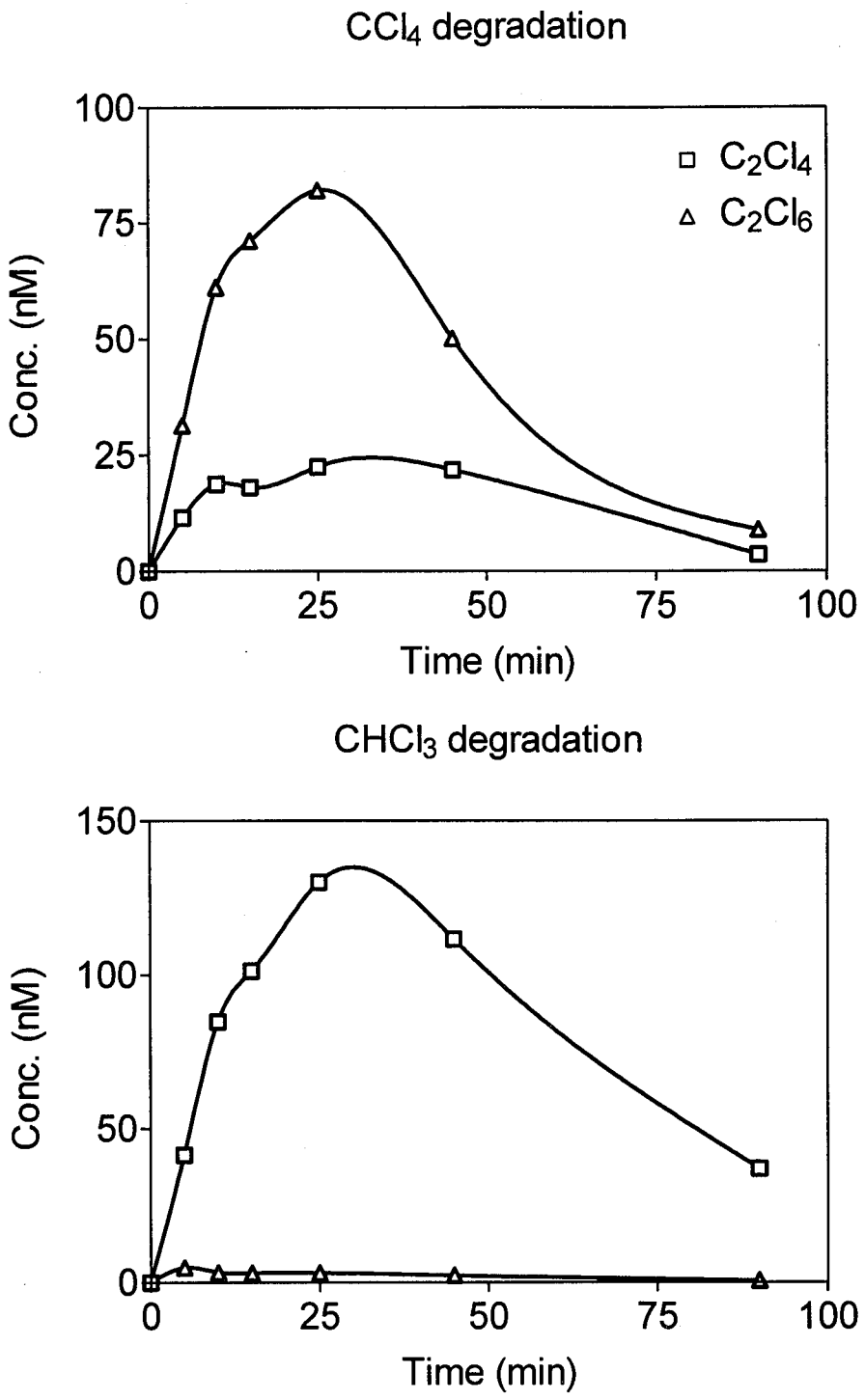

Figure 4. Variations in observed C_2Cl_4 and C_2Cl_6 concentrations vs. time during CCl_4 and $CHCl_3$ sonolyses at 205 kHz with an applied power of 50 W and an absorbed power of 35 W.

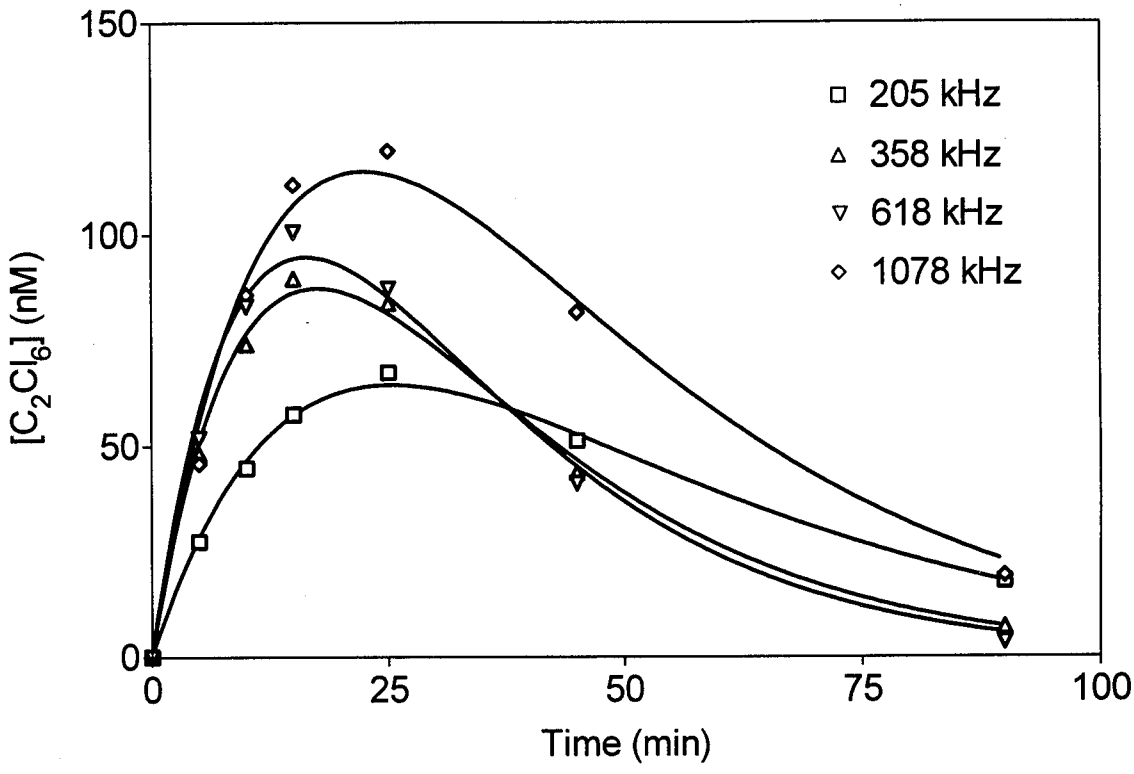

Figure 5. The comparison of experimental and modeled $[C_2Cl_6]$ vs. time during CCl_4 sonolysis. Lines are the fitting results from eq. 33.

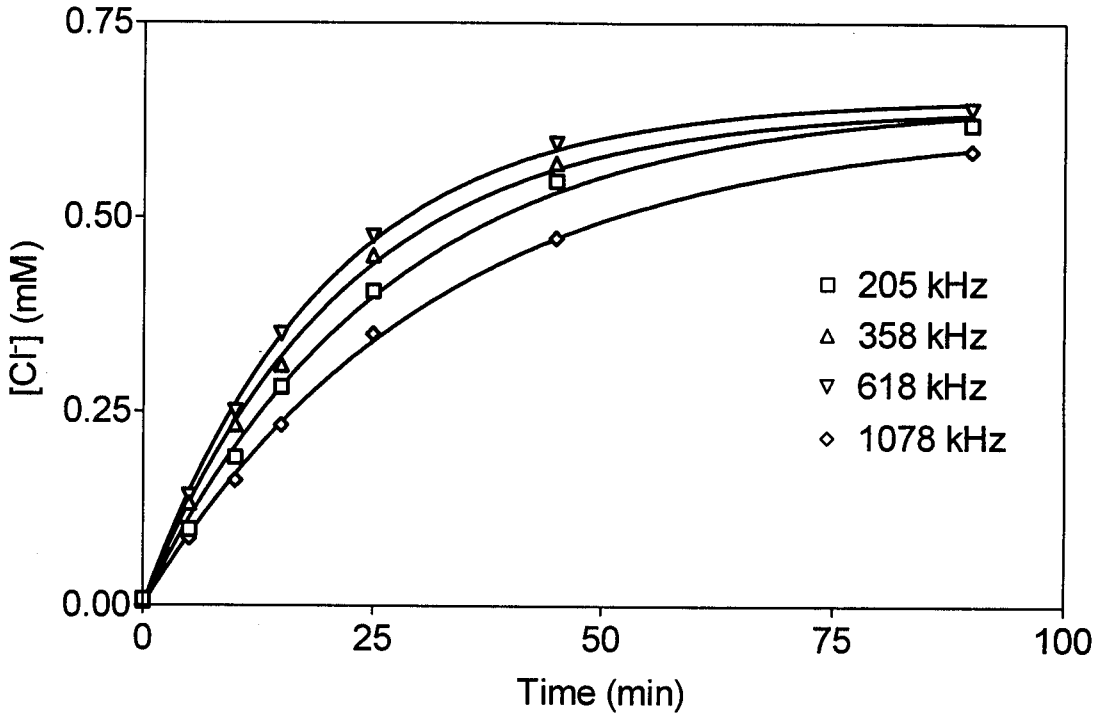

Figure 6. The comparison of experimental and modeled [Cl^-] vs. time during CCl_4 sonolysis. Lines are the fitting results from eq. 44.

Chapter 5

Kinetics and Mechanism of the Enhanced Reductive Degradation of CCl_4 by Elemental Iron in the Presence of Ultrasound

(*Environmental Science & Technology*, **1998**, 32: (19) 3011-3016)

Abstract

Enhanced rates of sonolytic degradation of CCl_4 in the presence of Fe^0 are demonstrated. In Ar-saturated solutions, the first-order rate constant for CCl_4 degradation is $k_{US} = 0.107\ min^{-1}$, while in the presence of Ar and Fe^0, the apparent first-order rate constant is found to depend on the total surface area of elemental iron in the following fashion: $k_{obs} = (k_{US} + k_{Fe^0} \cdot A_{Fe^0})\ min^{-1}$, where $k_{US} = 0.107\ min^{-1}$, $k_{Fe^0} = 0.105\ L\ m^{-2}\ min^{-1}$ and A_{Fe^0} = reactive surface area of Fe^0 in the units of $m^2\ L^{-1}$. In the coupled ultrasound and iron system, the contribution to the overall degradation rate by direct reaction with Fe^0 results in an overall rate enhancement by a factor of 40. These enhancements are attributed 1) to the continuous cleaning and chemical activation of the Fe^0 surface by the combined chemical and physical effects of acoustic cavitation, and 2) to accelerated mass transport rates of reactants to the Fe^0 surfaces. Additional kinetic enhancements are due to the production of H^+ during the course of the reaction. Furthermore, the concentrations of the principal reaction intermediates, C_2Cl_6 and C_2Cl_4, are influenced substantially by the total available surface area of Fe^0.

Introduction

Ultrasound is widely used for medical imaging, emulsification, plastic welding and a wide variety of synthetic applications (*1*). In addition, ultrasonic irradiation has been applied as an advanced oxidation technology for water treatment (*2,3*). Upon ultrasonic irradiation, organic compounds in water are degraded via several mechanisms. Three main pathways, which involve hydroxyl radical oxidation, pyrolytic degradation, and supercritical water reactions, have been proposed (*3*). In the case of an aqueous solution, water vapor present in the bubble is homolytically split to yield H• and •OH radicals. Chemical substrates present within the vapor phase or in the nearby liquid of the collapsing bubbles are subject to direct attack by •OH radical (*4,5*). Volatile compounds such as H_2S and CCl_4 partition into the gas phase (i.e., into the gaseous bubbles within the aqueous solution) and undergo direct pyrolysis (*1,5,6*). Furthermore, it has been found that hydrolysis reactions are accelerated by several orders of magnitude in the presence of ultrasound. These accelerated reaction rates have been attributed to the existence of transient supercritical water during ultrasonic irradiation (*7*).

The chemical effects of ultrasound are due to the phenomenon of acoustic cavitation (*1*). Sound travels through a liquid as a wave consisting of alternating compression and rarefaction cycles. If the sound wave has a sufficiently high pressure amplitude, it can overcome the intermolecular forces bonding the fluid. As a result, the liquid will break down and voids will be created, i.e., cavitation bubbles will be formed. In most liquids, cavitation is initiated with pre-existing microbubbles or weak spots which are

any type of inhomogeneity in the fluid. The inhomogeneity can be anything from particles to gas nuclei. These microbubbles grow sequentially during the compression and rarefaction cycles due to the phenomenon of rectified diffusion until they reach a critical size; then in subsequent compression cycles, these cavities can collapse violently releasing a large amount of energy. This rapid implosion is accompanied by an adiabatic heating of the vapor phase of the bubbles, which yields localized but transient high temperatures and pressures. Temperatures on the order of 5000 K have been obtained experimentally (*8*), and pressures of the order of 1000 bar have been calculated (*9*).

Elemental iron (Fe^0) is a mild reductant with an $E_H^0 = -0.44V$. It has been proposed as a suitable source of electrons for the in situ remediation of contaminated groundwater because of its low cost and nontoxicity (*10*). Fe^0 barrier systems have the potential to replace the pump-and-treat systems for the remediation of contaminated groundwater to reduce the chlorinated compounds to non-chlorinated products (*11,12*). The kinetics of carbon tetrachloride dechlorination at the presence of elemental Fe^0 have been reported by Tratnyek and co-workers (*10,13-15*). In addition to degrading chlorinated solvents, zero-valent metals may prove to be useful for the reduction of nitro aromatic compounds to anilines, which can be further degraded microbiologically (*16-19*).

Because acoustic cavitation can increase the surface area of the reactive solids by causing particles to rupture, sonication in the presence of Fe^0 has been explored for the dechlorination of trichloroethylene (TCE) (*20*). In this study, we investigate the combination of ultrasound and Fe^0 for CC_4 degradation. Carbon tetrachloride is degraded

by pyrolysis reaction inside the bubble, by reduction on the surface of Fe^0 and synergistically on Fe^0 surface sites created by ultrasonic effects. The combination of ultrasound and Fe^0 is a heterogeneous reaction system involving solid/liquid, gas/solid, and gas/liquid interfaces.

There are two modes of cavitational bubble collapse that can affect the surface of solids (*21*). First, cavitational bubble collapse directly on a surface may cause direct damage by shock waves produced upon implosion. These bubbles are formed on nuclei such as surface defects, entrapped gases or impurities on the surface of the material. Second, cavitational collapse near the solid surface in the liquid phase will cause microjets to hit the surface and produce a non-symmetrical shock wave. This phenomenon results in the well known cleaning action of ultrasound. As a consequence of these events, more reactant surface area is readily formed for further surface reactions.

In this paper, kinetics and mechanism of CCl_4 sonolysis in aqueous solution in the presence of two different Fe^0 samples are presented. In addition, the effect of Fe^0 on the fate and behavior of the primary reaction intermediates, tetrachloroethene (C_2Cl_4) and hexachloroethane (C_2Cl_6), is examined.

Technical Background

Mechanism of CCl_4 Sonolysis

The sonolytic degradation of CCl_4 has been studied by several research groups (*1,3,22-24*). The overall reaction mechanism (*3*) can be written as (where '))))' is

sonolysis):

$$CCl_4 \xrightarrow{)))} Cl\bullet + \bullet CCl_3 \quad (1)$$

$$CCl_4 \xrightarrow{)))} Cl_2 + :CCl_2 \quad (2)$$

$$\bullet CCl_3 \rightarrow \bullet Cl + :CCl_2 \quad (3)$$

$$\bullet CCl_3 + \bullet CCl_3 \rightarrow CCl_4 + :CCl_2 \quad (4)$$

$$\bullet CCl_3 + \bullet CCl_3 \rightarrow C_2Cl_6 \quad (5)$$

The trichloromethyl radical, produced via the pyrolysis of CCl_4 in eq.1, is an effective scavenger of the hydroxyl radical as follows:

$$\bullet CCl_3 + \bullet OH \rightarrow HOCCl_3 \quad (6)$$

$HOCCl_3$ reacts rapidly to yield phosgene, HCl and CO_2 as follows:

$$HOCCl_3 \rightarrow HCl + COCl_2 \quad (7)$$

$$COCl_2 + H_2O \rightarrow CO_2 + 2HCl \quad (8)$$

Dichlorocarbene, which is produced via eq. 2, can couple with itself to form tetrachloroethylene

$$:CCl_2 + :CCl_2 \rightarrow C_2Cl_4 \quad (9)$$

or it can react with water to form carbon monoxide and hydrochloric acid as follows:

$$:CCl_2 + H_2O \rightarrow 2HCl + CO \quad (10)$$

Chlorine atoms self-react to form molecular chlorine, which hydrolyzes to yield hypochlorous acid and chloride ion:

$$2Cl\bullet \rightarrow Cl_2 \xrightarrow{+H_2O} HOCl + HCl \qquad (11)$$

Mechanism of CCl_4 Reduction by Fe^0

The following mechanism (eqs. 12-16) for the reductive dehalogenation of CCl_4 by elemental iron has been proposed by Matheson and Tratnyek (*10*).

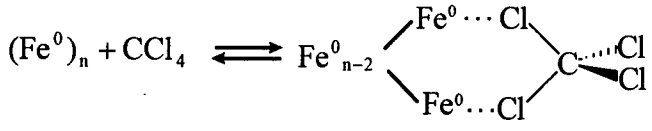

(12)

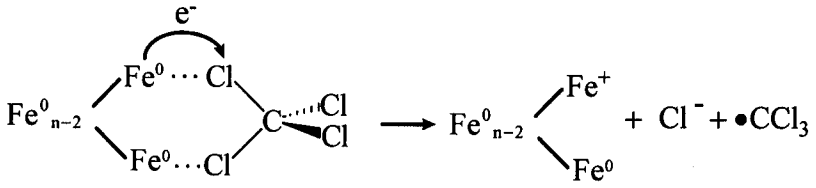

(13)

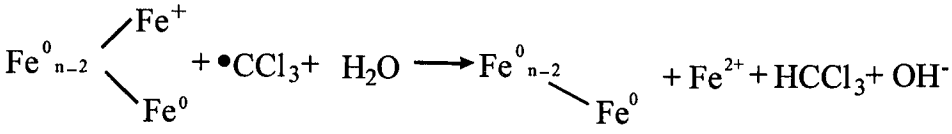

(14)

CCl_4 can also be degraded by H_2 produced from the reaction of H^+ with Fe^0.

$$Fe^0 + 2H^+ \longrightarrow Fe^{2+} + H_2 \qquad (15)$$

$$CCl_4 + H_2 \longrightarrow HCCl_3 + Cl^- + H^+ \qquad (16)$$

The primary product observed after several hours of reaction is chloroform. Neither C_2Cl_4

nor C_2Cl_6 are observed as intermediates. Matheson and Tratynek reported a pH increase during the course of the reaction that is consistent with the stoichiometry of eq.14. In addition, they observed that the rate of dehalogenation by Fe^0 was faster at low pH (*10*).

Experimental Procedures

Commercially available organic high-purity reagents were used without further purification. They included carbon tetrachloride, CCl_4, 99.9% (J. T. Baker); chloroform, LC grade; hexachloroethane, C_2Cl_6, 98% (Aldrich); and tetrachloroethene, C_2Cl_4, 99.9% (Sigma-Aldrich). Pentane (Omnisolv grade, EM Science) was used as the carrier solvent for the GC. Aqueous solutions were made with water obtained from a MilliQ UV Plus water purification system (18.2 mΩ-cm resistivity).

Two different sources of elemental iron were used in this study. Iron powder was obtained from J. T. Baker and electrolytic iron turnings were obtained from Fluka. The Fe^0 turnings were of a coarser grain size (mostly > 40 mesh) and were cleaner and smoother with a high metallic luster than the Fe^0 powder. The nominal purity of the Fe^0 turnings was 99.9% with the remainder consisting primarily of iron oxides. Trace impurities were less than 0.02% by weight of C, 0.008% by weight of S, 0.003% by weight of Si, 0.02% by weight of P, 0.02% by weight of Mn and 5 ppm of Mg (*19*). The desired concentrations of CCl_4 in Ar-saturated water were prepared by dilution of a saturated CCl_4 stock solution (5.1 mM) which was made by stirring excess CCl_4 with Ar-saturated water.

Sonolyses were performed with a Branson 200 sonifier operating at 20 kHz. The

temperature was maintained constant at 15 °C with a Haake A80 Refrigerated Bath and Circulator in order to compare the results with this study with those of Matheson and Tratnyek (*10*). Replaceable titanium tips on the 20 kHz transducer were polished and the transducer was tuned before each use to give a minimum power output when vibrating in air. The tuning process is a standard procedure to bring the transducer into resonance as part of the complete probe assembly. Sonolytic reactions at 20 kHz were performed in a 300 mL air-tight reactor cell. The physical dimensions and fundamental characteristics of the transducer are given in Table 1 while the reactor configuration has the similar design as shown in Hua and Hoffmann's paper (*3*).

In the kinetic experiments, 285 mL of 0.1 mM CCl_4 solution were transferred into a water-jacketed glass cell, which was closed from the atmosphere. The bottom of the glass reactor was designed with a 1 cm indentation in the center for reflection of the sound waves and for an even distribution of the cavitation bubbles in the solution. The reactor was made gas-tight with two O-ring seals in the threaded Teflon collar that connects the glass cell to the stainless steel probe. In addition, sampling ports were sealed with Teflon valves and covered with rubber septa. Sample aliquots were withdrawn with a 1 mL Hamilton syringe, filtered through a 0.45 μm nylon filter into a 2.5 mL glass vial with a PTFE/silicone septum-lined threaded cap, and mixed with 0.5 mL of pentane. For quantification of the concentrations of CCl_4, C_2Cl_4 and C_2Cl_6, 0.5 μL samples of the pentane extract were analyzed with an HP 5880A gas chromatograph-electron capture detector (GC-ECD) operated in the splitless mode and equipped with an HP-5 column.

The instrument was calibrated with commercial standards. Duplicate measurements were made for each sample. Time-sequenced samples were analyzed immediately by GC-ECD. The aqueous phase in the sample vial was analyzed by ion-exchange chromatography (IC) for Cl^-. The IC system was a Dionex Bio-LC system equipped with a conductivity detector and a Dionex OmniPac AS-II Column. The ultrasonic power output was measured by conventional calorimetry (*21*). The measured output power employed in this study was 62 W.

Results and Discussion

Experiments were performed at an initial CCl_4 concentration of 1×10^{-4} M and an initial pH of 7. Degradation of CCl_4 was found to be greater than 99% of its initial concentration after 90 min of exposure to ultrasound. Loss of CCl_4 was found to be less than 2% in the control experiments without ultrasound and iron. The pH at the completion of the reaction under ultrasound was 3.5; and with the combination of ultrasound and Fe^0, the final pH was 6 (presumably due to the formation of OH^- from Fe^0 reduction according to eq. 14).

First-order plots of $[CCl_4]$ vs. time during sonolysis and Fe^0 reduction of an Ar-saturated solution at 20 kHz are shown in Figure 1. The slopes from linear regression of the data yield the observed rate constants for CCl_4 degradation. The reaction rate for CCl_4 degradation by ultrasound in the presence of iron was also found to be first-order. In Figure 2, the results for enhanced rate constants (Δk = k (ultrasound + Fe^0) - k (ultrasound)) for different sizes of the Fe^0 particles (i.e., surface area) are shown. The iron

powder had a higher reactive surface area than iron turnings; as a consequence, Δk was enhanced by a factor of eight for Fe^0 powder at the same Fe^0 mass concentration. Figure 2 also shows that the rate constants for CCl_4 reduction increased linearly with increasing mass of Fe^0 per unit reaction volume (g L^{-1}) until it reached a saturation value for mass concentrations larger than 30 g L^{-1} (for iron turnings).

Assuming a constant specific surface area of 0.005 m^2/g for Fe^0 turnings (*19*), the following relationship for the reaction rates with the Fe^0 surface area was obtained by linear regression,

$$\Delta k\ (min^{-1}) = k_{Fe^0} \cdot A_{Fe^0} + 0.001$$

$$= 0.105\ (L\ m^{-2}\ min^{-1}) \cdot A_{Fe^0}\ (m^2\ L^{-1}) + 0.001\ min^{-1} \qquad (17)$$

where the differential rate constant (Δk) is in units of min^{-1} and the surface area concentration, A_{Fe^0}, is in units of $m^2\ L^{-1}$. These results (eq. 17) can be compared directly to the results reported by Matheson and Tratnyek (*10*) who measured the rate of CCl_4 degradation by Fe^0 without ultrasound as follows:

$$k = 0.0025 \cdot A_{Fe^0} + 0.017 \qquad (18)$$

This comparison confirms that ultrasonic irradiation enhances the rate of CCl_4 degradation due to Fe^0 by a factor of 40 compared to Fe^0 in the absence ultrasound.

The higher degradation rate contributed by Fe^0 in our study can be attributed to the indirect chemical effects associated with the continuous ultrasonic cleaning and activation

of the Fe^0 surface, the enhanced rate of mass transport resulting from the turbulent effects of cavitation, and the lower pH caused by CCl_4 sonolysis. The shock wave and microjets formed during cavitational bubble collapse are primarily responsible for the cleaning actions of ultrasound. Transient cavitation results in turbulent flow conditions within the reactor that enhance overall mass transport. The iron corrosion accelerated by ultrasound may also contribute to the reductive dehalogenation of CCl_4 via eq. 16. The effect of a drop in pH during sonication is to produce a faster rate of reduction of Fe^0. Since the sonolytic degradation of CCl_4 produces H^+ according to eqs. 10 and 11, we expect to see a faster rate in the combined system. The Fe^0 reduction reaction involving H^+ is as follows:

$$Fe + CCl_4 + H^+ \longrightarrow Fe^{2+} + CHCl_3 + Cl^- \qquad (19)$$

C_2Cl_4 and C_2Cl_6 were observed as intermediates during CCl_4 sonolysis discussed previously (*3, 25*). However, these intermediates were not measured by Matheson and Tratnyek (*10*). The principal products observed during CCl_4 reduction by Fe^0 are $CHCl_3$ and CH_2Cl_2. During CCl_4 sonolysis, the concentrations of C_2Cl_4 and C_2Cl_6 increased with time, then decreased during continued sonication after reaching maximum concentrations. The maximum concentrations of C_2Cl_4 and C_2Cl_6 are shown as functions of the mass concentration of Fe^0 in Figure 3. The measured C_2Cl_4 and C_2Cl_6 concentrations increase with increasing Fe^0 mass concentration up to 10 g/L. This effect can be explained by the production of higher levels of chloroform ($CHCl_3$) from the reductive dehalogenation of CCl_4 by Fe^0. We have previously shown that $CHCl_3$ sonolysis produces more C_2Cl_4 than C_2Cl_6 (*25*). The overall reactions consistent with these observations are as follows:

$$Fe + CCl_4 + H_2O \longrightarrow Fe^{2+} + CHCl_3 + OH^- + Cl^- \quad (20)$$

$$CHCl_3 \xrightarrow{)))} :CCl_2 + HCl \quad (21)$$

$$:CCl_2 + :CCl_2 \longrightarrow C_2Cl_4 \quad (22)$$

Another possible pathway involves CCl_4 sorption on the Fe^0 surface, which subsequently reacts with $\bullet CCl_3$ produced during sonolysis as follows:

$$CCl_4 \xrightarrow{)))} \bullet CCl_3 + \bullet Cl \quad (23)$$

$$CCl_4 + \frac{1}{2}Fe \longrightarrow \bullet CCl_3 + \frac{1}{2}Fe^{2+} + Cl^- \quad (24)$$

$$2 \bullet CCl_3 \longrightarrow C_2Cl_6 \quad (25)$$

The reactions of eqs. 20-25 help to explain the observed higher concentrations of C_2Cl_4 and C_2Cl_6 in the combination Fe^0/CCl_4 system.

Kinetic Analysis

The final reaction product observed during CCl_4 sonolysis is Cl^-. The overall degradation mechanism can be simplified as follows:

$$CCl_4 \xrightarrow{))) \ k_1} \bullet CCl_3 + \bullet Cl \quad (26)$$

$$2 \bullet CCl_3 \xrightarrow{k_2} C_2Cl_6 \quad (27)$$

$$C_2Cl_6 \xrightarrow{k_3} aCl^- + \text{other products.} \quad (28)$$

$$\bullet Cl + H_2O \xrightarrow{k_4} HCl + \bullet OH \quad (29)$$

with the corresponding kinetic equations:

$$\frac{d[CCl_4]}{dt} = -k_1[CCl_4] \quad (30)$$

$$\frac{d[\bullet CCl_3]}{dt} = k_1[CCl_4] - 2k_2[\bullet CCl_3]^2 \quad (31)$$

$$\frac{d[C_2Cl_6]}{dt} = 2k_2[\bullet CCl_3]^2 - k_3[C_2Cl_6] \quad (32)$$

$$\frac{d[\bullet Cl]}{dt} = k_1[CCl_4] - k_4[\bullet Cl] \quad (33)$$

$$\frac{d[Cl^-]}{dt} = k_4[\bullet Cl] + ak_3[C_2Cl_6] \quad (34)$$

The solution to the coupled differential eqs. 30-34 can be written as

$$[C_2Cl_6] = \frac{k_1}{2(k_1 - k_3)}[CCl_4]_0(e^{-k_3t} - e^{-k_1t}) \quad (35)$$

$$[Cl^-] = [CCl_4]_0[1 - e^{-k_1t} + \frac{ak_1}{2(k_1 - k_3)}(1 - e^{-k_3t}) - \frac{ak_3}{2(k_1 - k_3)}(1 - e^{-k_1t})] \quad (36)$$

for C_2Cl_6 and Cl^-, respectively (*25*). Based on our previous measurements, we know that k_1, which is CCl_4 degradation rate constant for sonolysis alone, $\approx k_3$, the corresponding

C_2Cl_6 degradation rate constant. Thus eq. 36 can be further simplified to

$$[Cl^-] \approx [Cl^-]_\infty (1 - e^{-k_{cl^-}t}) \tag{37}$$

The effect of Fe^0 can be treated as a simple step addition to the mechanism of eqs. 26-29 as follows:

$$CCl_4 + \frac{1}{2}\,Fe \xrightarrow{k'} \bullet CCl_3 + Cl^- + \frac{1}{2}\,Fe^{2+} \tag{38}$$

as a consequence, eq. 30 can be rewritten as

$$[CCl_4] = [CCl_4]_0 e^{-(k_1 + k')t} \tag{39}$$

where k′ (k′ = Δk) is the enhanced CCl_4 degradation rate in the presence of Fe^0. Since Fe^0 has a negligible influence on the rate of C_2Cl_6 degradation (*18*)), C_2Cl_6 degraded by Fe^0 can be ignored relative to the C_2Cl_6 sonolysis. This allows the modification of eqs. 35 and 36 to yield eqs. 40 and 41 as follows:

$$[C_2Cl_6] = \frac{(k_1 + k')}{2(k_1 + k' - k_3)} [CCl_4]_0 (e^{-k_3 t} - e^{-(k_1 + k')t}) \tag{40}$$

$$[Cl^-] = [CCl_4]_0 \{1 - e^{-(k_1 + k')t} + \frac{a(k_1 + k')}{2(k_1 + k' - k_3)}(1 - e^{-k_3 t}) - \frac{ak_3}{2(k_1 + k' - k_3)}(1 - e^{-(k_1 + k')t})\} \tag{41}$$

The $[Cl^-]$ concentration vs. time predicted by eq. 37 is used to fit all the kinetic data and

obtain k_{Cl^-} values as a function of [Fe^0]. In Figure 4, the fitted results for ultrasound alone and ultrasound + 2 g Fe^0 powder systems are shown. Furthermore, the comparison of the rate constant, k_{Cl^-}, for [Cl^-] production and the rate constant, k_{CCl_4}, for CCl_4 degradation as a function of [Fe^0] is shown in Table 2. If we suppose that eq. 41 can be simplified to eq. 37, the k_{Cl^-} obtained from Figure 4(b) embodies the contribution of k', the enhanced CCl_4 degradation rate by Fe^0. As mentioned above, k' is larger for Fe^0 powder than Fe^0 turnings. Based on the data summary in Table 2, we see that k' contributes more to k_{Cl^-}, which shows greater increases for Fe^0 powder than for Fe^0 turnings. From these comparisons, it is clear that k_{Cl^-} increases with [Fe^0] but the relative magnitude of the increase is less than that for k_{CCl_4}. This discrepancy could be due to the contribution of k′ in eq. 39; the difference between k_{Cl^-} and k_{CCl_4} is consistent with increasing Fe^0 mass concentration.

The degradation rate constant for ultrasound alone in this study is 0.107 min^{-1} (= 1.8×10^{-3} s^{-1}) at 62 W in 285 mL; this is equivalent to a first-order rate constant of 4.3×10^{-3} s^{-1} adjusted to 50 W in 95 mL through power density normalization. This value is faster than that reported by Hua and Hoffmann (*3*) (i.e., 3.3×10^{-3} s^{-1} in 50 W and 95 mL). The relative enhancement may have been due to a power density effect in which increased power results in enhanced chemical effects instead of simply heating the solution due to relative inefficiencies in energy transfer (*26*). For the combination of ultrasound and Fe^0, Reinhart et al. also observed similar rate enhancements for the reduction of trichloroethylene (TCE) by Fe^0 (*20*). In addition, they reported an increase in the final pH

of the mixture in the TCE- Fe^0 system compared with the application of ultrasound alone.

In this study, we demonstrated that the rate of sonolytic degradation of CCl_4 can be enhanced by the presence of Fe^0. The higher apparent rates of reaction in the coupled US/Fe^0 system compared to Fe^0 reaction alone can be attributed to the continuous cleaning and activation of the Fe^0 surface by the chemical and physical effects of ultrasound. Furthermore, faster mass transport rates resulting from the hydrodynamic cavitation and production of H^+ during the course of the reaction also contribute to the observed rate enhancements. The relative concentrations of the principal reaction intermediates, C_2Cl_4 and C_2Cl_6, which are observed during the course of the reaction, appear to be influenced significantly by total available surface area of Fe^0. In conclusion, the combination of ultrasound and Fe^0 has a positive synergistic effect on the dehalogenation of chlorinated hydrocarbons.

Acknowledgments

The authors appreciate the contributions by Dr. Linda Weavers's about the details of the kinetic and mechanisms. Financial support from the Office of Naval Research (NAV5-N0001492J1901; NAV1-N47408-97-M-0771) and the Department of Energy (DOE 1 963472402) is gratefully acknowledged.

References

1. Mason, T. J.; Lorimer, J. P. *Sonochemistry: Theory, Application and Uses of Ultrasound in Chemistry*; John Wiley &Sons: New York, 1988.

2. Cheung, H. M.; Bhatnagar, A.; Jansen, G. *Environ. Sci. Technol.* **1991**, *25*, 1510-12.

3. Hua, I.; Hoffmann, M. R. *Environ. Sci. Technol.* **1996**, *30*, 864-71.

4. Kotronarou, A.; Mills, G.; Hoffmann, M. R. *J. Phys. Chem.* **1991**, *95*, 3630-8.

5. Kotronarou, A.; Mills, G.; Hoffmann, M. R. *Environ. Sci. Technol.* **1992**, *26*, 1460-2.

6. Kotronarou, A. Ph. D. thesis; California Institute of Technology, Pasadena, **1991**.

7. Hua, I.; Hochemer, R.; Hoffmann, M. R. *J. Phys. Chem.* **1995**, *99*, 2335-2342.

8. Suslick, K. S.; Hammerton, D. A.; Cline, R. E. *J. Am. Chem. Soc.* **1986**, *108*, 5641-5642.

9. Shutilov, V. A. *Fundamental Physics of Ultrasound*; Gordon & Breach Science: New York, 1988.

10. Matheson, L. J.; Tratnyek, P. G. *Environ. Sci. Technol.* **1994**, *28*, 2045-2053.

11. Fairweather, V. *Civil Eng.* **1996**, *66*, 44-48.

12. Tratnyek, P. G. *Chem. Ind.* **1996**, 499-503.

13. Tratnyek, P. G.; Johnson, T. L.; Scherer, M. M.; Eykholt, G. R. *Ground Water*

Monitoring & Remediation **1997**, *XVII*, 108-114.

14. Scherer, M. M.; Westall, J. C.; Ziomek-Moroz, M.; Tratnyek, P. G. *Environ. Sci. Technol.* **1997**, *31*, 2385-2391.

15. Johnson, T. L.; Fish, W.; Gorby, Y. A.; Tratnyek, P. G. *J. Contam. Hydrol.* **1998**, *29*, 377-396.

16. Gillham, R. W.; Ohannesin, S. F. *Ground Water* **1994**, *32*, 958-967.

17. Lipczynskakochany, E.; Harms, S.; Milburn, R.; Sprah, G.; Nadarajah, N. *Chemosphere* **1994**, *29*, 1477-1489.

18. Johnson, T. L.; Scherer, M. M.; Tratnyek, P. G. *Environ. Sci. Technol.* **1996**, *30*, 2634-2640.

19. Agrawal, A.; Tratnyek, P. G. *Environ. Sci. Technol.* **1996**, *30*, 153-160.

20. Reinhart, D. R.; Clausen, C.; Geiger, C.; Ruiz, N.; Afiouni, G. F. *"Enhancement of In-Situ Zero-Valent Metal Treatment of Contaminated Groundwater"* in Non-aqueous phase liquids in surface environment: assessment and remediation; American Society of Civil Engineers: Washington, D. C., **1996**, 323-332.

21. Mason, T. J. *Practical Sonochemistry: User's Guide to Application in Chemistry and Chemical Engineering*; Ellis Horwood, 1991.

22. Wu, J. M.; Huang, H. S.; Livengood, C. D. *Environ. Prog.* **1992**, *11*, 195-201.

23. Francony, A.; Petrier, C. *Ultrasonic Sonochemistry* **1996**, *3*, S77-S82.

24. Bhatnagar, A.; Cheung, H. M. *Environ. Sci. Technol.* **1994**, *28*, 1481-6.

25. Hung, H.-M.; Hoffmann, M. R. *Environ. Sci. Technol.* **1998**, in review.

26. Hung, H.-M.; Hoffmann, M.R. "*The Effect of Frequency, Hydrostatic pressure, Temperature and Sonication Power on Sonochemical Reactions*" in preparing.

Table 1. Physical dimensions of the different frequency transducers.

Frequency	Emitting Dia., cm	Emitting Areas, cm^2	Sonication Volume
20 kHz + Fe^0 powder	1.27	1.27	245 mL
20 kHz + Fe^0 turnings	1.27	1.27	285 mL

Table 2. Comparsion of k values from CCl_4 degradation and Cl^- production, (a) Fe^0 powder and (b) Fe^0 turnings.

(a)

Fe^0 Powder mass conc. (g/L)	k_{CCl_4} (min^{-1})	k_{Cl^-} (min^{-1})
0	0.13	0.13
2.04	0.15	0.14
8.16	0.20	0.16
16.33	0.20	0.18
24.49	0.20	0.18

(b)

Fe^0 turnings mass conc. (g/L)	k_{CCl_4} (min^{-1})	k_{Cl^-} (min^{-1})
0	0.107	0.086
7.02	0.113	0.094
14.0	0.115	0.100
21.0	0.118	0.099
28.1	0.122	0.098
42.1	0.125	0.096

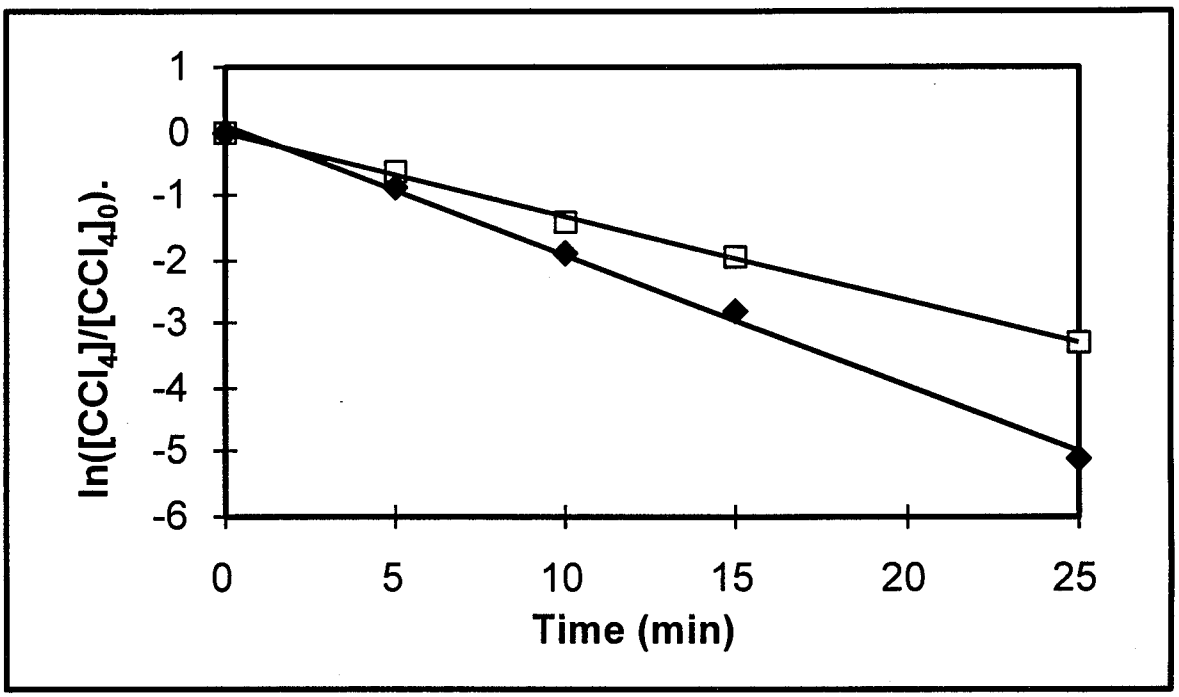

Figure 1. First-order plot for CCl_4 degradation; (□) by ultrasound alone; and by ultrasound + 2 g Fe^0 powder (◆); the solid lines are the fitting results.

Figure 2

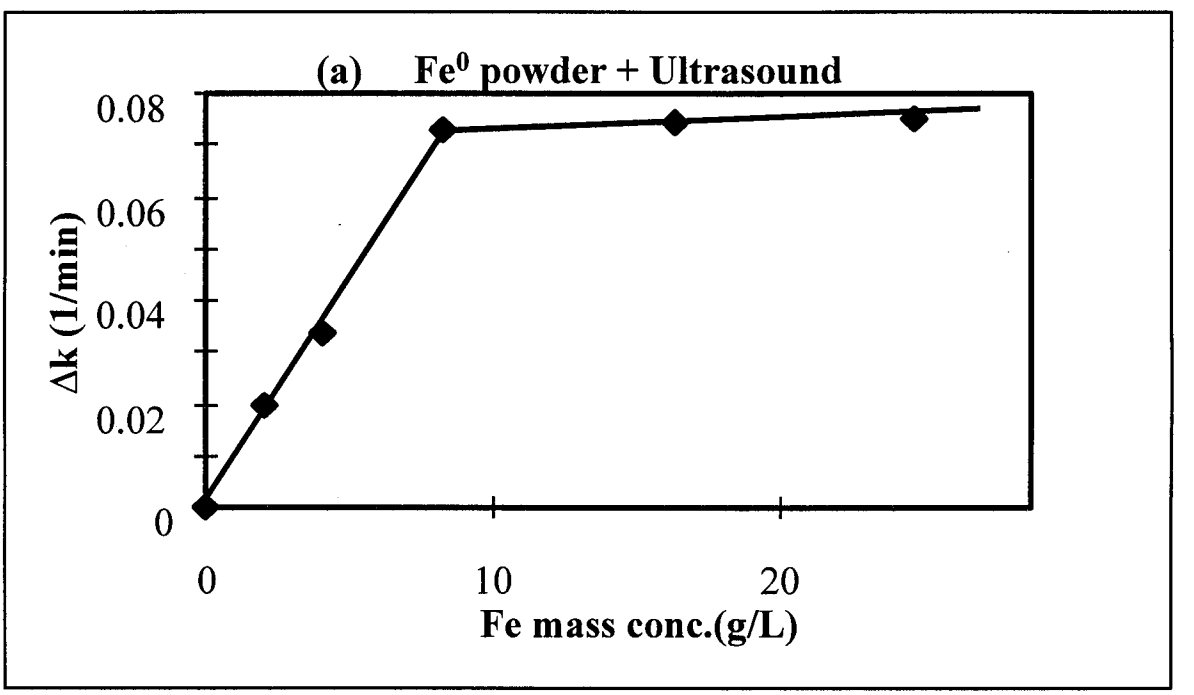
(a) Fe0 powder + Ultrasound
0.08
0.06
0.04
0.02
0
Δk (1/min)
0
10
20
Fe mass conc.(g/L)

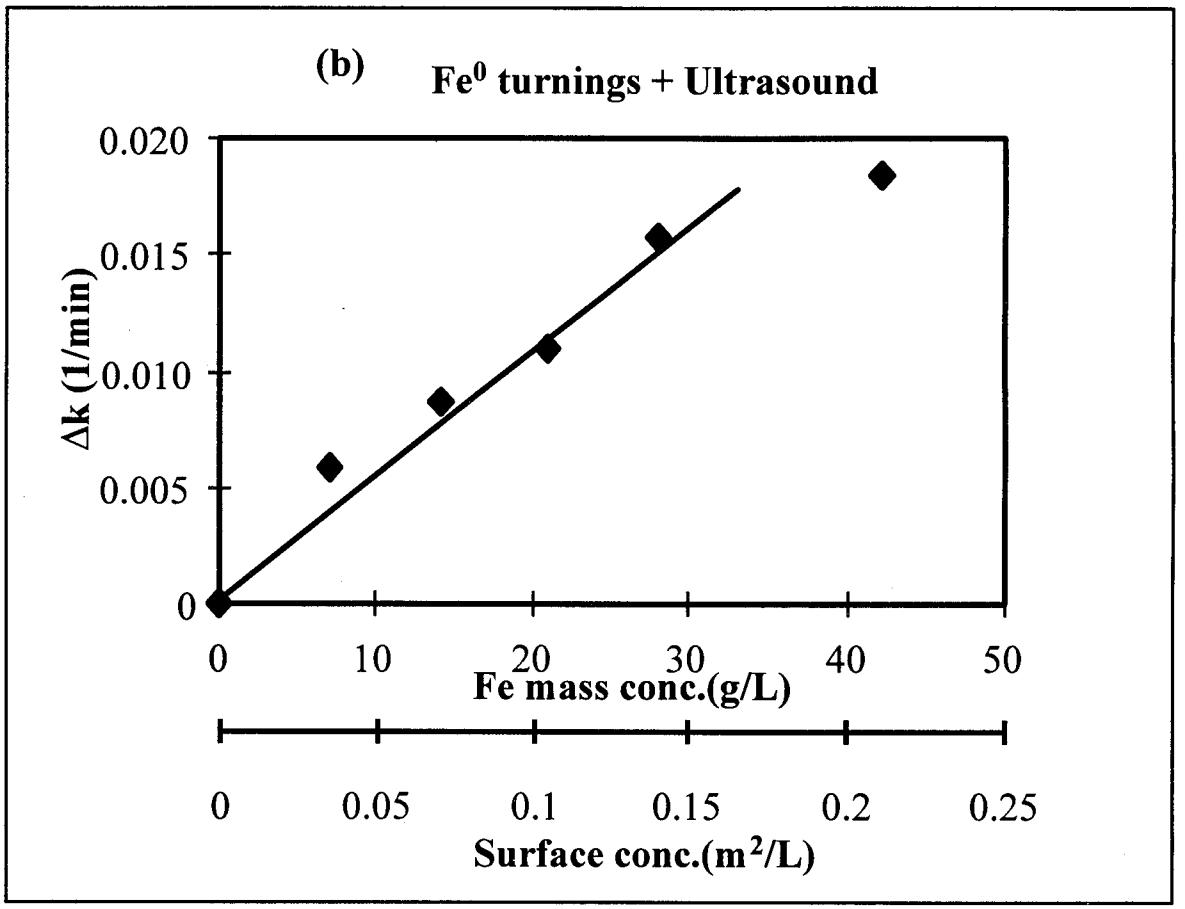

Figure 2. Effect of reactive surface area of Fe^0 on the pseudo-first-order rate constant for CCl_4 degradation by (a) Fe^0 powder and (b) Fe^0 turnings. { Δk = k (ultrasound + Fe^0) - k (ultrasound)}

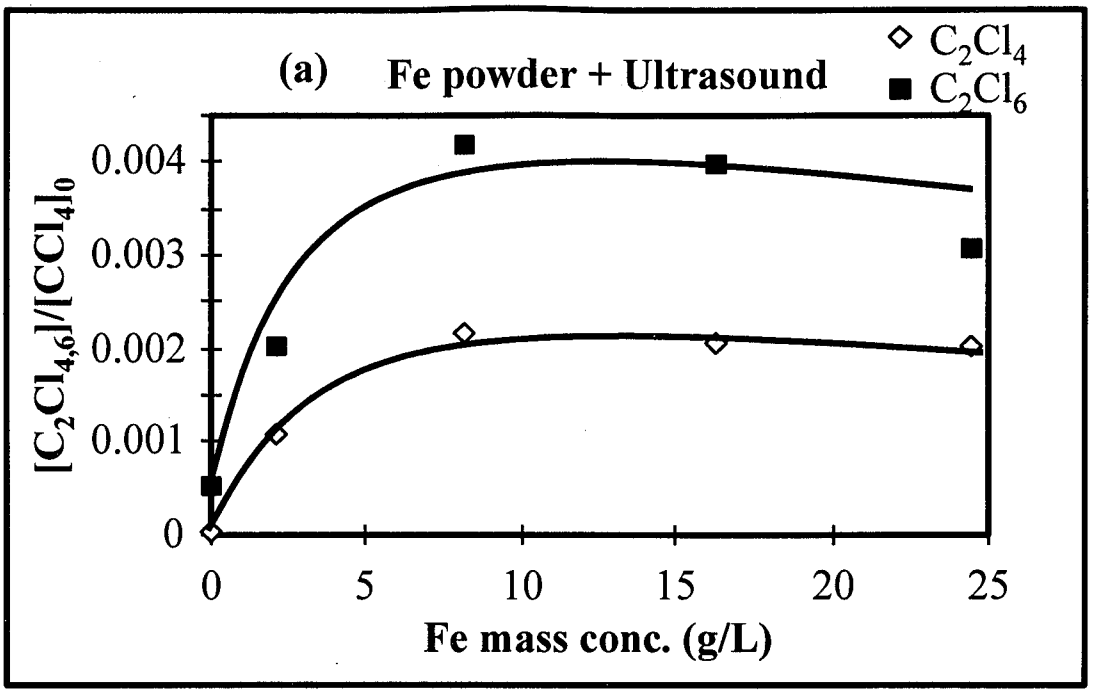

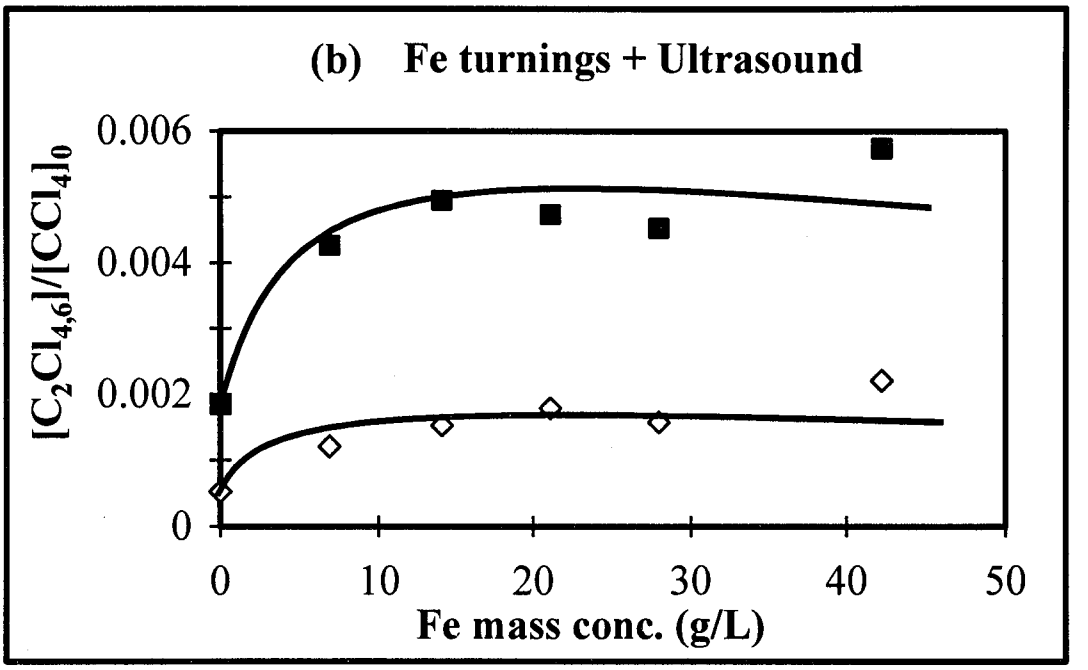

Figure 3. The ratio of maximum concentration of C_2Cl_4 and C_2Cl_6 as functions of $[Fe^0]$ respect to CCl_4 initial concentration, (a) for Fe^0 powder and (b) for Fe^0 turnings.

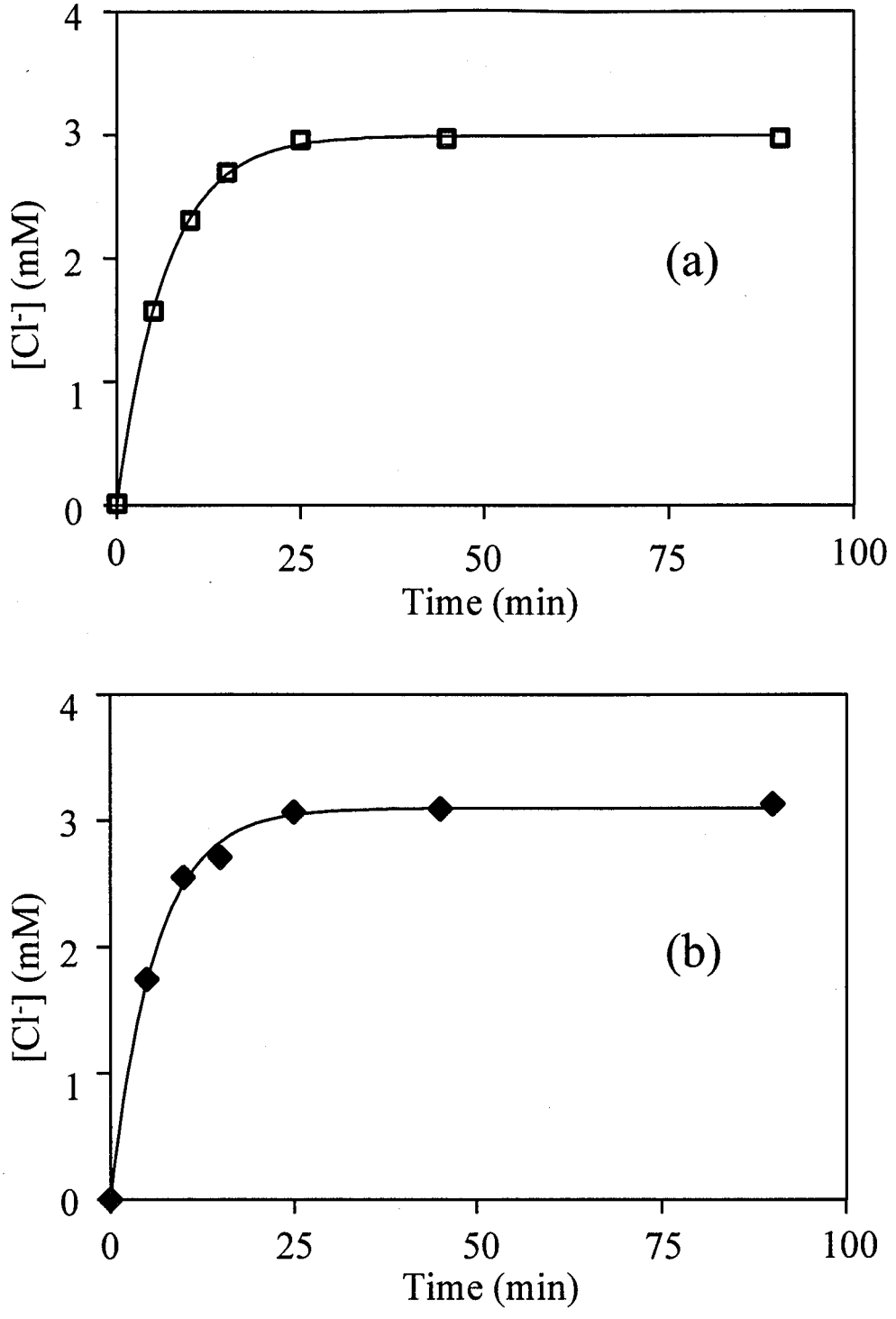

Figure 4. The fitting results for $[Cl^-]$ concentration by eq. 37, (a) ultrasound only; (b) ultrasound + 2 g Fe^0 powder.

Chapter 6

Kinetics and Mechanism of the Enhanced Reductive Degradation of Nitrobenzene by Elemental Iron in the Presence of Ultrasound

(In press, *Environmental Science & Technology*, **2000**)

Abstract

Sonolysis, reduction by elemental iron (Fe^0), and a combination of the two processes were used to facilitate the degradation of nitrobenzene (NB) and aniline (AN) in water. The rates of reduction of nitrobenzene by Fe^0 are enhanced in the presence of ultrasound. The first-order rate constant, k_{US}, for nitrobenzene degradation by ultrasound is 1.8×10^{-3} min^{-1}, while in the presence of Fe^0, the rate was found to be substantially faster. The observation of similar degradation rates for aniline in each system suggests that the sonication process was not affected by the presence of Fe^0. The observed rate enhancements for the degradation of nitrobenzene can be attributed primarily to the continuous cleaning and chemical activation of the Fe^0 surfaces by acoustic cavitation, and to accelerated mass transport rates of reactants, intermediates and products between the solution phase and the Fe^0 surface. The relative concentrations of nitrosobenzene and aniline, the principal reaction intermediates generated by Fe^0 reduction, are altered substantially in the presence of ultrasound.

Introduction

Ultrasonic irradiation has been applied as an advanced oxidation technology for water treatment (*1,2*). The chemical effects of ultrasound are due to the phenomenon of acoustic cavitation (*3-5*). Temperatures inside of the cavitation bubble are on the order of 5000 K (*4*), and pressures of the order of 1000 bar have been calculated (*4*). In homogeneous reactions, the destruction of organic compounds occurs inside the caviation bubbles by a pyrolysis reaction, or in the nearby interfacial region by hydroxylation (*3,5*). In heterogeneous reactions, the primary mode of action by sonication is erosion involving the removal of oxide layers and impurities together with pitting of metal surfaces. It is thought that sonication serves to sweep reactive intermediates or products from metal surfaces thereby reactivating and cleaning the surfaces for subsequent reactions (*3,5*).

Elemental iron (Fe^0) has been proposed as a suitable source of electrons for the *in situ* remediation of contaminated groundwater (*6-14*). Tratnyek and co-workers (*7-10*) have used Fe^0 to reduce chlorinated hydrocarbons to non-chlorinated products and to reduce nitroaromatic compounds (NACs) to anilines (*13,14*). A linear correlation between the observed rate constants for the reduction of nitrobenzene and the square-root of mixing rate (rpm) indicated that the observed reaction rates were controlled by mass transfer of the substrates to the Fe^0 surfaces (*14*).

Since acoustic cavitation is known to increase the surface area of reactive solids by causing particles to rupture, Reinhart et al. (*15*) investigated the dechlorination of trichloroethylene by Fe^0 in the presence of ultrasound. In our previous paper (*16*), the kinetics and mechanism of carbon tetracholoride degradation by Fe^0 in the presence of ultrasound was reported and it was noted that the rate of CCl_4 degradation was enhanced by a factor of 40 compared to the same reaction system in the absence of ultrasound.

In this study, we investigate the combination of ultrasound and Fe^0 for the reduction of nitrobenzene and aniline, the by-product from the nitrobenzene reduction by Fe^0. The influence of ultrasonic power density is also discussed.

Technical Background

Mechanism of Nitrobenzene Sonolysis

The sonolytic degradation of nitrobenzene has been studied by Weavers *et al.* (*17*). Pyrolysis and hydroxylation are the main pathways for the sonolytic degradation of nitrobenzene as follows, where ')))' refers to the application of ultrasound, and [O] refers to the ·OH radical or other oxidants (e.g., H_2O_2) produced by ultrasound:

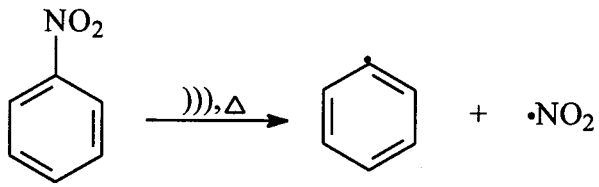

(1)

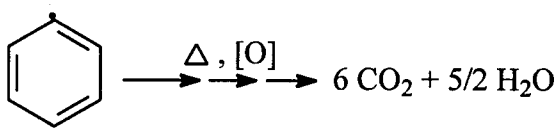

(2)

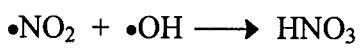

(3)

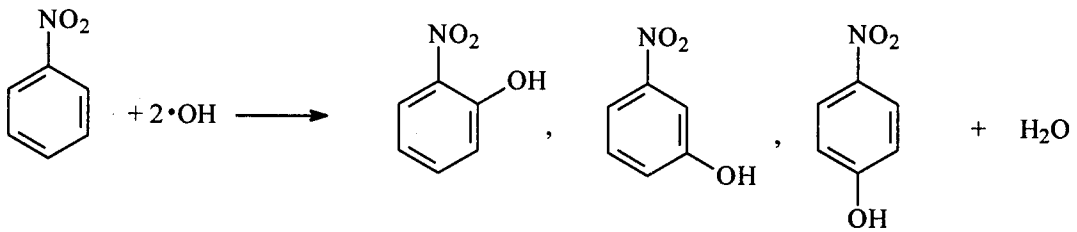

isomeric intermediates

(4)

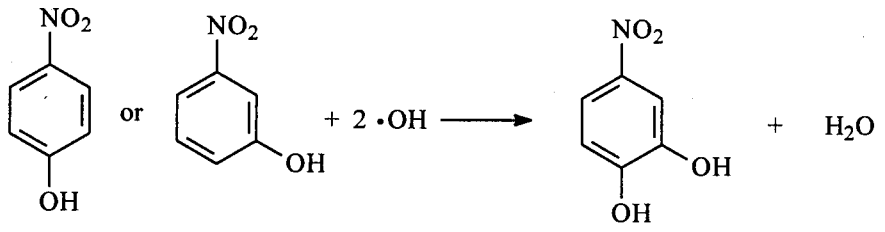

(5)

The formation of *meta*-nitrophenol (MNP), *para*-nitrophenol (PNP), and 4-nitrocatechol (4-NC) was observed during sonolysis of nitrobenzene in water at 20 kHz (*17*). However, at 500 kHz, *o*-nitrophenol (ONP) was also observed as an intermediate. With continuous irradiation these intermediates are further degraded to inorganic products, e.g., HNO_3, CO_2 and H_2O.

Mechanism of Nitrobenzene Reduction by Fe^0

According to Agrawal and Tratnyek (*14*), the pathway for nitrobenzene reduction by elemental iron can be described by the following stoichiometric reactions:

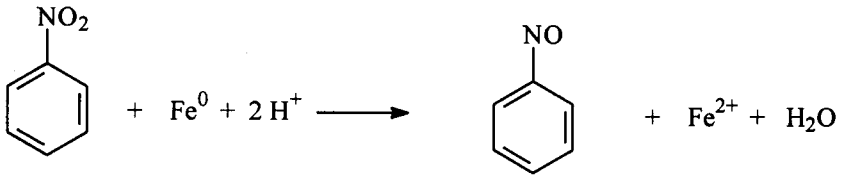

(6)

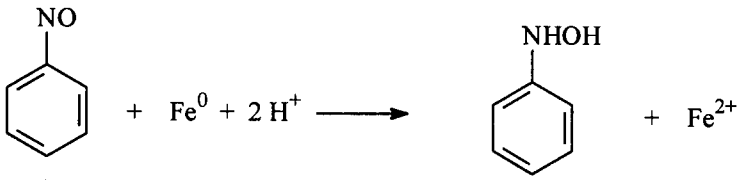

(7)

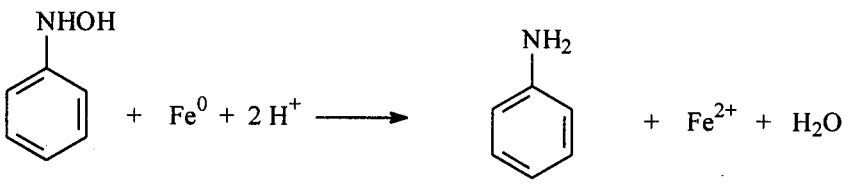

(8)

where the overall stoichiometry is given by

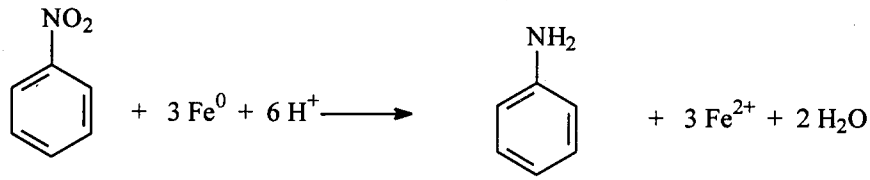

(9)

Based on the overall reaction depicted in eq. 9, the primary product observed after several hours of reaction is aniline with nitrosobenzene found as the only intermediate (eq.6).

Experimental Procedures

High-purity reagents, nitrobenzene (Aldrich, 99%), nitrosobenzene (Fluka, 99%), and aniline (Fluka) were used without further purification. Standard solutions of nitrobenzene and aniline were made with water purified by a Millipore Milli-Q UV Plus system (18.2 MΩ-cm resistivity). For nitrosobenzene, the stock solution was prepared with 50% acetonitrile (EM Science, GR). The initial reaction volume was 0.285 L and the initial nitrobenzene concentration was 25 μM. Solutions were not buffered.

Zero-valent iron particles (Fluka) were prepared by sieving raw particles through a 20-mesh screen (1.0 mm opening size). The elemental iron was not pretreated with acid prior to use. The degradation reactions with Fe^0 were carried out in tightly closed systems with reaction volumes of 300 mL. Sample aliquots were obtained by syringe through a Teflon septum. The reaction vessels were wrapped in aluminum to limit exposure to light. Reaction solutions were pre-equilibrated at 15° C in a circulating water bath.

Kinetic runs were initiated by adding a measured amount of Fe^0 to the reactor system which was placed on a variable-speed rotary shaker. The entire shaker was kept in an air-cooled refrigeration unit at a constant temperature of 15 °C.

Sonolyses were performed with a VCX-400 Vibracell™ (Sonics and Materials, Inc., Danbury, CT) operating at 20 kHz. The temperature was maintained at 15 ± 2 °C

with a Haake A80 Refrigerated Bath and Circulator. Replaceable titanium tips with diameter of 1.27 cm on the transducer were polished and the transducer was tuned before each use to give a minimum power output when vibrating in air. The tuning process is a standard procedure to bring the transducer into resonance as part of the complete probe assembly. Sonolytic reactions at 20 kHz were performed in a 300 mL air-tight reactor cell with air equilibrium. The physical dimensions and fundamental characteristics of the transducer and the reactor configuration have been presented (*16*). The bottom of the glass reactor was designed with a 1 cm indentation in the center for reflection of the sound waves and for an even distribution of the cavitation bubbles in the solution. The reactor was made gas-tight with two O-ring seals in a threaded Teflon collar that connects the glass cell to the stainless steel probe. In addition, sampling ports were sealed with Teflon valves and covered with rubber septa. The ultrasonic power output was measured by calorimetry.

Chemical Analyses

Sample aliquots of 0.5 mL were collected at designated times and were filtered through Teflon syringe filters (Gelman Acrodisc) into amber colored liquid chromatography vials. Quantification of nitrobenzene and its intermediates was performed on a Hewlett-Packard Series II 1090 Liquid Chromatograph with a 3 μm 100 x 4 mm Hypersil BDS-C18 column (Hewlett Packard). The method called for a 1 mL min^{-1} flow rate, 40° C temperature, and a 25 μL injection volume. The runs were 6 minutes long with an isocratic mixture (70:30) of water to acetonitrile (EM Science, HPLC grade). The post-run time was 1 minute.

Results and Discussion

Experiments were performed at an initial nitrobenzene concentration of 25 μM and an initial pH of 6 without an added buffer. The loss of nitrobenzene was found to be less

than 5% in control experiments in the absence of ultrasound and iron. After completion of each kinetic run with ultrasound alone, the final observed pH was close to 5.5. With Fe^0 alone the final observed pH was close to 7, and with the combination of ultrasound and Fe^0, the observed pH was near 8. In the reactions involving Fe^0, a rise in pH is consistent with the following stoichiometries:

$$Fe^0 + 2\,H_2O \rightleftharpoons Fe^{2+} + H_2 + OH^- \quad (10)$$

$$2\,Fe^0 + O_2 + 2\,H_2O \rightleftharpoons 2\,Fe^{2+} + 4\,OH^- \quad (11)$$

The observed higher pH with the combined US/Fe^0 systems indicates that more Fe^0 is involved in the degradation of nitrobenzene or oxidized by water and oxygen in the presence of ultrasound.

Nitrosobenzene (NSB) and aniline (AN) were the major products observed in the reduction of nitrobenzene by Fe^0. However, during sonication the principal observed intermediates were *ortho*-nitrophenol (ONP), *meta*-nitrophenol (MNP), *para*-nitrophenol (PNP), and 4-nitrocatechol (4-NC). The key UV-vis spectroscopic and chromatographic data for nitrobenzene and its intermediates are presented in Table 1.

First-order plots of $\ln\{[NB]/[NB]_0\}$ vs. time during sonolysis at 20 kHz and during reduction by Fe^0 are shown in Figure 1. The slopes obtained from linear regression of the data yield the observed first-order rate constants for nitrobenzene degradation. The corresponding reaction rate for nitrobenzene degradation by ultrasound in the presence of iron was also found to be first-order at lower Fe^0 loadings, $[Fe^0]$. At higher $[Fe^0]$, the second-order polynomial function (dashed line) gives a better experimental fit than a simple first-order relationship (solid line) as shown in Figure 1. The average deviation for nitrobenzene reductions determined in replicate experiments was < 10%.

Reduction by Elemental Iron Surfaces

Agrawal and Tratnyek (*14*) reported that the nitrobenzene reduction rate constants exhibited a linear relationship with respect to the square root of the stirring rate (i.e., rate $\propto \omega^{0.5}$), which indicated that the apparent reaction rate was limited by mass transport. In this study, we mixed the suspension with a 360° rotary shaker at ω = 10 rpm. The rate of reduction of nitrobenzene by Fe^0 is observed to be first-order. The observed reaction rate constants, k_{10rpm/Fe^0}, as a function of [Fe^0] are listed in Table 2. As expected, k_{10rpm/Fe^0} increases with [Fe^0].

In the combined US/Fe^0 systems, the overall rate of nitrobenzene disappearance can be described by a linear combination of first-order terms (*17*):

$$-\frac{d[NB]}{dt} = k_{US}[NB] + k_{Fe^0}[NB] + k'[NB] = \left(k_{US} + k_{Fe^0} + k'\right)[NB] \qquad (12)$$

where k_{US}, k_{Fe^0}, and k' are respectively, the first-order degradation rate constants for sonolysis, reduction by Fe^0, and the synergistic kinetic effect achieved by combining the two systems. k' may be related to the generation of increased surface area or reactive intermediates, which are capable of degrading nitrobenzene. The k' should be dependent on the newly created reactive surface sites and on the concentration of the reactive intermediates. k' can be expressed by the following generalized equation:

$$k' = k_{\text{sec}}[X_{i,j}] \qquad (13)$$

where k_{sec} is the average second-order rate constant for the reaction between the Fe^0 surface sites, or the reactive intermediates and nitrobenzene, and $[X_{i,j}]$ is effective concentration of the newly generated Fe^0 surface sites (i) and the reactive intermediates (j). Since the reactive intermediates will be consumed very fast with any reactants in the solution, the contribution in $[X_{i,j}]$ from the reactive intermediates can be ignored. If we assume that $[X_{i,j}]$ is mainly contributed from the newly generated Fe^0 surface by ultrasound, the total

activated Fe^0 surface (x) increasing rate is proportional to x with a rate constant, k_a, as follows:

$$\frac{dx}{dt} = k_a x \tag{14}$$

x as a function of time can be solved as follows:

$$x = x_0 + [X_{i,j}] = x_0 \, e^{k_a t} \tag{15}$$

where x_0 is the initial activated Fe^0 surface before ultrasound is applied. Since the influence of ultrasound at low [Fe^0] can be ignored, the exponential term in eq. 15 could be expanded into polynomial terms. Without consideration of the high order terms, $[X_{i,j}]$ can be expressed as follows:

$$[X_{i,j}] = x_0 k_a t = k_p t \tag{16}$$

where $k_p = x_0 \, k_a$ is a zero-order rate constant that increases with added [Fe^0]. Substitution of eqs. 13 and 16 into eq. 12 yields the following time-implicit equations:

$$-\frac{d[NB]}{dt} = (k_{US} + k_{Fe^0} + k_{\sec} k_p t)[NB] \tag{17}$$

The integration of eq.17 gives:

$$-\ln\left[\frac{[NB]}{[NB]_0}\right] = (k_{US} + k_{Fe^0})t + \frac{1}{2} k_{\sec} k_p t^2 \tag{18}$$

Values of k_{US} were determined from the separate sonication-only experiments. Figure 2 shows the fitted results from eq.18 for various [Fe^0]. The individual rate constants are listed in Table 2.

The values of k_{Fe^0} in the combined US/Fe^0 system are slightly higher than k_{10rpm/Fe^0} values in part because of the higher relative mixing rates achieved during sonication. The

new surface area and species created by ultrasound are reflected in '$k_{sec}k_p$', which increases with Fe^0 loading at higher [Fe^0]. The higher values of '$k_{sec}k_p$' obtained with increasing [Fe^0] are due primarily to the effects related to the direct reactions with elemental iron. Since k_{sec} is a rate constant quantifying the impact of the secondary effects on nitrobenzene, it is independent of [Fe^0]. On the other hand, k_p should increase with [Fe^0] as mentioned above.

The higher degradation rates observed in the combined US/Fe^0 systems can be attributed to the indirect chemical effects associated with the continuous ultrasonic cleaning and activation of the Fe^0 surface, the enhanced rate of mass transport resulting from the turbulent effects of cavitation, and the H^+ released to solution from the HNO_3 produced during the sonolysis of nitrobenzene and water (eq. 3). The shock wave and microjets formed during cavitational bubble collapse are primarily responsible for the surficial cleaning actions of ultrasound. Transient cavitation results in turbulent flow conditions within the reactor that enhance overall mass transport. The iron corrosion accelerated by ultrasound may also contribute to the reduction of the nitro group to an amine group via eq. 9.

It has long been recognized that air-saturated water, which is exposed to the action of ultrasound, leads to the formation of NO_2^-, and to a lesser extent NO_3^-, as well as H_2O_2 (*18-21*). The observed pH decrease during sonication should result in a faster rate of reduction of Fe^0 (eq. 6). Since the sonolytic degradation of nitrobenzene produces HNO_3 according to eqs. 1 - 3, we expect to see a faster reduction rate in the combined reaction system, but this contribution can be ignored because of higher pH observed at US/Fe^0 systems. The H^+ produced during sonolysis should be consumed by Fe^0 oxidation or nitrobenzene reduction according to the following stoichiometry:

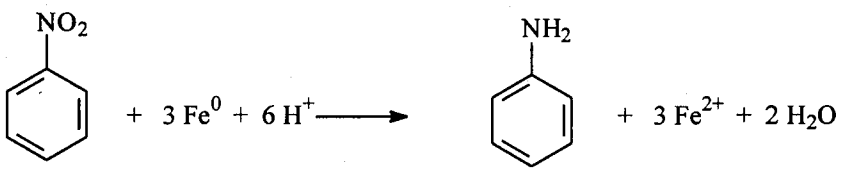

(19)

Aqueous-phase Fe^{2+} (*i.e.*, $Fe(H_2O)_6^{2+}$) and the Fe^{2+} sorbed on the surface of Fe^0 can also react with H_2O_2, which is produced from the sonication of H_2O (*20*) as follows:

$$Fe(H_2O)_6^{2+} + H_2O_2 \longrightarrow Fe(H_2O)_6^{3+} + OH^- + \cdot OH \quad (20)$$

$$\{Fe{\cdot}Fe^{2+}\} + H_2O_2 \longrightarrow \{Fe{\cdot}Fe^{3+}\} + OH^- + \cdot OH \quad (21)$$

The ·OH radical will be available for further reactions such as the degradation of nitrobenzene and aniline. Since high concentrations of Fe^{2+} are produced from oxidation of Fe^0, the subsequent Fenton's Reagent reaction should be independent of $[Fe^0]$. The contribution of the Fenton's reaction in the combined US/Fe^0 systems should be relatively constant, and thus reflected in the second term of eq.18. Since a similar degradation rate for aniline is observed in both the US and combined US/Fe^0 systems, the secondary Fenton's reaction appears to be negligible compared to other secondary effects. Ultrasound also enhances the mass transfer of the product, aniline, away from the Fe^0 surface.

The observed nitrobenzene reduction rates in our study are somewhat lower than those reported by Agrawal and Tratnyek (*14*). These differences may be due to the specific nature of the buffers and the elemental iron used in each case. In our study, the elemental iron was used without pretreatment, and therefore the initial reactive surface areas may have been somewhat different than those used by Agrawal and Tratnyek (*14*).

Aniline Sonolysis

The final observed product of nitrobenzene reduction by Fe^0 is aniline, which is a well-known corrosion inhibitor. The mechanism of inhibition is believed to involve an

interference with mass transport of the primary oxidant to the metal surface, which in turn is strongly influenced by the orientation of the sorbed aniline. The sonolytic degradation of aniline is a first-order reaction with an apparent rate constant of 2.4×10^{-3} min^{-1} at 20 kHz with an input power density of 139 W L^{-1}. In this case, there is no enhancement due to the presence of Fe^0 surfaces because aniline cannot be reduced by Fe^0. The observed rate enhancements in the reduction of nitrobenzene in the combined US/Fe^0 system could also be due to the degradation of aniline by sonolytic cavitation. The degradation of aniline with US or the combined US/Fe^0 (35 g L^{-1}) system has the same observed rate constants. This result indicates that the sonolyses are not affected by Fe^0 and the enhancement of nitrobenzene degradation by US/Fe^0 is mainly due to a faster rate of nitrobenzene reduction by Fe^0 in the presence of ultrasound.

The rate constants, for the sonolytic degradations of nitrobenzene and aniline are smaller than those observed for CCl_4 (*16*). This may be due to the lower tendency for the substituted benzenes to partition into the vapor phase of the cavitation bubbles due to their lower Henry's Law constants (*17*). The principal observed intermediate during aniline sonolysis is benzoquinone. The possible mechanism for the degradation of aniline by sonication is as follows:

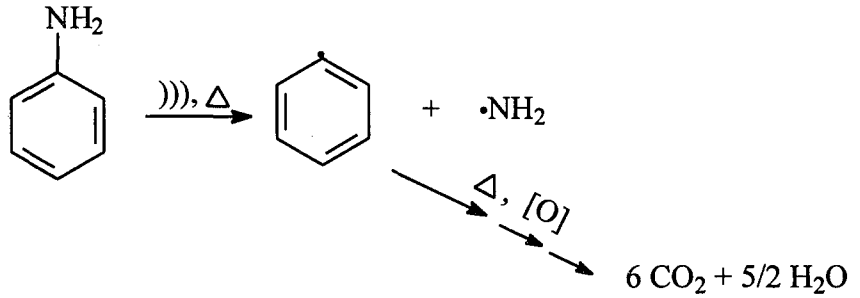

(22)

$$\bullet NH_2 + \bullet OH \longrightarrow NH_2OH \xrightarrow{+\bullet OH} NHOH + H_2O \qquad (23)$$

$$NHOH + {}^{\bullet}OH \longrightarrow {}^{\bullet}NHO + H_2O \quad (24)$$

$${}^{\bullet}NHO + {}^{\bullet}OH \longrightarrow NO + H_2O \quad (25)$$

$$NO + {}^{\bullet}OH \longrightarrow HONO \quad (26)$$

$$HONO + {}^{\bullet}OH \longrightarrow NO_2 + H_2O \quad (27)$$

$$NO_2 + {}^{\bullet}OH \longrightarrow HNO_3 \quad (28)$$

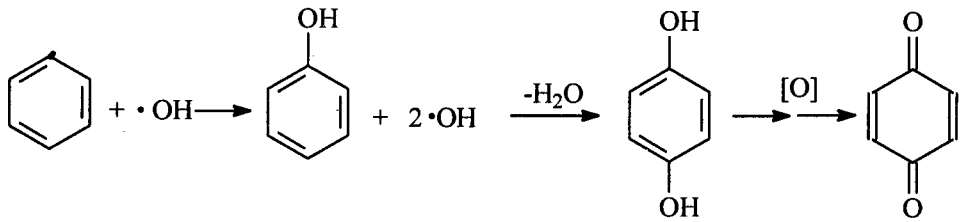

(29)

Identification of By-products and Reaction Intermediates

The intermediates observed at relatively high concentrations during nitrobenzene sonication at 20 kHz are meta-nitrophenol, para-nitrophenol and 4-nitrocatechol (*17*). These intermediates are eventually decomposed sonochemically to CO_2 and HNO_3. In this study, nitrosobenzene and aniline were observed as the main intermediates in the presence of Fe^0. Other reaction intermediates such as 4-nitrocatechol and benzoquinone have concentrations less than 1 μM in the combined US/Fe^0 systems and are ignored in Figure 3 (a). The nitrophenols (eq. 4) were not observed. This may be due to a fast transformation rate to 4-nitrocatechol such that the nitrophenols concentrations were kept below the detection limits under current experimental conditions. The relative effects of sonication on the observed intermediates and the total mass balance around nitrobenzene are shown in Figure 3. After 3 hours of reaction, the total mass of aromatic compounds does not change in the mechanically agitated Fe^0 system but is decreased by 12% in US system and by 40%

in the combined US/Fe^0 system. The principal intermediate, aniline, which is not degraded by Fe^0, is eventually destroyed by ultrasound. The array of aromatic compounds observed during nitrobenzene degradation should be more efficiently decomposed in the combined US/Fe^0 systems. The higher concentration of aniline in US/Fe^0 systems suggests that the nitrobenzene degradation rate is apparently enhanced from the reduction of nitrobenzene by Fe^0.

Effects of Ultrasonic Power Density

The reduction of nitrobenzene by Fe^0 occurs at the Fe^0/H_2O interface. The heterogeneous reactions involves five steps (*3,22*): (i) mass transfer of the reactant to the Fe^0 surface from the bulk solution; (ii) adsorption of the reactant on the surface; (iii) chemical reaction at the surface; (iv) desorption of the products from the surface; and (v) mass transfer of the products into the bulk solution. Any one of these steps may be rate limiting and, therefore, be reflected in the values of k_{obs} reported in this study. To properly interpret trends in the observed reaction rates, it is important to distinguish between mass transport and reaction-limited kinetics.

A common criterion for detecting mass transfer-limited kinetics is a variation in the reaction rate with the intensity of mixing. An increase in ultrasonic power will increase the mixing intensity due to the turbulence generated by cavitational bubble collapse. The ultrasonic power levels adjusted by changing the ultrasound power amplitude and the corresponding calorimetry results are given in Table 3. The reactions taking place at an Fe^0 loading of 35 g L^{-1} are pseudo first-order. Under these conditions, the relative enhancement in the nitrobenzene reduction rate increases with increasing sonication power. For example, when the applied power density is increased from 39 to 73 W L^{-1}, the reaction rate is approximately doubled. However, when the power density is increased further to 139 W L^{-1}, the reaction rate is only increased another 50%. As reported

previously (*16*), the efficiency of energy transfer to solution decreases with higher power densities due to a greater loss of input energy as heat. The observed rate constants are directly proportional to the power density at low power inputs; however, at high input powers the relationship becomes non-linear. Furthermore, at higher sonication intensities, the Fe^0-corrosion pathways (eqs. 10, 11) are enhanced and thus the net degradation rate of nitrobenzene is no longer directly proportional to the sonication power.

In this study, we demonstrated that the rate of nitrobenzene reduction by Fe^0 could be enhanced in the presence of ultrasound. The higher apparent rates of reaction in the combined US/Fe^0 systems compared to Fe^0 reaction alone can be attributed primarily to the continuous cleaning and activation of the Fe^0 surface by the chemical and physical effects of ultrasound. Furthermore, the rates of mass transport rates of nitrobenzene, nitrosobenzene and aniline to and from the Fe^0 surface are enhanced by hydrodynamic cavitation. Oxidation of the reaction intermediates during sonication also contributes to the observed rate enhancements. The relative concentrations of the principal reaction intermediates in US/Fe^0 systems, nitrosobenzene and aniline appear to be influenced significantly by total available surface area of Fe^0. In conclusion, the combination of ultrasound and Fe^0 appears to have a positive synergistic effect on the reduction of nitro aromatic compounds.

Acknowledgments

Financial support from the Office of Naval Research (NAV5-N0001492J1901; NAV1-N47408-97-M-0771) and the Department of Energy (DOE 1 963472402) is gratefully acknowledged.

References

1. Cheung, H. M.; Bhatnagar, A.; Jansen, G. *Environ. Sci. Technol.* **1991**, *25*, 1510-1512.
2. Hua, I.; Hoffmann, M. R. *Environ. Sci. Technol.* **1996**, *30*, 864-871.
3. Mason, T. J.; Lorimer, J. P. *Sonochemistry: Theory, Application and Uses of Ultrasound in Chemistry*; John Wiley &Sons: New York, 1988.
4. Suslick, K. S.; Hammerton, D. A.; Cline, R. E. *J. Am. Chem. Soc.* **1986**, *108*, 5641-5642.
5. Mason, T. J. *Practical Sonochemistry: User's Guide to Application in Chemistry and Chemical Engineering*; Ellis Horwood, 1991.
6. Fennelly, J. P.; Roberts, A. L. *Environ. Sci. Technol.* **1998**, *32*, 1980-1988.
7. Matheson, L. J.; Tratnyek, P. G. *Environ. Sci. Technol.* **1994**, *28*, 2045-2053.
8. Tratnyek, P. G.; Johnson, T. L.; Scherer, M. M.; Eykholt, G. R. *Ground Water Monitoring & Remediation* **1997**, *XVII*, 108-114.
9. Scherer, M. M.; Westall, J. C.; Ziomek-Moroz, M.; Tratnyek, P. G. *Environ. Sci. Technol.* **1997**, *31*, 2385-2391.
10. Johnson, T. L.; Fish, W.; Gorby, Y. A.; Tratnyek, P. G. *J. Contam. Hydrol.* **1998**, *29*, 377-396.
11. Gillham, R. W.; Ohannesin, S. F. *Ground Water* **1994**, *32*, 958-967.
12. Lipczynskakochany, E.; Harms, S.; Milburn, R.; Sprah, G.; Nadarajah, N. *Chemosphere* **1994**, *29*, 1477-1489.

13. Johnson, T. L.; Scherer, M. M.; Tratnyek, P. G. *Environ. Sci. Technol.* **1996**, *30*, 2634-2640.

14. Agrawal, A.; Tratnyek, P. G. *Environ. Sci. Technol.* **1996**, *30*, 153-160.

15. Reinhart, D. R.; Clausen, C.; Geiger, C.; Ruiz, N.; Afiouni, G. F. *"Enhancement of In-Situ Zero-Valent Metal Treatment of Contaminated Groundwater"* in Non-aqueous phase liquids in surface environment: assessment and remediation; American Society of Civil Engineers: Washington, D. C., **1996**, 323-332.

16. Hung, H.-M.; Hoffmann, M. R. *Environ. Sci. Technol.* **1998**, *32*, 3011-3016.

17. Weavers, L. K.; Ling, F. H.; Hoffmann, M. R. *Environ. Sci. Technol.* **1998**, *32*, 2727-2733.

18. Wakeford, C. A.; Blackburn, R.; Lickiss, P. D. *Ultrasonics Sonochemistry* **1999**, *6*, 141-148.

19. Carvalho, L. R. F.; Souza, S. R.; Martinis, B. S.; Korn, M. *Analytica Chimica Acta* **1995**, *317*, 171-179.

20. Hua, I.; Hoffmann, M. R. *Environ. Sci. Technol.* **1997**, *31*, 2237-2243.

21. Kotronarou, A.; Mills, G.; Hoffmann, M. R. *J. Phys. Chem.* **1991**, *95*, 3630-3638.

22. Spiro, M. *"Heterogeneous Catalysis of Solution Reactions"* in Chemical Kinetics; Elsevier: Amsterdam, **1989**, 69-166.

Table 1. HPLC retention times and specific topic data for nitrobenzene (NB) and its sonolysis reaction intermediates.

	λ	Average Retention Time	ε
NB	267 nm	~4.5 min	6.36×10^6 M^{-1} cm^{-1}
NSB	307 nm	~5.5 min	6.60×10^6 M^{-1} cm^{-1}
AN	224 nm	~2.0 min	4.85×10^6 M^{-1} cm^{-1}
ONP	224 nm	~1.5 min	4.56×10^6 M^{-1} cm^{-1}
MNP	224 nm	~2.4 min	7.37×10^6 M^{-1} cm^{-1}
PNP	318 nm	~2.2 min	8.53×10^6 M^{-1} cm^{-1}
4-NC	224 nm	~3.7 min	5.71×10^6 M^{-1} cm^{-1}

NB = nitrobenzene

NSB = nitrosobenzene

AN = aniline

ONP = o-nitrophenol

MNP = m-nitrophenol

PNP = p-nitrophenol

4 – NC = 4-nitrocatechol

Table 2: Comparison of k values for nitrobenzene degradation in the combined US/Fe^0 system (ultrasound power amplitude: 35%) and on the rotary shaker system.

$[Fe^0]$, g L^{-1}	$k_{US} + k_{Fe^0}$, $min^{-1} \cdot 10^3$	k_{Fe^0}, $min^{-1} \cdot 10^3$	$k_{sec}\, k_p$, $min^{-2} \cdot 10^5$	$k_{10\ rpm/Fe^0}$, $min^{-1} \cdot 10^3$
0	1.8 (± 0.1)	0	0	0
18	2.9 (± 0.1)	1.1	0	0.8
35	5.9 (± 0.2)	4.1	~ 0	1.5
53	6.9 (± 0.4)	5.1	2.8 ± 0.5	3.5
70	7.8 (± 0.4)	6.0	9.8 ± 0.5	4.8
88	12.4 (± 1.5)	10.6	21.0 ± 2.4	9.9

Table 3. The ultrasonic applied power and the corresponding absorbed power as determined by calorimetry.

Applied Power (W)	140	80	40
Absorbed power (W)	40	21	11
Power density, W L^{-1}	139	73	39
k_{US}, min^{-1}	1.8×10^{-3}	1.4×10^{-3}	0.7×10^{-3}
$k_{US+35gL^{-1}Fe^0}$, min^{-1}	6.1×10^{-3}	4.8×10^{-3}	2.4×10^{-3}

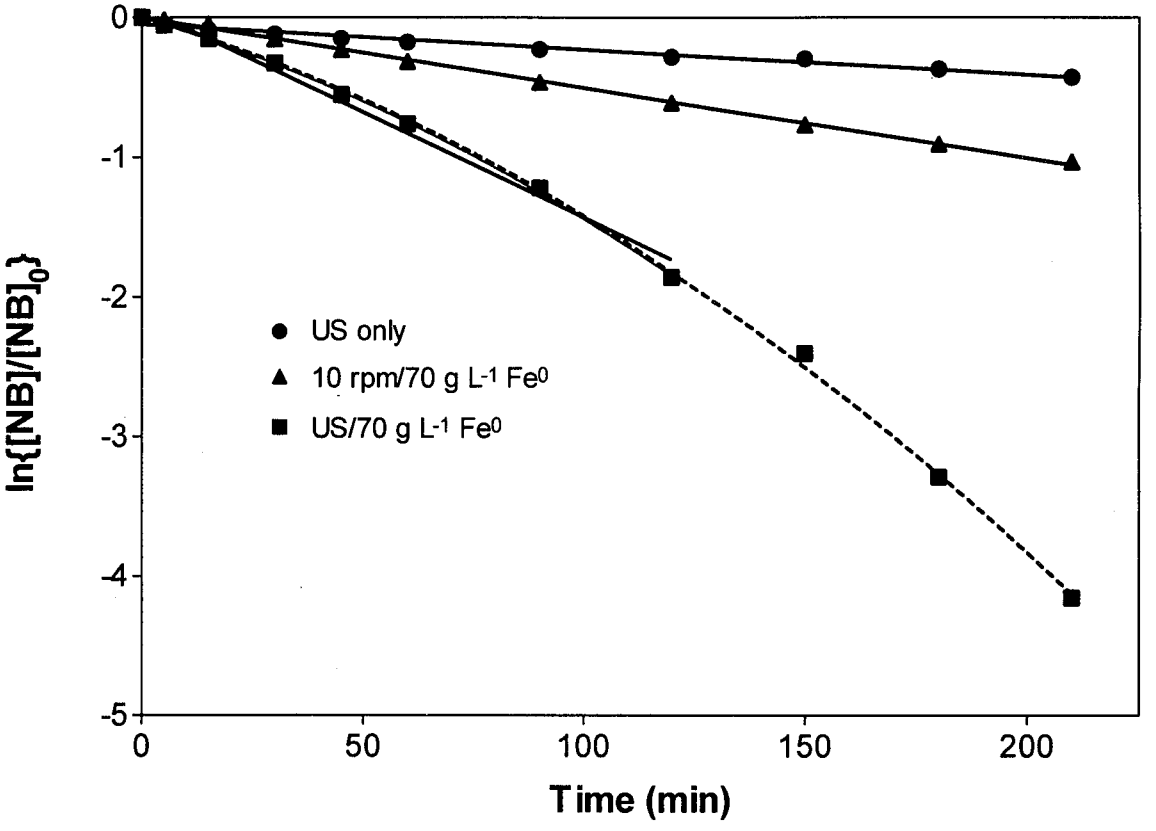

Figure 1. The degradation of nitrobenzene by ultrasound (•), 10 rpm/70 g L^{-1} Fe^0 (▲) and US/70 g L^{-1} Fe^0 (■); the solid lines are the fitted results from the first-order analysis and the dashed line is the second-order fitting from eq. 16 for US/70 g L^{-1} Fe^0.

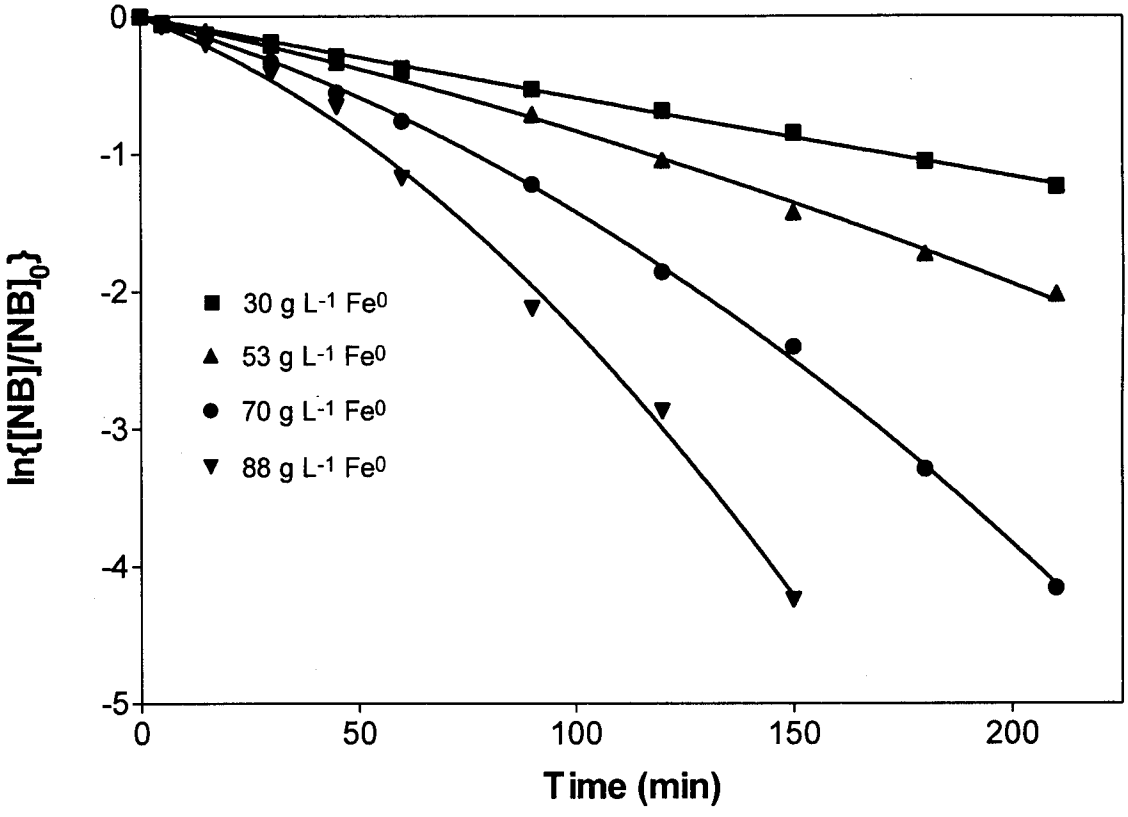

Figure 2. The fitted results from eq.16 in the combined US/Fe^0 systems as a function of [Fe^0].

Figure 3(a)

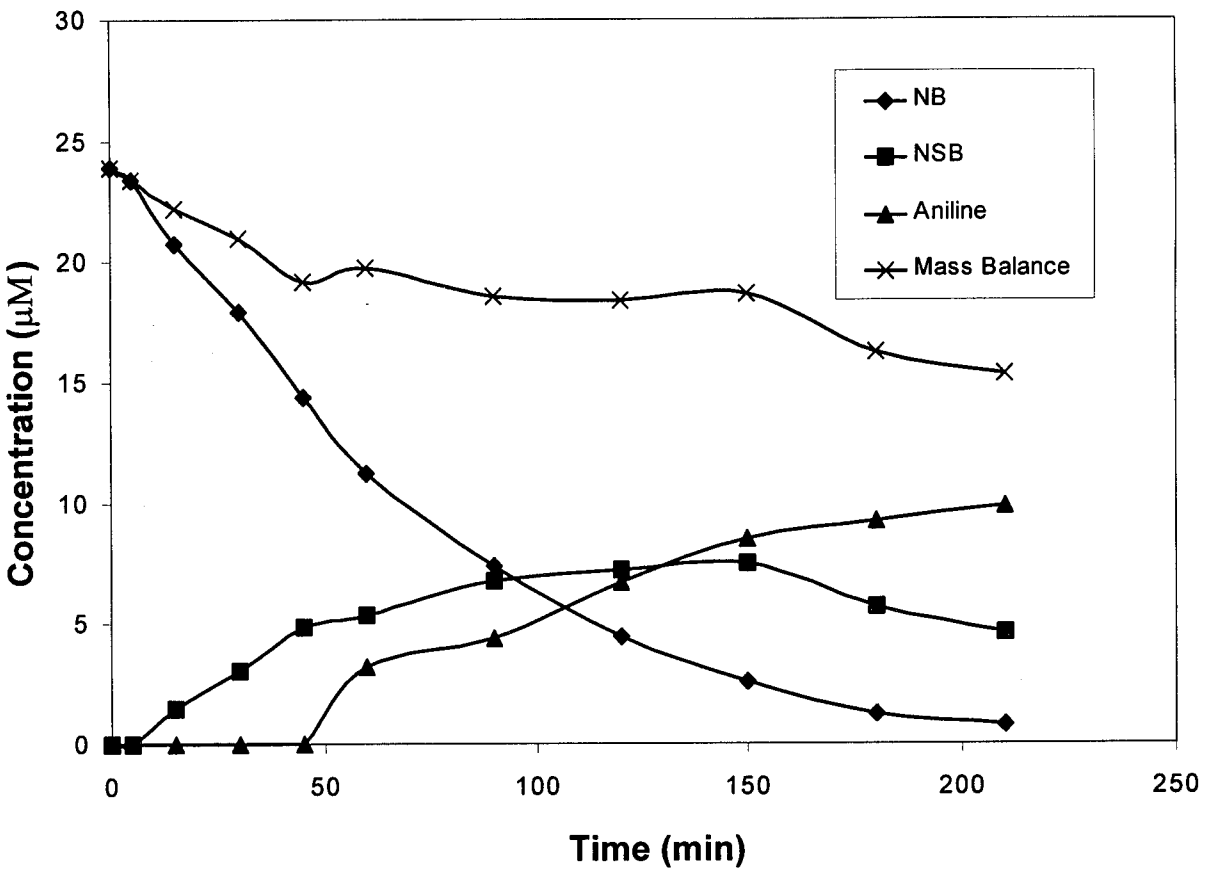
30
25
20
15
10
5
0
Concentration (μM)
0
50
100
150
200
250
Time (min)
NB
NSB
Aniline
Mass Balance

Figure 3(b)

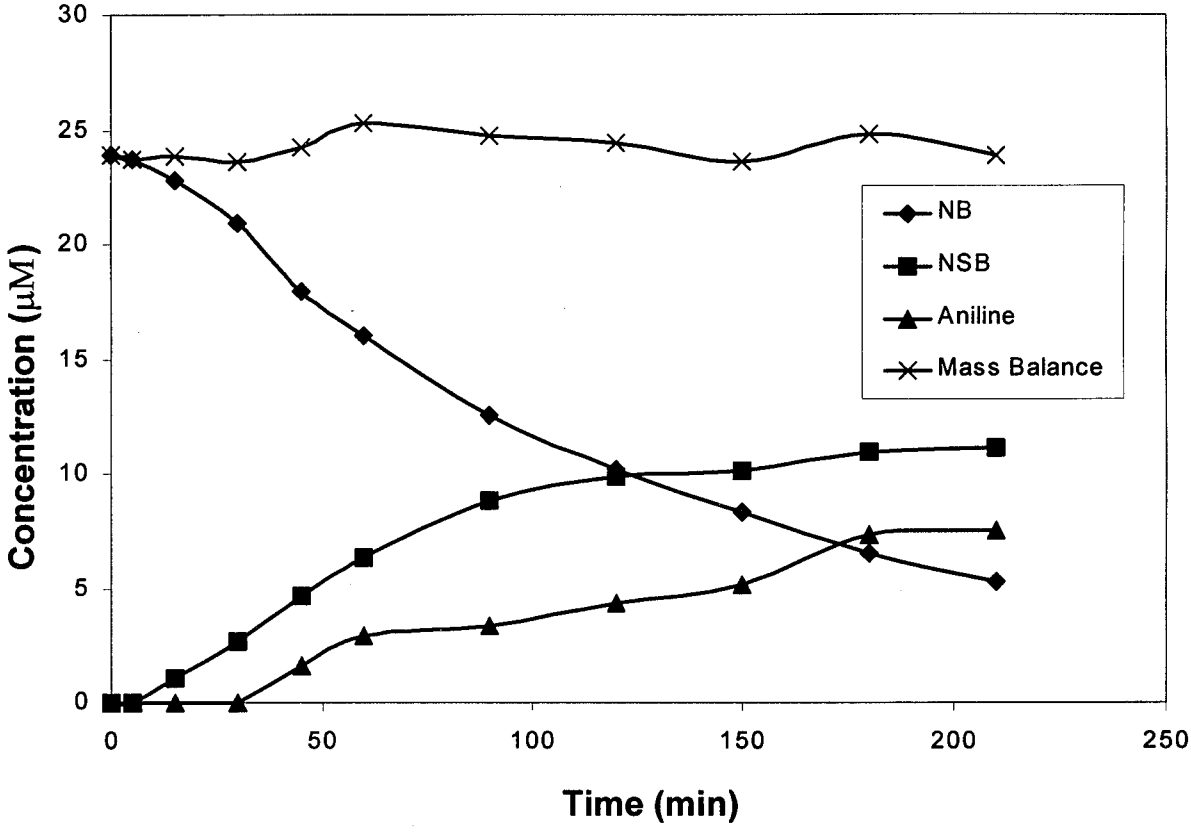

Figure 3. The concentrations of the reactant, intermediates and products as a function of time. (a) in the US/70 g L^{-1} Fe^0 system; and (b) in the10 rpm/70 g L^{-1} Fe^0 system.

Chapter 7

The Sonolytic Destruction of Methyl Tertiary Butyl Ether (MTBE) by Ultrasonic Irradiation: The Role of O_3, H_2O_2, Frequency and Power Density

(*Environmental Science & Technology*, **1999**, 3: (18) 3199-3205)

Abstract

The sonolysis in the presence of ozone has been used to investigate the degradation of methyl tertiary-butyl ether (MTBE). The effects of different ultrasonic frequencies and power levels combined with various ozone concentrations were also investigated. Experiments were performed at the frequency range of 205 to 1078 kHz. For sonolysis only or sonolysis in the presence of ozone, the higher overall reaction rates were observed at 358 and 618 kHz than at 205 and 1078 kHz. The pseudo first-order rate constant, k_o, for MTBE degradation increased with increasing power density up to 250 Watts/L. A linear dependence of the first-order rate constant for the simultaneous degradation of O_3 on power density was also observed. In addition, the naturally-occurring organic matter (NOM), which might affect the oxidation rate of advanced oxidation process (AOP), has a negligible affection in this study.

Introduction

Methyl tertiary butyl ether, which is blended into gasoline, is frequently found in groundwater, where it is slowly degraded by aerobic and anaerobic processes (*1*).

The use of ultrasound for the treatment of chemical contaminants in water has been investigated in recent years (*2-8*). Ultrasonic waves, which consist of compression and rarefaction cycles, produce cavitation bubbles in liquid solution. After several compression cycles, the cavitation bubbles collapse violently and adiabatically with extremely high temperatures up to 5000 K and pressures of 975 bar (*9,10*). Under these extreme conditions, volatile chemical compounds are destroyed by direct pyrolysis reactions and indirectly by reactions with H•, •OH, O•, and H_2O_2. The addition of ozone into sonolytic systems often enhances the overall rate of destruction of a wide variety of compounds (*6,11,12*).

The thermal decomposition of ozone in the cavitation bubbles leads to the formation of •OH as shown in eqs. 1 and 2 (*11,13*):

$$O_3 \longrightarrow O_2 + O(^3P) \qquad (1)$$

$$O(^3P) + H_2O \longrightarrow 2 \cdot OH \qquad (2)$$

In addition, the direct reaction of ozone with substrates may occur.

In our proceeding paper (*14*), the kinetics and mechanism of sonolytic degradation of MTBE were investigated at a single ultrasonic frequency of 205 kHz. The addition of ozone into the aqueous sonolytic system resulted in an increased rate of MTBE destruction. The generalized reactions can be described by the following equations.

$$(CH_3)_3COCH_3 \xrightarrow{))),\ H_2O} (CH_3)_3COH + CH_3OH \qquad (3)$$

$$(CH_3)_3COCH_3 \xrightarrow{))),\ O_3,\ H_2O} (CH_3)_3COH + HCO_2H \quad (4)$$

$$(CH_3)_3COH \xrightarrow{))),\ H_2O} \rightarrow (CH_3)_3CO_2H, CH_3OH, HCHO \quad (5)$$

$$(CH_3)_3COCH_3 \xrightarrow{))),\ O_3} \rightarrow (CH_3)_3COOCH_3 \xrightarrow{)))} \rightarrow CH_3OH, HCO_2H \quad (6)$$

where the symbol,))), indicates ultrasonic irradiation. The main intermediates observed during MTBE sonolysis and ozonolyis are tert-butyl formate, tert-butyl alcohol. In this paper, the combined effects of sonolysis and ozonolysis on the kinetics of MTBE degradation are explored over a broader frequency range.

Experimental Methods

MTBE (99.9%; EM science) and sodium bicarbonate (Reagent Grade; EM Science) were used without further purification. A humic acid reagent was prepared by dissolving solid humic acid obtained from Fluka AG in a 0.1 N NaOH solution and then filtered through 0.45-μm filter paper.

Ultrasonic irradiations were performed with an Ultrasonic Transducer USW 51 (AlliedSignal ELAC Nautik, Inc.) in a glass and titanium reactor having vibrational area of 25 cm^2, and operated at four different frequencies: 205, 358, 618, and 1078 kHz. The reactor as shown in Figure 1 is a 600 mL cylindrical double-walled (cooling jacket) reaction vessel that has 4 sampling ports on the top that are used for gas venting, for withdrawing aqueous samples, and for the introduction of background gases.

Temperature was maintained constant at 23 ± 3 °C with a 20 °C water bath (Haake Co., model A80). Aqueous solution were made with water obtained from a MilliQ UV plus purification system, while O_3 solutions were prepared with an Orec Ozonator (Model V10-0) by bubbling ozone into deionized water at a flow rate of 100 mL min^{-1} through a

glass fritted diffuser until the desired ozone concentration in the aqueous phase was obtained. A HP 8452 Diode Array Spectrophotometer was used to determine the target ozone concentration. The molar extinction coefficient for O_3 in water at 260 nm is 3300 M^{-1} cm^{-1}.

MTBE stock solutions (100 mM) were prepared and stored at 4 °C. After the desired aqueous ozone concentration was obtained, an appropriate volume of the MTBE stock solution was spiked into 500 mL of ozonated solution; it was mixed further by bubbling additional O_2/O_3 gas for a few more seconds at a low flow rate in order to minimize any sparging effects. The first sample was taken right after the closing of ozone supply and then the sonolytic irradiation was started. 1 mL of sample was taken at appropriate time intervals during each run and stored in 20 mL Teflon-faced aluminum sealed vials. In the case of dissolved ozone, 10 μL of 1 N-$Na_2S_2O_3$ was used to quench the residual aqueous ozone to preserve samples prior to the analysis. Since the total amount of samples withdrawn from the reactor was kept less than 15 mL, only a small error (< 3%) was introduced due to the differential volume change. During each run, the ultrasonic power inputs was kept in the range of 50 Watts to 240 Watts depending on the particular frequency that was used. For frequencies greater than 600 kHz, the maximum power was 50 Watts.

Compounds extracted into the gas phase of head-space sample in the HP 7694 Headspace sampler were auto-injected into a HP 5890 series II GC-FID equipped with a HP-624 capillary column (30 m x 0.32 mm x 1.8 um) with 70 °C isothermal oven temperature. Sample aliquots for hydrogen peroxide analysis were taken at 10 minute intervals and were measured by spectrofluorometer (*9*). Samples taken for TOC (Total

Organic Carbon) analysis were filtered with 0.45-μm Teflon syringe filters (Gelman) before injection and were measured with a Shimadzu 5000A total organic carbon analyzer.

For some runs, the aqueous ozone concentrations were continuously measured spetrophotometrically with circulating the aqueous solution from the reactor through the spectrophotometer and back into the reactor.

Results and Discussion

Effects of Applied Power Input

In our earlier study, which was carried out at 205 kHz, the sonolytic degradation of MTBE was shown to follow pseudo first-order kinetics. Plots of the pseudo first-order rate constants, k_0, versus the input power density are shown in Fig. 2 for sonolytic irradiation 205 kHz and 358 kHz with initial MTBE concentrations of 1 mM and 0.05 mM, respectively. The apparent rate constant, $k_{0,358}$, at 358 kHz is higher than $k_{0,205}$. by a factor of 5. From our previous study (*14*), the MTBE sonication rate constant at 205 kHz was found to be faster with $[MTBE]_0$ = 0.05 mM than for $[MTBE]_0$ = 1 mM by a factor of 2 (i.e., the rate decreases with increase initial substrate concentration). Furthermore, as shown in Fig. 2, k_0 increases rapidly with an increase in power density up to 240 Watts/L. In general, an increase in power density results in an increase in the observed sonochemical reaction rate. However, the cavitation bubble size, the bubble collapse time, the transient temperature, and the internal pressure in the cavitation bubble during collapse are all dependent on the power intensity. For example, the power intensity which is proportional to the applied power density, is a function of the acoustic amplitude, P_A, as follows:

$$I = P_A^2 / 2\rho c \qquad (7)$$

where I is the sound intensity (amount of energy flowing per unit area per unit time), ρ is the density of the medium and c is the velocity of sound in the medium.

For a cavitation bubble, the maximum bubble size is dependent on the density of the liquid, the applied frequency, the hydrostatic pressure, and the acoustic pressure as follows (*9*):

$$R_{\max} = \frac{4}{3\omega_a}(P_A - P_h)\left(\frac{2}{\rho P_A}\right)^{1/2}\left[1 + \frac{2}{3P_h}(P_A - P_h)\right]^{1/3} \qquad (8)$$

where ω_a is the applied acoustic frequency and P_h is the external (hydrostatic) pressure, which is 1 atm under our experimental conditions. In addition, the bubble collapse time, τ, is proportional to the maximum bubble size, R_m (*9*):

$$\tau = 0.915 R_m (\rho / P_m)^{1/2}(1 + P_{vg} / P_m) \qquad (9)$$

where P_m is the pressure in the liquid, (i.e., $P_m = P_h + P_a$), and P_{vg} is the vapor pressure in the bubble. Therefore, at high acoustic intensity (i.e., large P_A values) the cavitation bubbles are able to grow to a larger size during a rarefaction cycle such that insufficient time is available for complete collapse during a single compression cycle. As the above equations predict and the experimental results show, there is an optimum power density which can be applied during sonochemical irradiation in order to obtain the maximum reaction rate.

Effects of Variable Frequencies on H_2O_2 Production

In an attempt to determine the optimum frequency to obtain the most beneficial chemical effects, hydrogen peroxide production was used as a direct indicator of free radical production. Hydrogen peroxide is known to be produced during sonolysis of water

(*5,9,13*). During sonolysis, hydrogen atoms and hydroxyl radicals are formed due to the pyrolytic decomposition of water.

$$H_2O \rightarrow H\cdot + \cdot OH \qquad (10)$$

Hydroxyl radicals can recombine to form hydrogen peroxide:

$$\cdot OH + \cdot OH \rightarrow H_2O_2 \qquad (11)$$

If O_2 is present in the vapor phase of bubble, peroxide can also be produced via the production of the hydroperoxyl radical as follows:

$$H\cdot + O_2\cdot \rightarrow HO_2\cdot \qquad (12)$$

$$HO_2\cdot + HO_2\cdot \rightarrow H_2O_2 + O_2 \qquad (13)$$

Since the recombination reaction rate constants of $HO_2\cdot$ and $\cdot OH$ at 298 K are 8.3×10^5 M^{-1} s^{-1} and 5.5×10^9 M^{-1} s^{-1} in solution (*15*) and 3×10^{-12} cm^3 $molecule^{-1}$ s^{-1} (*16*) and 1.5×10^{-11} cm^3 $molecule^{-1}$ s^{-1} (*17*) in gas phase, respectively, the $\cdot OH$ recombination reaction should be the major route for the hydrogen peroxide formation. The sonolytic production rates of H_2O_2 in O_2 saturated solutions relative to Ar-saturated solutions were compared at 205 kHz with a power density of 240 Watts/L. The apparent H_2O_2 production rates for these two conditions were found to be identical, i.e., $d[H_2O_2]/dt = 3.5 \times 10^{-4}$ mM min^{-1}. This result supports the argument that the self-reaction (eq. 11) of OH is the principal pathway for H_2O_2 production.

Recombination of $OH\cdot$ to form H_2O_2 most likely takes place in the bubble phase instead of the liquid phase (*18*). It should also noted that hydrogen peroxide is the most likely $OH\cdot$ scavenger ($k_{OH,\,H_2O_2} = 2.7 \times 10^7$ $M^{-1}s^{-1}$) in the absence of other $OH\cdot$ scavengers (*19*).

$$OH\cdot + H_2O_2 \rightarrow HO_2\cdot + H_2O \qquad (14)$$

The rate of hydrogen peroxide production during the sonolysis of water is given by the eq. 15:

$$\frac{d[H_2O_2]}{dt} = k_{OH,OH}[OH][OH] + k_{HO_2,HO_2}[HO_2][HO_2] - k_{OH,H_2O_2}[OH][H_2O_2] - k_{pyr}[H_2O_2] \quad (15)$$

The actual production rates of ·OH and H_2O_2 during sonolysis will be affected by the bubble collapse temperature, the collapse pressure, and the bubble lifetime.

Plots of hydrogen peroxide (H_2O_2) production versus time with a power input of 240 Watts/L is shown in Fig. 3(a) for four different sonolytic frequencies: 205, 358, 618, and 1078 kHz. At a power input of 100 Watts/L, a similar trend with a variation in frequency is observed in Fig. 3(b). However, in this case the rates of H_2O_2 production are lower due to the lower applied power density (i.e., lower P_A). $d[H_2O_2]/dt$ at 240 Watts/L is approximately twice that at 100 Watts/L and is clearly highest at 358 kHz and lowest at 1078 kHz. From the data shown in Fig. 3(a), it is worthwhile to note that peroxide production at 358 kHz is non-linear whereas for the other frequencies it is linear. This may be due to the fact that the self-scavenging reaction between OH radical and H_2O_2 (eq. 14) becomes significant as peroxide accumulate in the liquid phase. Hua and Hoffmann (*5*) reported that $d[H_2O_2]/dt$ increased with increasing frequency for 20, 40, 80, and 500 kHz. However, it is noted that the peroxide production rate is the lowest at the highest applied ultrasonic frequency of 1078 kHz. At these very high frequencies, the rarefaction (and compression) cycles are very short. The time required for the rarefaction cycle is too short to permit a cavitation bubble to grow to a size sufficient to cause optimal disruption of the liquid.

The I_2 (I_3^-) production rate during sonolysis at four different frequencies is shown in Fig. 4. The iodine formation rate can be related to the ·OH production rate by a stoichiometric factor of two. The sequence of I^- oxidation is as follows:

$$\cdot OH + I^- \longrightarrow OH^- + I\cdot \quad (16)$$

$$I\cdot + I^- \longrightarrow I_2^{\cdot -} \quad (17)$$

$$I_2^{\cdot -} + I\cdot \longrightarrow I_3^- \quad (18)$$

$$I_2^{\cdot -} + OH\cdot \longrightarrow I_2 + OH^- \quad (19)$$

$$I_2 + I^- \rightleftharpoons I_3^- \quad (20)$$

Again, the optimum frequency for I_2 (I_3^-) production at 293 K and I_a = 84 Watts L^{-1} is located between 358 and 618 kHz. This result is similar to that observed for H_2O_2 production although the reaction volume for H_2O_2 can be with the vapor phase of the collapsing bubble or within the interfacial region of the bubble, whereas I_3^- formation is restricted to the liquid phase (*20*).

Enhancement Effects of O_3 on MTBE degradation at 205 kHz and 358 kHz

The combination of O_3 and ultrasound at 205 kHz has been shown to enhance the MTBE degradation rate (*14*). In this study, the enhancement effect of O_3 in sonolytic MTBE degradation at 358 kHz was investigated and compared with the 205 kHz data (Table 1). The direct reaction of MTBE with ozone has pseudo-first-order constant of 6×10^{-5} s^{-1} for $[MTBE]_0 = 0.01$ mM and 6.7×10^{-6} s^{-1} for $[MTBE]_0 = 1$ mM. These reaction rates are small enough to be ignored when compared with the effects of sonication. From Table 1, it is clear that the combination of O_3 and ultrasound increases k_0. The

enhancement in k_0 is greater at lower $[MTBE]_0$. The enhancement factors (k_0 (O_3-Ultrasound)/k_0 (Ultrasound)) for 205 kHz and 358 kHz are very similar at higher initial MTBE concentrations and increase slowly as $[MTBE]_0$ decreases. However, at lower concentrations (i.e., 0.01 mM), the enhancement factor for 358 kHz (5.4) is higher than it is at 205 kHz (3.9). The k_o ratios at 358 kHz and 205 kHz for the US system alone and the combined O_3-US system are also given in Table 1. For the US alone system, k_o at 358 kHz was greater than at 205 kHz by a factor of 1.7 to 2.2. Similarly, in the case of the O_3-US system, the k_o at 358 kHz was greater at lower $[O_3]_0$.

The Role of Ozone in Sonochemistry

The combination of ozone and sonolysis was found to be signnificantly more effective in degrading MTBE than either ultrasound or O_3 alone (*14*). To illustrate the mechanism of ozone enhancement in the sonochemical process, the role of ozone in the sonolysis process was studied at the other target frequencies. In this study, the sonolysis rate of ozone was investigated as a function of frequency, power density, and $[MTBE]_0$. Aqueous ozone concentrations were determined by using continuous flow spectrophotometry at $\lambda = 260$ nm, where $\varepsilon = 3300\ M^{-1}\ cm^{-1}$.

In order to observe the relative effects of frequency on the ozone decomposition rate during sonication, initial aqueous ozone concentrations were adjusted to 0.13 - 0.15 mM before sonication and the aqueous ozone concentrations were monitored at 10-second intervals. Experiments were performed at a fixed power density of 100 Watts/L for all frequencies in a 1.0 mM bicarbonate [HCO_3^-] solution. As shown in Fig. 5, the sonolytic degradation rate of ozone is found to be first-order at all frequencies. Thus, the apparent rate equation for the sonolytic degradation of O_3 by sonolysis is given by eq. 21:

$$-d[O_3]/dt = k_d[O_3] \quad (21)$$

where k_d is the apparent first-order degradation rate constant. Based on the data, k_d is lowest at the highest ultrasonic frequency, 1078 kHz, while the measured rates at the other frequencies are nearly the same.

The relative effect of applied power density on the ozone decay rate was investigated at 358 kHz in 1.0 mM bicarbonate spiked distilled water. As shown in Fig. 6, a linear dependence of the first-order rate constant for ozone with a variation of power density can be quantified as follows:

$$k_d = \gamma_o + \gamma P \quad (22)$$

Where γ_o is the ozone decay rate in the absence of ultrasound (0.0011 s^{-1}), i.e., the rate due to the base catalyzed reaction ($k_{O_3,OH^-}[OH^-]$), γ is the slope of the k_d vs. P line (7.0 x 10^{-5} L sec^{-1} $Watt^{-1}$), and P is the power density in Watts/L. The overall decomposition rate, k_d, is the sum of the rate due to the base-catalyzed reaction pathway, the in situ thermal (pyrolysis) decomposition rate, and the ozone decay rate due to the conjugate base of H_2O_2 produced as a sonolysis intermediate.

$$H_2O_2 \rightleftarrows HO_2^- + H^+, \quad pK_a = 11.8 \quad (23)$$

Thus, k_d is given by:

$$k_d = k_{O_3,OH^-}[OH^-] + k_{O_3,pyr} + k_{O_3,HO_2^-} 10^{pH-pKa}[H_2O_2] \quad (24)$$

The effects of $[MTBE]_o$ on the ozone sonolytic decomposition rates are shown in Fig. 7. In the absence of sonication, the ozone decay rates were not affected by the $[MTBE]_o$ due to the negligibly low rate of the direct reaction of ozone with MTBE at ambient temperature. However, the effect of $[MTBE]_o$ on ozone decomposition rate is

significant for sonolytic ozonolysis as shown in Fig. 7. In this case, the ozone decomposed at a faster rate with increasing $[MTBE]_o$. Furthermore, as $[MTBE]_o$ increases, the ozone decomposition rates deviates from a strict first-order relationship. This effect may be attributed to the direct reaction of MTBE with ozone at the cavitation bubble interface area or to the enhanced ozone decomposition rate due to the increased H_2O_2 production in the presence of MTBE (*14*). Thus, in the presence of MTBE, the sonolytic decomposition rate of ozone, $d[O_3]/dt$, is given by:

$$-d[O_3]/dt = (k_d + k_{o_3,MTBE}[MTBE] + k_{O_3,HO_2^-}10^{pH-pKa}[H_2O_2])[O_3] \qquad (25)$$

where the first term represents the ozone decay rate in the absence of MTBE, and the 2nd and 3rd terms are the net increased rates of ozone decay when MTBE is present.

Under these conditions, the sonolytic degradation of MTBE in the presence of O_3 is given by:

$$[MTBE]_t = [MTBE]_o e^{-k_o t} \qquad (26)$$

$\Delta[H_2O_2]$ is the net increase of $[H_2O_2]$ in the combined system in the presence of MTBE compared to the MTBE-free sonolysis. The $\Delta[H_2O_2]$ vs. time profile obtained from measuring the $[H_2O_2]$ production rate at $[MTBE]_o$ = 0.5 mM relative to $[MTBE]_o$ = 0 mM is shown in Fig. 8. The apparent increase in $d[H_2O_2]/dt$ can be attributed to the following reactions (*14*):

$$H_2O \xrightarrow{)))\,\Delta} H\cdot + \cdot OH \qquad (27)$$

$$O_3 \xrightarrow{)))\,\Delta} O_2 + O\cdot \qquad (28)$$

$$(CH_3)_3COCH_3 + \cdot OH \rightarrow (CH_3)_3COCH_2\cdot + H_2O \qquad (29)$$

$$(CH_3)_3COCH_2\cdot + O_2 \rightarrow (CH_3)_3COCH_2O_2\cdot \quad (30)$$

$$(CH_3)_3COCH_2O_2\cdot + \cdot OH \rightarrow (CH_3)_3COCHO + H_2O_2 \quad (31)$$

The $[H_2O_2]$ contributed from MTBE is a complicated process. If we suppose the $\Delta[H_2O_2]$ vs. time is a 2nd-order polynomial equation as given by:

$$\Delta[H_2O_2]_t = A_2t^2 + A_1t \quad (32)$$

The fitted result is shown in Fig. 8 with $A_2 = 5.56 \times 10^{-8}$ and $A_1 = 2.0 \times 10^{-4}$. The influence to $[H_2O_2]$ from the first term is smaller than the second one at $t < 100$ min.

Substituting eqs. 26 and 32 into eq. 25, and rearranging in an integrated form yields:

$$-\ln[O_3]/[O_3]_o = k_d + (1-e^{-k_o t})k_{O_3,MTBE}[MTBE]_o/k_o + k_{O_3,HO_2^-}10^{pH-pKa}(A_1t^2/2 + A_2t^3/3) \quad (33)$$

where k_{O_3, HO_2^-} is the second order rate constant of O_3 and HO_2^- ($k_{O_3, HO_2^-} = 5.6 \times 10^6\ M^{-1}s^{-1}$) (*21*). The pK_a for H_2O_2 = 11.8 and the pH = 8.25 in the 1.0 mM of $[HCO_3^-]$. The rate constant, $k_{O_3, MTBE}$, is estimated by fitting the eq. 33 to the experimental data. The fitted result is shown in Fig. 9. In this case, $k_{O_3, MTBE} = 2.5\ M^{-1}\ s^{-1}$. This implies that the third term of eq. 33 mainly accounts for the deviation from the pseudo first-order kinetics. In addition, the apparent enhancement in $k_{O3,MTBE}$ may be due to enhanced mass transfer between the bubble and liquid in the presence of ultrasound.

Effects of Frequency and Ozone Concentration

The effects of frequency and ozone dose on the net MTBE degradation reaction rate were explored in order to obtain the overall optimal conditions. The pseudo first-order rate constant, k_o, versus ozone concentration and frequency is shown in Fig. 10. For each

frequency, ozone doses were varied from 0 to 0.19 mM at $[MTBE]_o$ = 0.5 mM at a power density of 100 Watts/L. From the 3-D plot, it can be seen that ultrasonic frequencies of 358 and 618 kHz are the most effective for MTBE degradation. Without O_3, the rate constant of the sonolysis of MTBE has an optimal value at 358 kHz with power density 100Watts/L. At the same power density, Petrier and Francony (*22*) reported the sonolysis of phenol, a less volatile compound than CCl_4, has an optimal rate constant at 200 kHz compared to 20, 500 and 800 kHz. Both studies have the similar trend: the rate constant increases with frequency before 500 kHz then decreases.

The resonance radius of the bubble as described by Mason (*21*) is proportional to frequency^{-1} so the surface area-to-volume ratio is larger at higher frequencies. The rectified diffusion rate could also be enhanced at higher frequencies. That is the reason that the rate constant is faster for 358 kHz than 205 kHz. For more higher frequencies, less transition bubbles happen, so H_2O in the bubble phase could not decompose without the extreme high temperature and pressure.

Effect of Background Organics

Naturally-occurring organic matter (NOM) and certain inorganic species in natural waters are potential competitive reactants for ·OH. Therefore, these background compounds might affect the oxidation rate of AOP processes. In order to test the potential impact of this competition during sonication, MTBE was sonolytically degraded in the absence and presence of NOM (2.1 and 4.2 mg/L). The prescribed concentration of NOM was prepared using commercial humic acid reagent (Fluka AG). As shown in Fig. 11 (a), the effect of NOM on the MTBE decomposition rate is negligible. The concentration of TOC as a function of time in the presence of humic acid is shown in Fig. 11(b). This result

confirms previous observations that the major reaction site for the MTBE with ·OH radical is in the vapor-phase cavitation bubble and not in the bulk aqueous phase (i.e., volatile compounds such as MTBE and CCl_4 are more rapidly decomposed during sonolysis than are the semi-volatile or non-volatile compounds).

The results of this study demonstrate that the combination of ozonation and sonication can degrade MTBE more effectively at an ultrasonic frequency of 358 kHz compared to the other three frequencies.

Acknowledgments

Financial support from the U. S. Department of Energy (DOE 1 963472402) via the Argonne National Laboratory (Dr. Robert Peters) is gratefully acknowledged.

References

1. Suflita, J. M.; Mormile, M. R. *Environ. Sci. Technol.* **1993**, *27*, 976-978.
2. Serpone, N.; Terzian, R.; Hidaka, H.; Pelizzetti, E. *J. Phy. Chem.* **1994**, *98*, 2634-2640.
3. Kotronarou, A.; Mills, G.; Hoffmann, M. R. *Environ. Sci. Technol.* **1992**, *26*, 1460-1462.
4. Kotronarou, A.; Mills, G.; Hoffmann, M. R. *J. Phy. Chem.* **1991**, *95*, 3630-3638.
5. Hua, I.; Hoffmann, M. R. *Environ. Sci. Technol.* **1997**, *31*, 2237-2243.
6. Hua, I.; Hoffmann, M. R. *Environ. Sci. Technol.* **1996**, *30*, 864-871.
7. Hua, I.; Hochemer, R. H.; Hoffmann, M. R. *J. Phy. Chem.* **1995**, *99*, 2335-2342.
8. Hua, I.; Hochemer, R. H.; Hoffmann, M. R. *Environ. Sci. Technol.* **1995**, *29*, 2790-2796.
9. Mason, T. J.; Lorimer, J. P. *Sonochemistry: Theory, Application and Uses of Ultrasound in Chemistry*; John Wiley & Sons: New York, 1988.
10. Flint, E. B.; Suslick, K. S. *Science* **1991**, *253*, 1397-1399.
11. Hart, E. J.; Henglein, A. *J. Phy. Chem.* **1986**, *90*, 3061-3062.
12. Olson, T. M.; Barbier, P. F. *Water Res.* **1994**, *28*, 1383-1391.
13. Hart, E. J.; Henglein, A. *J. Phy. Chem.* **1985**, *89*, 4342-4347.
14. Kang, J. W.; Hoffmann, M. R. *Environ. Sci. Technol.* **1997**, *32*, 3194-3199.
15. Buxton, G. V.; Greenstock, C. L.; Helman, W. P.; Ross, A. B. *J. Phy. Chem. Ref. Data.* **1988**, *17*, 513-886.
16. Tsang, W.; Hampson, R. F. *J. Phy. Chem. Ref. Data.* **1986**, *15*, 1087-1279.
17. Zellner, R.; Ewig, F.; Paschke, R.; Wagner, G. *J. Phy. Chem.* **1988**, *92*, 4184-4190.

18. Henglein, A.; C., K. *Int. J. Radiat. Biol. Relat. Stud. Phys. Chem. Med.* **1985**, *48*, 251-258.

19. Christensen, H.; Sehested, K.; Corfitzen, H. *J. Phy. Chem.* **1982**, *86*, 1588-1590.

20. Hung, H.-M.; Hoffmann, M. R. "*The Effect of Frequency, Hydrostatic Pressure, and Sonication Power on Sonochemical Reactions*" in preparation. **1999**.

21. Staehelin, J.; Hoigne, J. *Environ. Sci. Technol.* **1982**, *16*, 676-681.

22. Petrier, C.; Francony, A. *Wat. Sci. Tech.* **1997**, *35*, 175-180.

Table 1. Enhancement effect of ozone on the pseudo-first-order rate constants of MTBE destruction.

[MTBE]- mM	k_o, 10^{-4} s^{-1} at 205 kHz				k_o, 10^{-4} s^{-1} at 358 kHz				R[b]	
	O_3-mM	US	O_3-US	E[a]	O_3-mM	US	O_3-US	E[a]	US	O_3-US
0.01	0.30	8.5	33.2	3.9	0.20	16.5	88.3	5.4	1.9	2.7
0.25	0.31	6.9	14.9	2.2	0.23	15.3	32.2	2.1	2.2	2.1
0.50	0.34	5.4	12.2	2.3	0.23	10.4	18.6	1.8	1.9	1.5
1.00	0.26	4.1	6.3	1.5	0.23	6.8	12.3	1.8	1.7	2.0

[a] Enhancement Factor = k_o (O_3-Ultrasound)/k_o(Ultrasound)

[b] Ratio = k_o (358 kHz)/k_o (205 kHz)

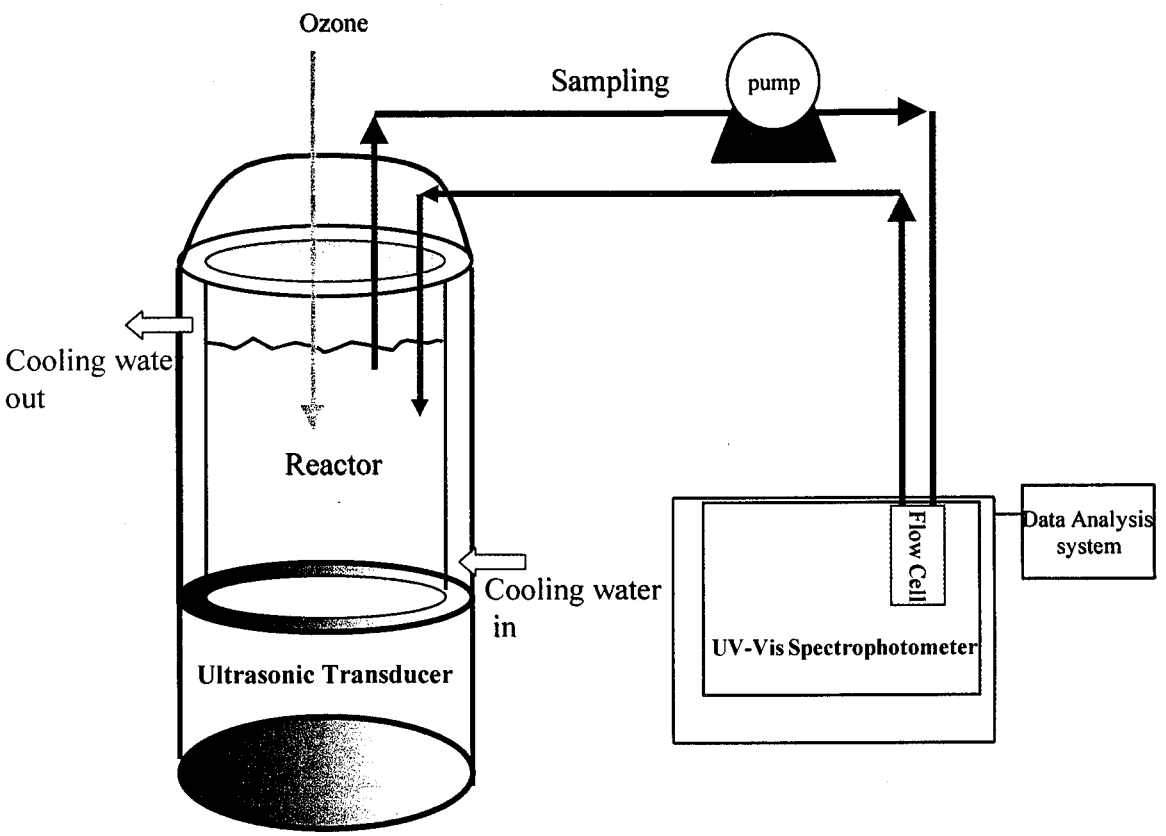

Ultrasonic System
Frequencies: 205, 358, 618, 1078kHz
Reactor Volume: 500mL

Figure 1. Schematic diagram of the sonochemical-reactor system.

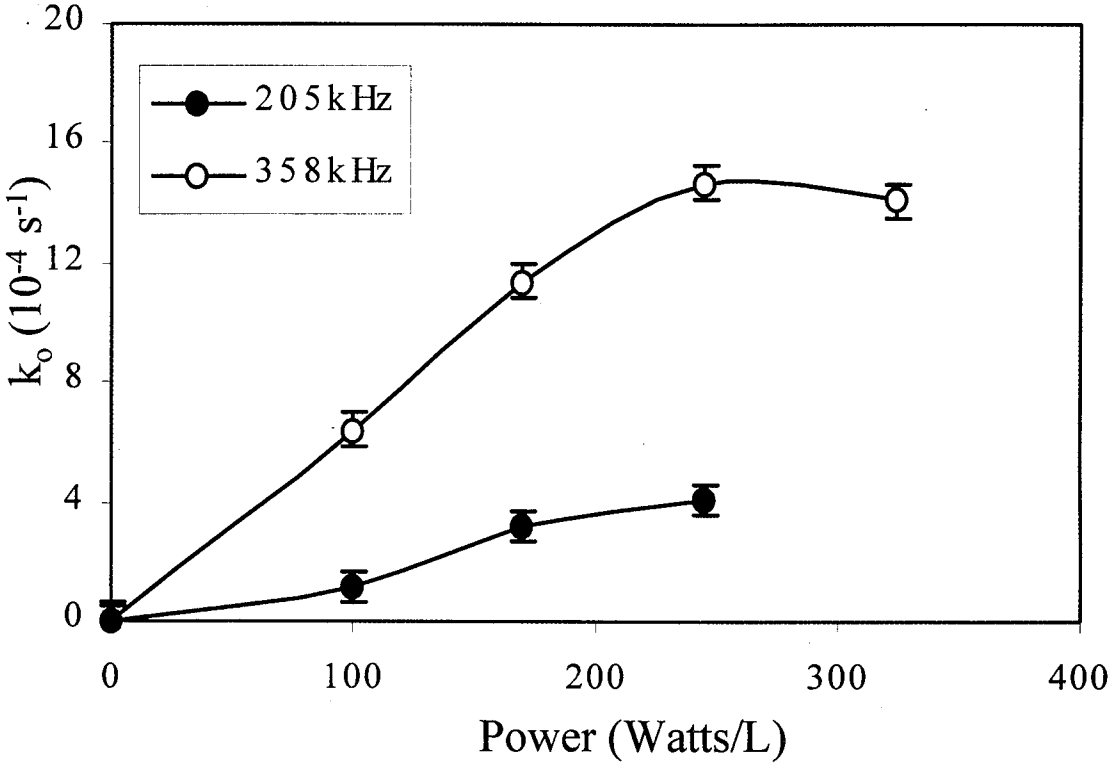

Figure 2. Effect of power density on the pseudo first-order rate constant, k_o, for the destruction of MTBE by ultrasonic irradiation at 205 kHz and 358 kHz, $[MTBE]_o$ = 1mM at 205 kHz, $[MTBE]_o$ = 0.05 mM at 358 kHz.

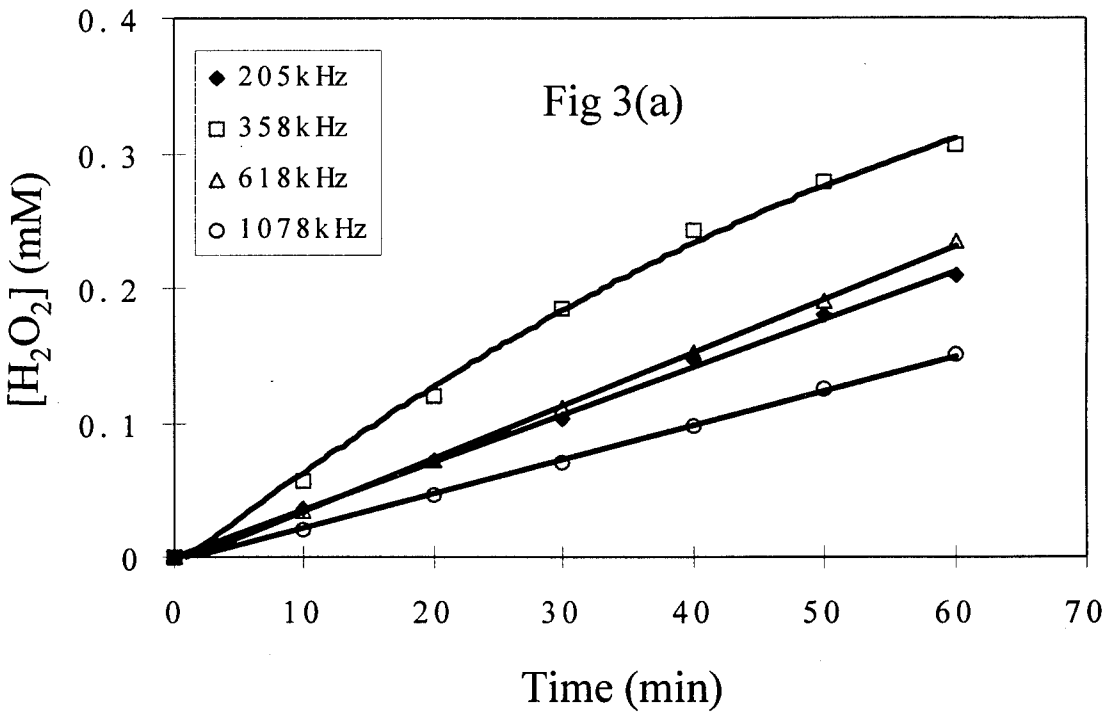

Figure 3(a). Effect of frequency on hydrogen peroxide production rate at power density = 240 Watts/L.

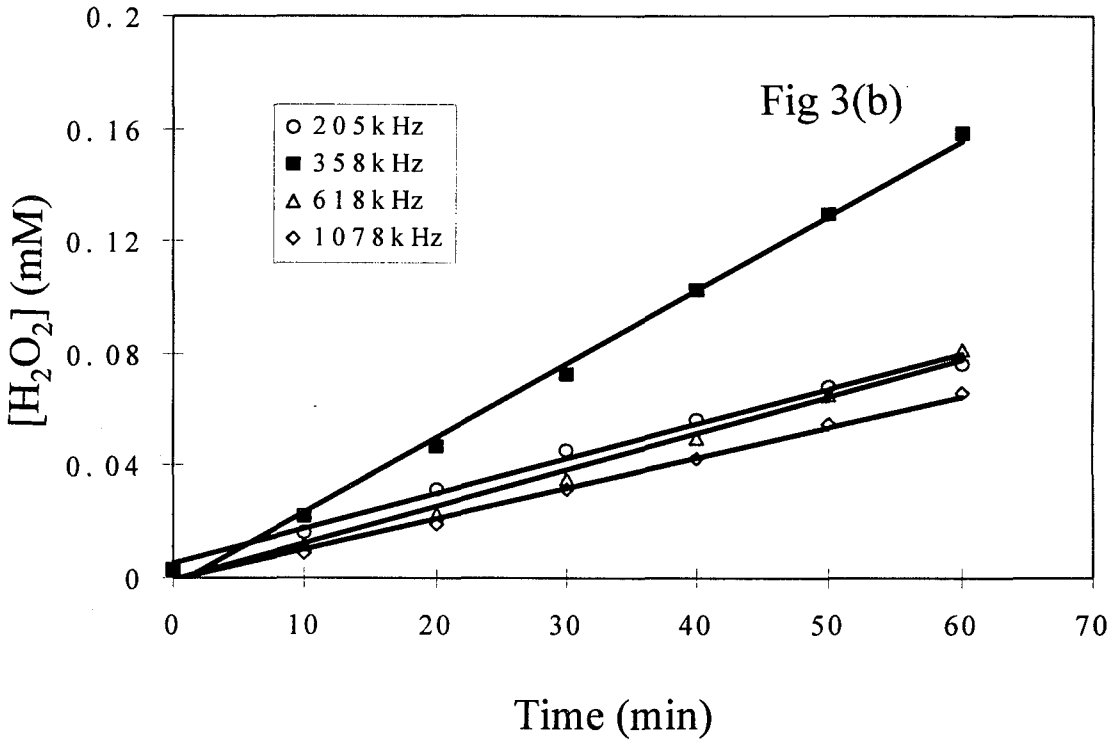

Figure 3(b). Effect of frequency on hydrogen peroxide production rate at power density = 100 Watts/L.

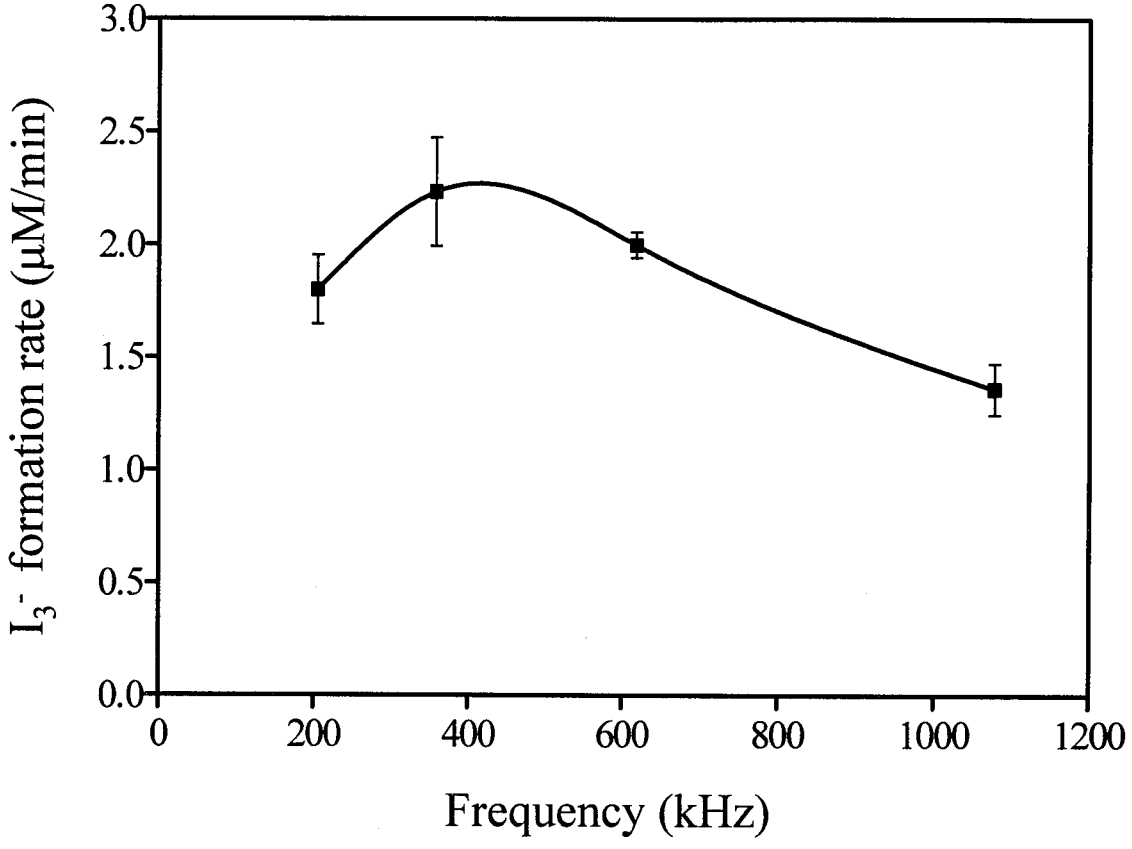

Figure 4. The I_3^- production rate at 205, 358, 618 and 1078 kHz with $[KI]_0$ = 0.1 M, temperature 23 ± 3 ^{0}C and power density 84 Watts L^{-1}.

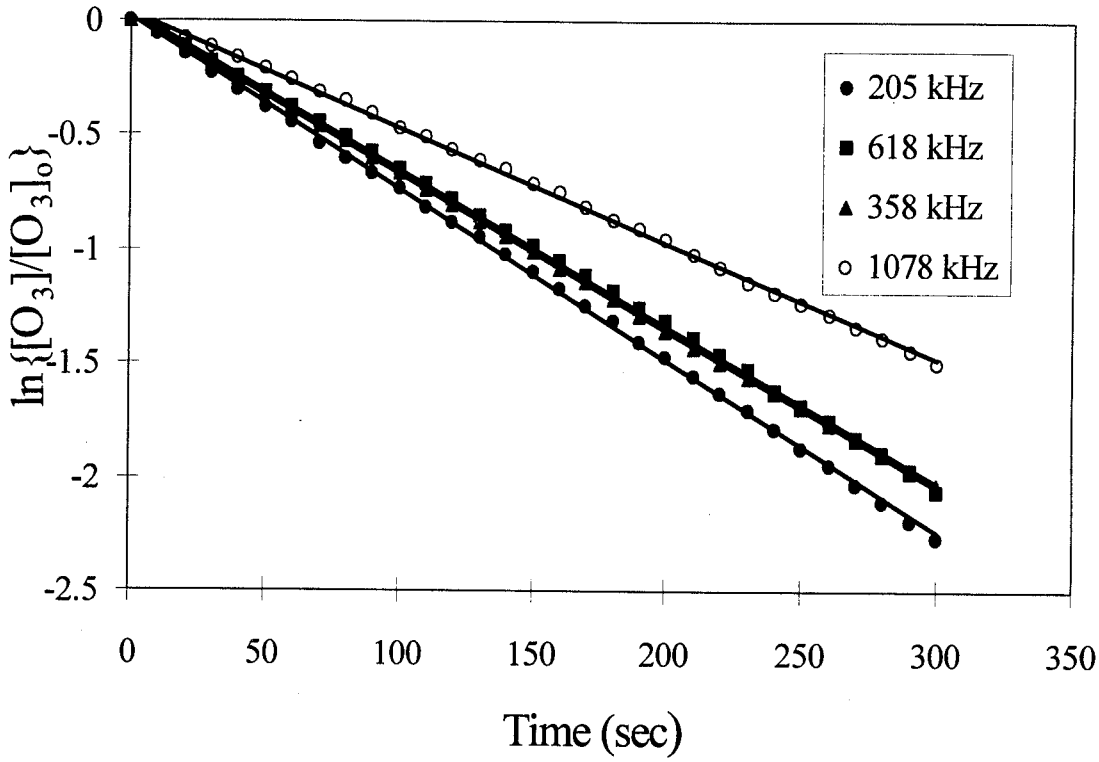

Figure 5. Effect of frequency on the first-order ozone degradation rate with power Intensity = 100 Watts/L, $[O_3]$ = 0.14 – 0.15 mM, $[HCO_3^-]$ = 1 mM, and pH = 8.25.

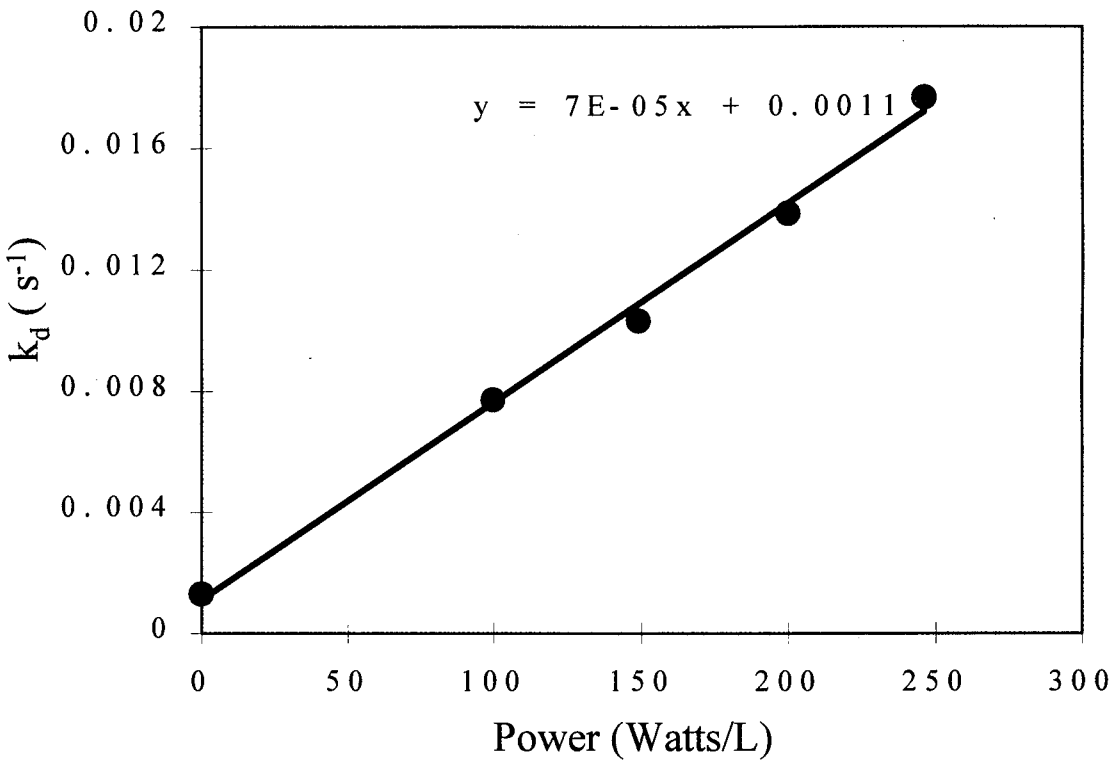

Figure 6. Effect of power density on the first-order ozone decay rate constant, k_d, for the sonolytic ozonolysis at 358 kHz, $[O_3] = 0.17 - 0.18$ mM, $[HCO_3^-] = 1$ mM, and pH = 8.25.

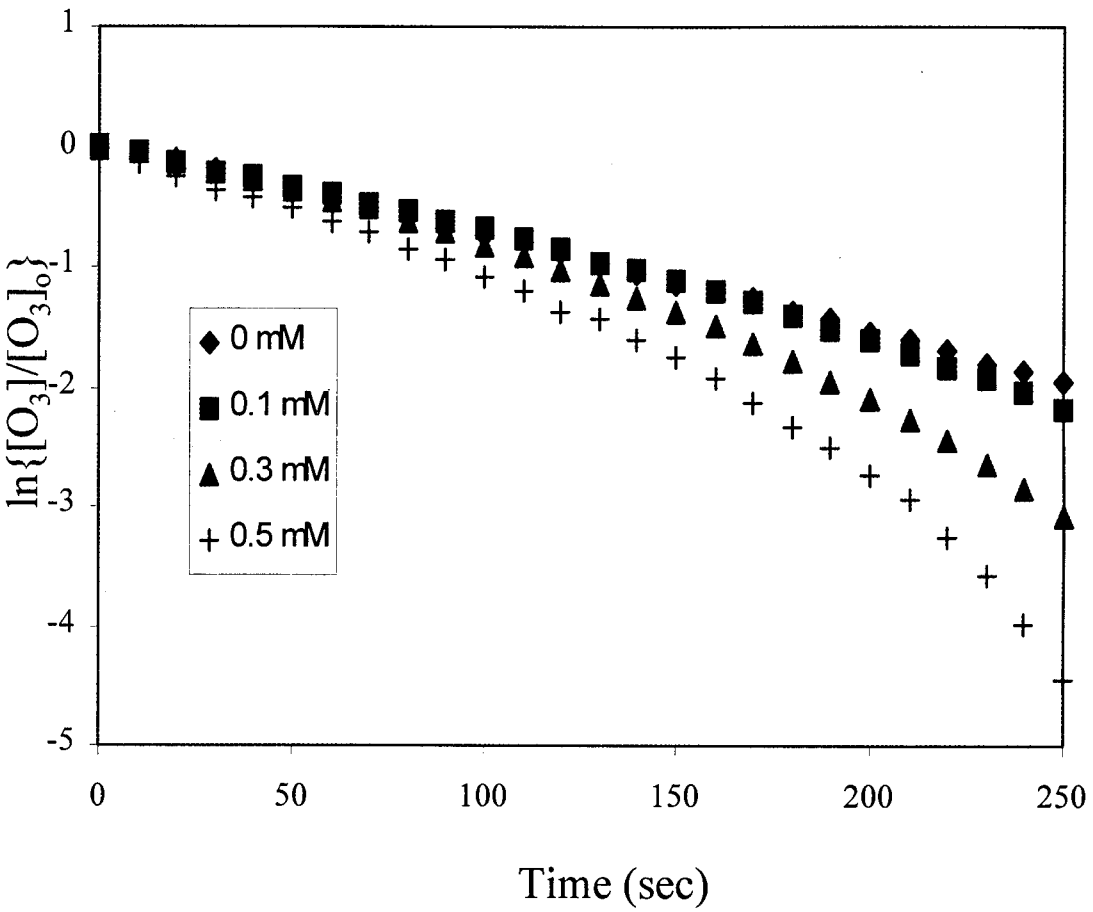

Figure 7. Effect of $[MTBE]_o$ on the first-order ozone degradation rate for the O_3-US process at 358 kHz, power density = 100 Watts/L, $[O_3]$ = 0.16 – 0.18 mM, $[HCO_3^-]$ = 1 mM, and pH = 8.25.

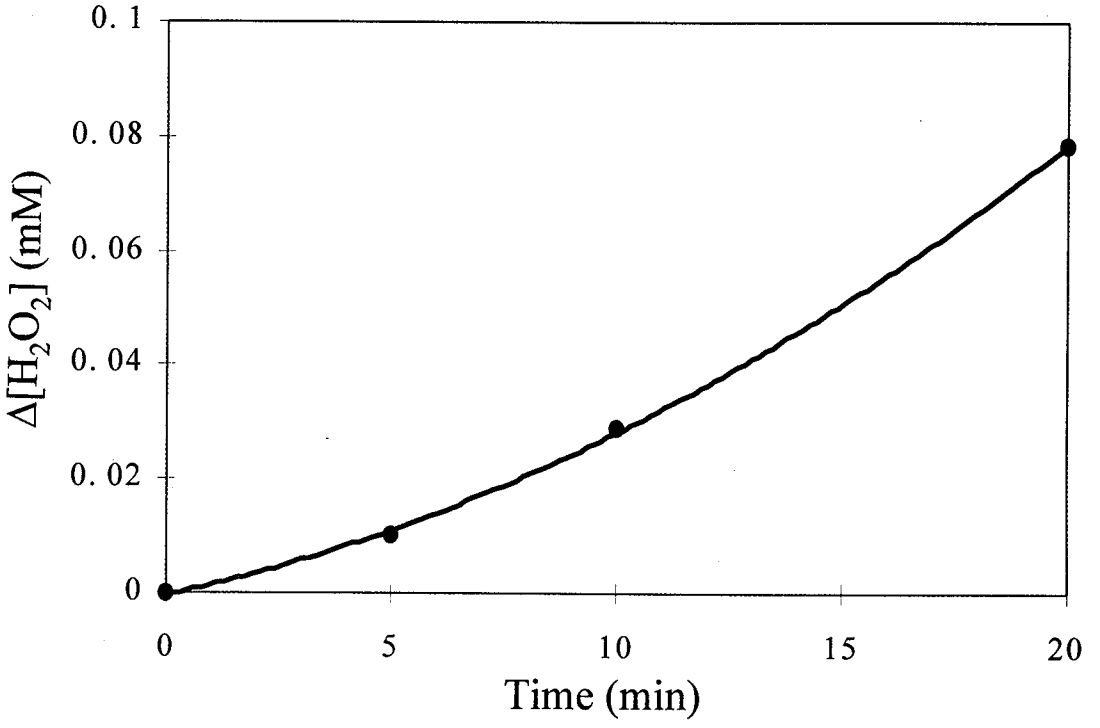

Figure 8. The net increased peroxide concentration, $\Delta[H_2O_2]$ versus time profile by O_3-US process at 358 kHz, power density = 100 Watts/L, $[MTBE]_o$ = 0.5 mM, $[O_3]$ = 0.16 mM, $[HCO_3^-]$ = 1 mM, and pH = 8.25.

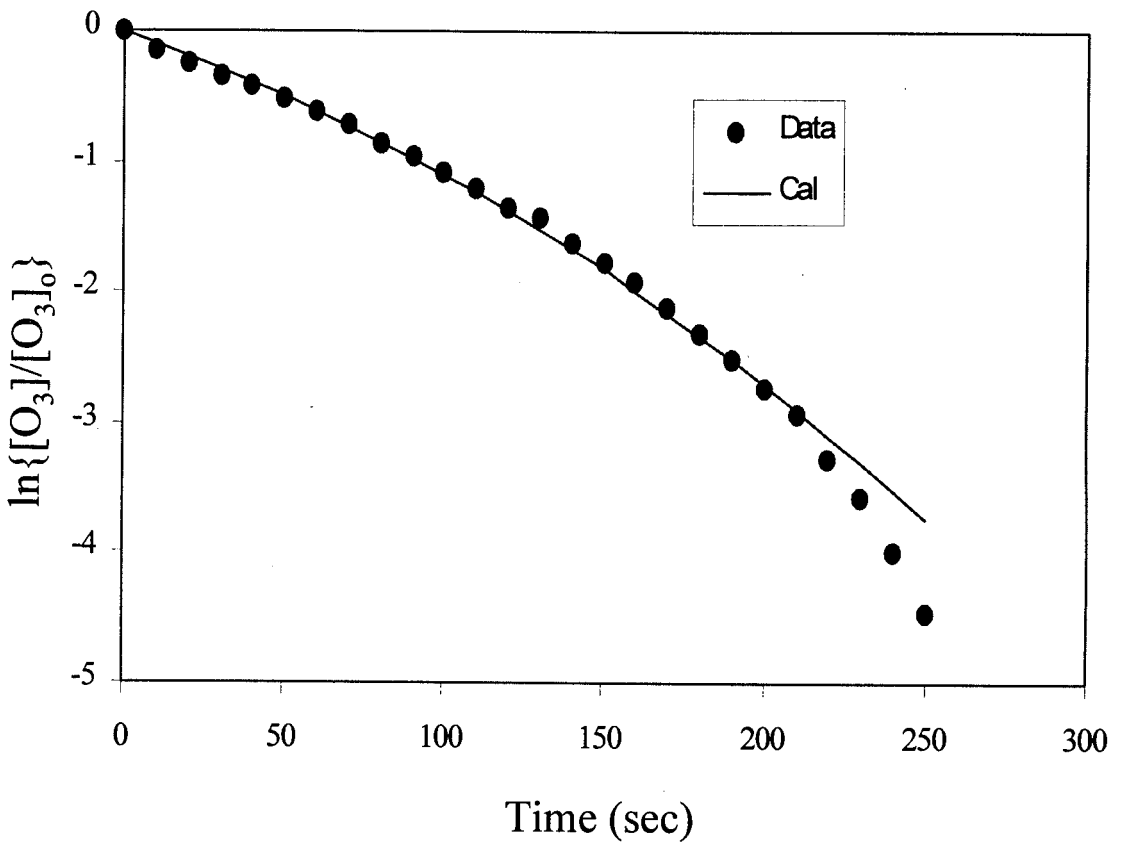

Figure 9. Comparison of the calculated and measured ozone degradation rate by the O_3-US process at 358 kHz, power density = 100 Watts/L, $[MTBE]_o$ = 0.5 mM, $[O_3]$ = 0.16 mM, $[HCO_3^-]$ = 1 mM, and pH = 8.25.

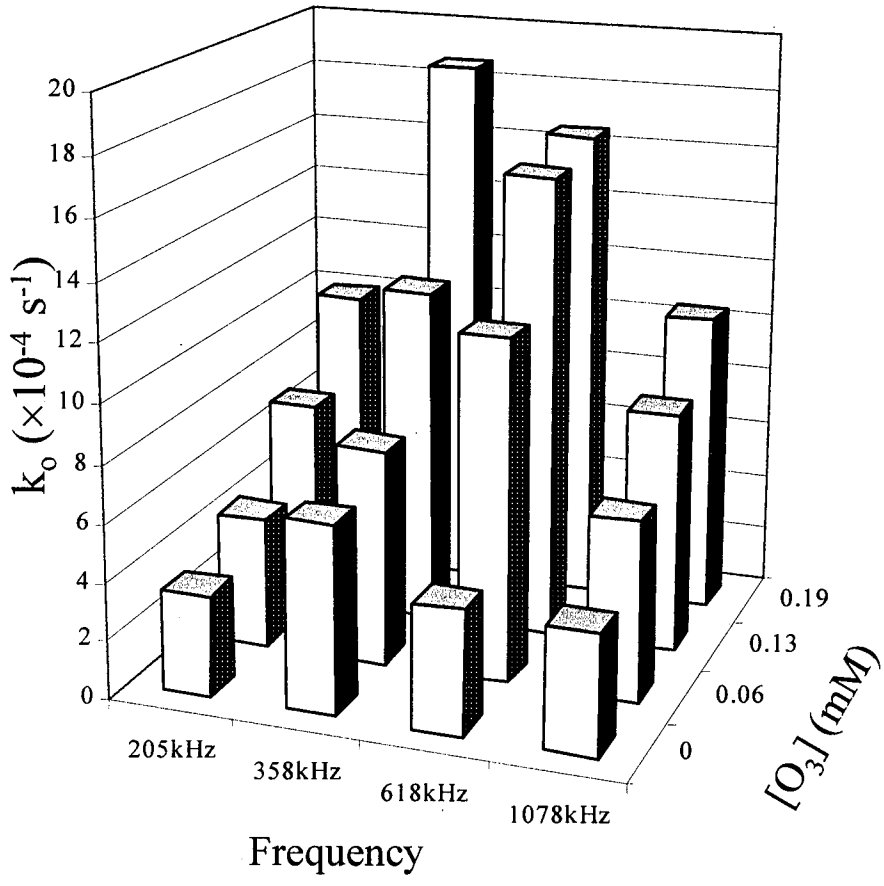

Figure 10. Effects of ozone and frequency on the pseudo-first-order rate constants for MTBE destruction with power density = 100 Watts/L, and $[MTBE]_o$ = 0.05 mM.

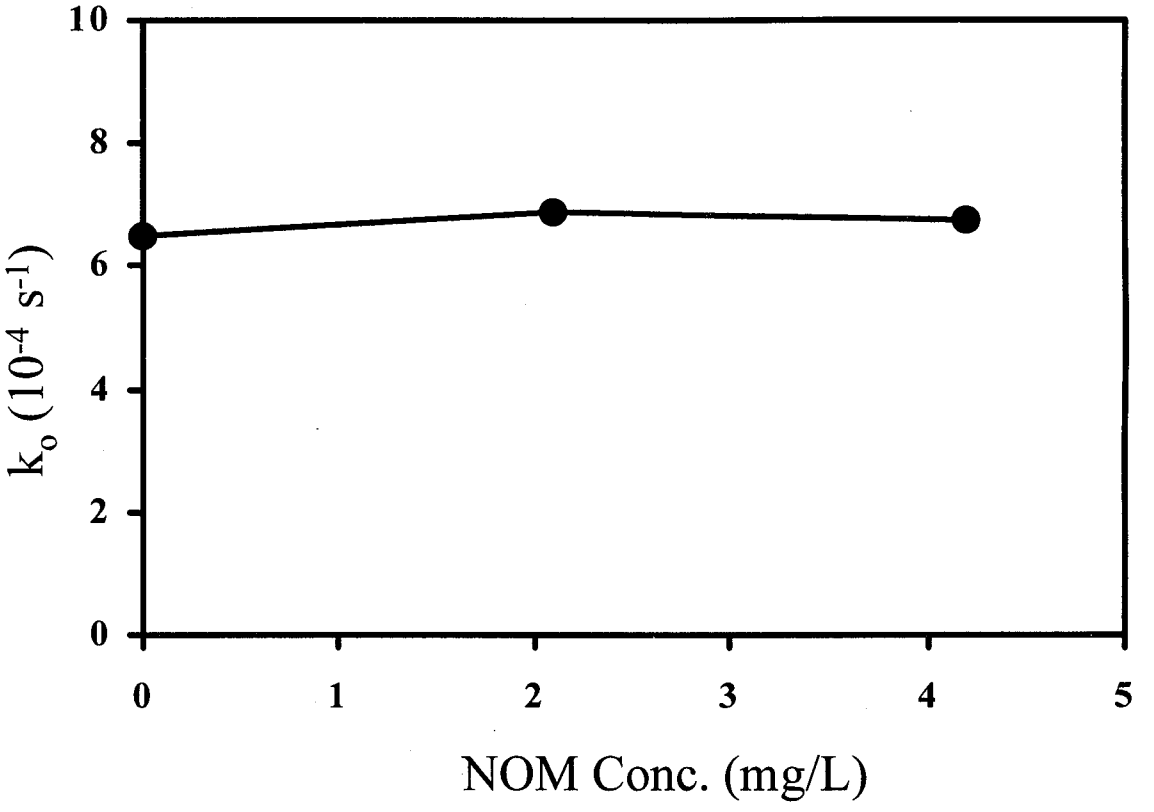

Figure 11(a). Effect of NOM on the MTBE destruction rate by the ultrasound process at 358 kHz, and power density = 100 Watts/L.

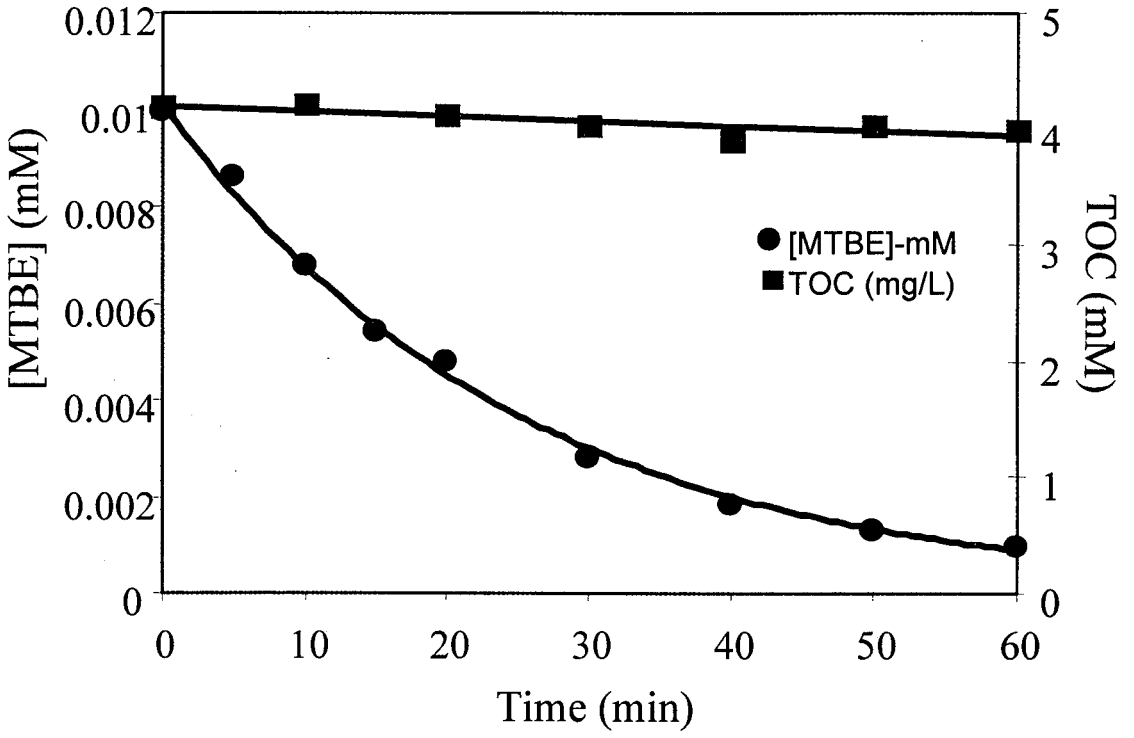

Figure 11(b). The concentration of TOC as a function of time in the presence of humic acid.

Chapter 8

The Sonolytic Destruction of Methyl Tertiary Butyl Ether (MTBE) Present in Contaminated Groundwater

(Submitted to *Water Environment Research*, **1999**)

Abstract

Ultrasonic irradiation in the presence of ozone was used to efficiently eliminate methyl tert-butyl ether (MTBE) from the groundwater. The sonolytic degradation of MTBE has been investigated in three different reactor configurations and frequencies: Allied Signal ELAC (AST, 358 kHz), Near Field Acoustical Processor (NAP, 20 & 16 kHz) and Radial Tube Resonator (RTR, 20 kHz). The sonochemical reactors can be ordered in terms of their efficiency with respect to the degradation of MTBE in the following way, AST (358 kHz) > RTR > NAP. The higher elimination rates of MTBE in groundwater by combined ultrasound/O_3 systems is attributed to the effective conversion of O_3 to OH radical even in the presence of high alkalinity. Carbonate radicals, which formed from the oxidation of bicarbonate by hydroxyl radicals, are shown to react with MTBE via a hydrogen-atom abstraction pathway. MTBE is also rapidly eliminated from groundwater underlying a major international airport by the direct chemical oxidation with a mixture of hydrogen peroxide and ozone.

Introduction

Since 1990, MTBE (Methyl tert-butyl ether) has been used on a large scale as a gasoline additive to lower the emissions of reductive hydrocarbons to the atmosphere (*1,2*). However, as a consequence of its large-scale production and use, MTBE has become the focus intensive investigation because of its negative impact on water quality due to leakage of petroleum products containing MTBE from the underground storage tanks and to evaporative losses to the atmosphere. For example, MTBE, which is highly soluble in water (*3*), has been detected at significant concentrations in a wide range of surface waters. MTBE is added to gasoline at a level of approximately 15% by volume. The addition of MTBE to gasoline has resulted in an apparent reduction in the relative ozone-producing capacity of gasoline vapors and combustion by-products by approximately 15% and benzene emissions to the atmosphere by 50% over regular gasoline (*1,2*).

In California, 184 underground storage sites were found to be contaminated with MTBE, while 156 of those sites had MTBE concentrations in excess of 35 $\mu g\ L^{-1}$ (0.4 μM) (*4*). In the same study, 13 California lakes were found to be contaminated with MTBE. However, in the case of drinking water wells, only 17 wells were found to be contaminated with MTBE. Groundwater plumes contaminated with MTBE are often prevented from reaching drinking water wells by several factors such as well head protection, well seals, geological separation (deep source wells vs. shallow groundwater sources of MTBE), dilution during water withdrawal, dilution by source blending, and through losses of MTBE due to volatilization.

MTBE has a relatively high vapor pressure of 0.32 atm (i.e., 205 mm Hg at 20

°C). For comparison, MTBE is three times more volatile than benzene (P_v^o = 0.1 atm). Given this relatively high vapor pressure, MTBE will be preferentially volatilized from the vadoze zone. However, the high vapor pressure is offset somewhat by the relatively high solubility of MTBE in water (C_{sat} = 0.54 M) and its water-to-air partition tendencies (as quantified by its Henry's law constant, k_H = 0.49 atm-L mol^{-1}) which are one-tenth of benzene. This implies that dissolved MTBE will volatilize to a lesser extent than benzene from the aqueous phase to the vapor phase.

MTBE does not sorb readily to soil organic matter and thus its retardation tendency is quite low with typical retardation factors of close to 1.00. With this low retardation factor, MTBE will move at nearly the same rate as groundwater while the BTEX (benzene, toluene, ethylbenzene, and xylene) components will move at slower rates through contaminated aquifers. For example, benzene, which has a typical retardation factor of 1.2, will move 20% slower than MTBE through a typical saturated zone. Given the high mobility of MTBE in aquifers, the early arrival of MTBE at a well head can often be a warning sign of BTEX contamination. For drinking water, the odor threshold for MTBE contamination is 15 μg L^{-1} (0.17 μM).

MTBE is reported to be relatively resistant to both aerobic and anaerobic microbial degradation by bacteria (*5*). However, recent studies show that the rates of biodegradation of MTBE are measurable but quite slow (e.g., k_{bio} = 0.000 to 0.001 day^{-1} which translates to $k_{bio} = 7.0 \times 10^{-7}$ min^{-1}) (*6-9*). In general, the biodegradation of MTBE is substantially slower than the biodegradation of BTEX.

Due to its low Henry's Law constant, air stripping is not a viable process for the

removal of MTBE from water (*3*). In addition, MTBE is poorly adsorbed on granular activated carbon; on the other hand, the treatment of MTBE by ozone and combinations of ozone and hydrogen peroxide have been reported. For example, Velleitner et al. (*10*) investigated the reaction of MTBE and O_3 in water and reported that 5.5 moles of ozone per moles of MTBE were required for a net 80% destruction of MTBE. Barreto, *et al.* (*11*) explored the use photocatalytic oxidation by oxygen on titanium dioxide to degrade MTBE; they reported MTBE degradation rates that were faster than those obtained for the oxidation of MTBE by O_3.

Over the last several years, ultrasonic irradiation (i.e., sonolysis or sonication) has been explored for the treatment of chemical contaminants in aqueous solution (*12-15*). The chemical effects of sonolysis are the direct consequence of acoustic cavitation. Sonolytically-induced microbubbles grow with each successive ultrasonic frequency cycle until they reach a critical size resonance-frequency that results in the violent collapse of gas bubbles. The rapid implosion of cavitation bubbles is accompanied by adiabatic heating of the vapor phase of the bubble that yields localized transient high temperature and pressure. Temperatures and pressures obtained upon bubble collapse have been estimated to be on the order of 4,200 K and 975 bar, respectively (*16*). Temperature exceeding 5000 K have been reported in the ultrasonic cavitation of organic and polymeric liquids (*17*). Water vapor under these conditions undergoes a thermal dissociation to yield extremely reactive radicals, H· and ·OH. In the presence of O_2, H· atom leads to the formation of the hydroperoxyl radical, HO_2·. As a result, organic compounds that are present near bubble/water interface may undergo thermal decomposition, or they may react with high-redox potential free radicals that are generated within the collapsing bubbles.

Our preliminary research into the sonolytic oxidation of MTBE in the presence of ozone shows that MTBE can be readily oxidized by hydroxyl radical (·OH) over a wide range of ultrasonic frequencies (*18,19*). At an ultrasonic frequency of 205 kHz and an applied power of 200 W L^{-1}, the observed first-order degradation rate constant for the loss of MTBE was found to increase from 4.1×10^{-4} s^{-1} to 8.5×10^{-4} s^{-1} as the concentration of MTBE decreased from 1.0 mM to 0.01 mM. These rate constants correspond to reaction half-lives for MTBE of 28 and 13.6 min, respectively. In the presence of O_3, the sonolytic rates of destruction of MTBE were accelerated significantly. The rates of MTBE sonolysis with ozone were found to be enhanced by a factor of 1.5 to a factor of 3.9 depending on the initial concentration of MTBE. The primary reaction intermediates were determined to be tertiary-butyl formate, tertiary-butyl alcohol, methyl acetate, and acetone.

The goal of this study was to investigate the feasibility of using ultrasound for the treatment of MTBE present in contaminated groundwater.

Experimental Methods

MTBE (99.9%; EM Science), tert-butyl formate (99%; Aldrich), tert-butyl alcohol (99%; EM Science), acetone (99.5%; EM Science), methyl acetate (99.5%, Aldrich), sodium bicarbonate (Reagent Grade; EM Science) and other chemicals were used without further purification. Three ultrasound systems, Allied Signal ELAC (AST, 358 kHz) (*18*), Near Field Acoustical Processor (NAP, 20 & 16 kHz) (*12*) and Radial Tube Resonator (RTR, 20 kHz), were used in this study. The physical parameters for those three systems are listed in Table 1. In AST system, the reactor had 4 sampling ports to withdraw aqueous samples, and to allow gases to be introduced and to be vented. The interior diameter of the

reaction vessel was 6 cm. Temperature was maintained constant at 20 °C throughout all runs.

Sonolytic irradiations were performed in water purified by a Milli-Q UV Plus system (R > 18 Ω) and groundwater samples were collected from beneath the John F. Kennedy International Airport. The groundwater characteristics are listed in Table 2. Solutions containing O_3 were prepared by bubbling ozone, that was generated via the corona discharge process on O_2 with an Orec Ozonator (Model V10-0) into deionized water through a glass fritted diffuser until the desired aqueous phase ozone concentration was obtained. The target aqueous ozone solution was monitored by UV spectrophotometry, using the molar extinction coefficient of 3300 M^{-1} cm^{-1} for O_3 in water at 260 nm (*20*).

All kinetic runs were made in the batch mode without the addition of a buffer. MTBE stock solutions (100 mM) were prepared and stored at 4 °C until use. During each kinetic run, 1 mL of sample was taken at appropriate time intervals and stored in Teflon-faced aluminum sealed vials. In ozonation runs, the residual aqueous ozone was quenched with 10 μL of 1 N-$Na_2S_2O_3$. The total amount of samples withdrawn from the reactor was less than 15 mL, which introduced a small error (≤ 3%) due to differential volume changes (dV/dt) during a given kinetic run.

MTBE and its identifiable oxidation by-products were analyzed by gas chromatography. For the routine kinetic runs, compounds were analyzed by the headspace GC with FID detection. The compounds extracted in the gas phase of head-space sample in the HP 7694 headspace sampler were auto-injected into a HP 5890 series II GC-FID equipped with a HP-624 capillary column (30 m x 0.32 mm x 1.8 um) with 80 °C

isothermal oven temperature for 10 minutes. By-products of MTBE were identified by injecting 100 μL of the extracted head space sample into a Hewlett-Packard 5890 series II gas chromatograph connected to a quadruple-type mass spectrometer (HP 5989A) equipped with a HP-5 MS capillary column (30 m x 0.25 mm x 1 μm). The temperature ramp was programmed to 30 °C for 6 minutes and increased at 10 °C/min to 150 °C. Sample aliquots for hydrogen peroxide analysis were taken at 10 minutes intervals over a 60 minutes run time and were measured fluorometrically (*21*).

Ozone concentration in the sparging feed gas was measured by a standard method in which the ozone is trapped in a bubbler tube containing KI solutions. The molecular iodine formed by the redox reaction of ozone with iodide was titrated with a 0.1 N $Na_2S_2O_3$ solution. Hydrogen peroxide feed solutions were prepared from 31% reagent grade hydrogen peroxide (EM Science). Residual hydrogen peroxide was determined by the horseradish peroxidase-catalyzed fluorescence method, while residual ozone concentration were measured by UV spectrophotometer at $\lambda = 260$ nm. The molar extinction coefficient for O_3 is $\varepsilon = 3300\ M^{-1}\ cm^{-1}$.

Kinetic runs involving the combination of ozone and hydrogen peroxide were made in the batch mode in a 2 L - cylindrical reactor. The cylindrical Pyrex reactor is 12″ high with a 4″ inner diameter; it is fitted with a disk-type fritted-glass gas sparger for ozone introduction and dispersion. The reactor is surrounded by a double-wall water jacked for temperature control at 15 °C. Ozone was generated from oxygen with the OREC generator (Maximum output: 3 W/W %) using a current setting appropriate for the desired dose. Gas (O_3/O_2) flow rate was fixed at 240 mL min^{-1}. At time zero, the ozone and hydrogen

peroxide solutions were 0.5 to 2 mL min^{-1} depending on the ozone dose rate.

Results and Discussion

Based on our previous work (*18,19*), we determined that the kinetics of degradation of MTBE in the presence of ultrasound followed pseudo first-order kinetics for most of the duration of the reactions. The rate of disappearance of MTBE is given by

$$-\frac{d[MTBE]}{dt} = k_o[MTBE] \quad (1)$$

with the corresponding integrated solution:

$$[MTBE]_t = [MTBE]_o e^{-k_o t} \quad (2)$$

where $[MTBE]_t$ = concentration of MTBE at time = t and $[MTBE]_o$ is the concentration of MTBE at t = 0. The kinetic data given in this report are expressed in terms of k_o values and the corresponding half-lives for the first-order reactions, where

$$t_{1/2} = \frac{\ln 2}{k_o} = \frac{0.693}{k_o} \quad (3)$$

The integrated solution to the first-order rate expression can also be expressed simply as

$$\ln\left(\frac{[MTBE]_t}{[MTBE]_o}\right) = -k_o t \quad (4)$$

Degradation Kinetics of MTBE in the Presence of Ozone in the AST system

The most efficient frequency for MTBE degradation in AST reactor occurs at 358 kHz (*19*). In these sets of experiments, the frequency was set at 358 kHz. Groundwater from JFK was used to probe the effects of variable power and ozone dosage levels on the

rate of degradation of MTBE. The reactor volume was 0.5 L, T = 15 °C, and $[MTBE]_o$ = 0.72 mM.

Under these conditions, the first-order degradation rate constant for MTBE increased from $k_o = 0.77 \times 10^{-4}$ s^{-1} at an applied power density of 50 W L^{-1} to $k_o = 0.77 \times 10^{-4}$ s^{-1} at an applied power density of 246 W L^{-1}. With the addition of ozone to the reaction mixture the rates of degradation were enhanced even further as shown in Table 3. In the combined treatment experiments, ozone was sparged into the reactor for 10 min before the start of sonication such that the initial ozone concentration was $[O_3]_o$ in the range of 0.21 to 0.24 mM (i.e., 10 to 12 mg L^{-1}). Overall, these experiments show that the rate of water-to-air gas transfer of MTBE is low and that ozone alone can degrade MTBE in real groundwater. The later result indicates the JFK groundwater contains other constituents that appear to accelerate the decomposition of ozone to yield hydroxyl radical, ·OH.

The combined effects of a variation in ozone dosage at power density of 246 W L^{-1} are shown in Figure 1. These results are summarized in Table 4. This series of experiments show clearly that the combination of ozone and ultrasound results in enhanced degradation rates for MTBE; however, the net ozone utilization rate in the reactor due to continuous sparging was low (≤ 30%). The minimum half-life for MTBE degradation under these conditions is 6 min.

With an applied ultrasonic frequency of 358 kHz (246 W/L) and an ozone concentration of 20.6 mg/L, the total organic carbon (TOC) in the JFK groundwater was dropped from 68 mg/L to 9 mg/L after 60 min of sonication. More than 85% of TOC was

converted to inorganic carbon.

pH Effects

In a series of experiments, the effects of initial pH on the relative rates of MTBE degradation in the JFK samples were observed in combined O_3 + US runs with a preset O_3 dose of 20.6 mg/L-min and an applied power of 123 W in the AST reactor. pH was adjusted to 4.9 by adding 6 mL of 1 N HCl into 500 mL water; the reference pH was 6.8. For comparison, under these conditions the observed first-order rate constant at pH 4.9 was $k_o = 18.9 \times 10^{-4}\ s^{-1}$; while at pH 6.8, $k_o = 20.2 \times 10^{-4}\ s^{-1}$. From this comparison, there appears to be relatively little dependence of the MTBE degradation rate on the initial pH of the reaction mixture.

Effects of Bicarbonate

Since CO_3^{2-} and HCO_3^- are potential competitive reagents for ·OH, the effect of bicarbonate on the oxidation rate of MTBE was investigated. For example, in the MTBE contaminated groundwater wells, typical bicarbonate levels are in the range of 1 to 4 mM. Glaze and Kang (*22*) reported that high levels of bicarbonate ion in groundwater significantly decrease the rate of removal of TCE and PCE because of the direct competition due to the following reactions:

$$\cdot OH + HCO_3^- \rightarrow CO_3^- \cdot + H_2O \qquad (5)$$

$$\cdot OH + CO_3^{2-} \rightarrow CO_3^- \cdot + OH^- \qquad (6)$$

Under most circumstances, the carbonate radical, $CO_3^- \cdot$, is much less reactive than hydroxyl radical; however, there are a significant number of examples of reactions

involving the $CO_3^{-\cdot}$ radical and organic substrates for which the rate constants vary from 10^8 to 10^9 M^{-1} s^{-1} (*23*). On the other hand, some of the reported second-order rate constants involving the carbonate radical are as low as 10^3 to 10^4 M^{-1} s^{-1} (*23,24*).

In order to test the impact of a possible competition for hydroxyl radical during the treatment of MTBE, sonication of 0.01 mM MTBE in the presence of variable bicarbonate concentrations were performed. The initial MTBE concentration for this study was determined based on the similarities of the second-order rate constants of ·OH with bicarbonate ion ($k_{OH\bullet}$ = 1.5 x 10^7 $M^{-1}s^{-1}$) (*25*) and MTBE ($k_{OH\cdot}$ = 1.57 x 10^9 $M^{-1}s^{-1}$) (*26*). However, the effect of HCO_3^- on the rate of ultrasonic decomposition of MTBE is negligible over the range of [HCO_3^-] from 1 to 2 mM. This result suggests that the major reaction site for MTBE with ·OH is within the cavitation bubble or on the surface of the bubble but not in the bulk aqueous phase.

Near Field Acoustical Processor (NAP) Treatment

Initial kinetic runs under continuous-flow conditions were run with a NAP reactor (*12-15*). These were run with MTBE added to Milli-Q water, with JFK-1, and with JFK-2 groundwater (Table 2). The total reactor volume including the reservoir was 8.9 L with the temperature maintained at ~ 15 °C. A series of kinetic runs were made with $[MTBE]_o$ = 0.05, 0.1 and 0.5 mM at applied powers of 1200 W and 1800 W. The kinetics of these reactions were again first order in [MTBE]. The kinetic runs are summarized in Table 5. The O_3 dose rate for these experiments was 5.3 mg L^{-1} min^{-1}. A variation of sonication power at a $[MTBE]_o$ = 0.5 mM showed no discernable effect on the measured reaction rate when ultrasound alone was applied. In kinetic runs with Milli-Q water, the pH dropped

during the course of the reaction, while in the JFK-1 samples, the pH rose during the reaction promoted by ultrasound alone. Based on these results, the half-life for the degradation of MTBE in the JFK-1 sample with an initial $[MTBE]_o$ = 0.35 mM was 28 min.

An additional set of experiments with the NAP reactor system were performed on the JFK-2 sample in which the initial MTBE concentration was $[MTBE]_o$ = 0.72 mM. The reactor conditions were the same as described above for JFK-1. In the case of sonication alone, no loss of MTBE was observed. However, when ozone and ultrasound were combined, MTBE was degraded at rates similar to those found in the Milli-Q water systems. The results of these experiments in which the applied power and ozone dosage rates were varied are summarized in Table 6. Under optimal conditions in the NAP reactor with an ozone dose rate of 5.3 mg L^{-1} min^{-1}, the half-life for MTBE degradation was 33 min.

Radial Tube Resonator (RTR) Reactor Treatment

Experiments with the RTR system were run at 20 kHz and at an applied power of 533 W in the batch mode with a total reaction volume of 2.0 L, with the temperature held at ~ 15 °C, and with an initial MTBE concentration of $[MTBE]_o$ = 0.5 mM. In the initial runs, ultrasound alone was used to degrade MTBE with a measured rate constant of k_o = 2.38×10^{-4} s^{-1} ($t_{1/2}$ = 48 min). In general, the RTR reactor appeared to be more effective at degrading MTBE, when ultrasound alone was applied. For comparison, the corresponding rate constant for the NAP reactor at the similar power density (i.e., 200 W L^{-1}) was 0.30×10^{-4} s^{-1} ($t_{1/2}$ = 385 min). However, the reactor operated at 358 kHz was the most efficient

system for the degradation of MTBE.

In another set of experiments using the RTR reactor but without sonication, O_2 and O_3 were sparged into the reactor through a disk type of gas diffuser installed at the bottom of sonoreactor. Oxygen gas was sparged at a flow rate of 240 mL min^{-1} while ozone was dosed with a maximum current setting on the ozone generator with the same gas flow rate as for oxygen. The resulting ozone dose rate was 11.9 mg L^{-1} min^{-1}. These "control" experiments showed that the losses of MTBE by gas transfer at a net gas flow rate of 240 mL min^{-1} were negligibly small. The rate constant for the degradation of MTBE in the presence of ozone alone under these conditions was found to be 0.57×10^{-4} s^{-1} ($t_{1/2}$ = 202 min.).

In another set of experiments using the RTR reactor system, ozone and ultrasound were combined at a fixed ultrasonic power of 533 W (power density = 267 W L^{-1}). Ozone dosage rates were varied from 0 (oxygen alone) to 11.9 mg O_3 L^{-1} min^{-1} at a fixed gas flow rate. These results are tabulated in Table 7. The MTBE degradation rate with O_2 and US was low. With the combination of O_3 and US, the oxidation rate is enhanced by a factor of five at an ozone dose of 7.3 mg L^{-1} min^{-1} at 267 W L^{-1} of ultrasonic power intensity. Furthermore, an increase in the ozone dosage rate results in faster MTBE reaction rates as shown in Figure 2.

The RTR reactor conditions were the same as described above with $[MTBE]_o$ = 0.72 mM at an ultrasonic frequency of 20 kHz, and an irradiation intensity of 267 W L^{-1}. The observed first-order rate constants for MTBE degradation in the JFK-2 groundwater sample are summarized in Table 8. From this data it is clear that rate of degradation of

MTBE in actual JFK groundwater was substantially faster than the corresponding rates in Milli-Q water. For example, the relative enhancement in the rate of MTBE destruction in JFK-2 groundwater is by a factor of 7. In addition, the MTBE degradation rate constant ($k_{O_3} = 1.97 \times 10^{-4}$ s^{-1}) in the RTR reactor with a disk type diffuser installed at bottom was clearly faster than in NAP reactor system ($k_{O_3} = 1.77 \times 10^{-4}$ s^{-1}) even with a smaller ozone dosage and lower gas flow rate (i.e., 240 mL min^{-1} vs. 480 mL min^{-1}). This difference is most likely due to the enhanced ozone mass transfer rates achieved with the disk type diffuser in the RTR system as compared to the tubular glass frit diffuser used with the NAP system.

Treatability of JFK Groundwater with Peroxone ($O_3 + H_2O_2$)

Ozone gas was introduced through a disk type of gas diffuser installed at the bottom of the 2 L glass reactor into Milli-Q water containing 0.7 mM MTBE at 15 °C. The gas flow rate was maintained at 240 mL min^{-1}. Ozone was dosed at a rate of 11.9 mg L^{-1} min^{-1}. Two different peroxone kinetic runs were made; they included a kinetic run with an added bicarbonate and a run in bicarbonate free water. In the bicarbonate system, 1.5 g of $NaHCO_3^-$ were added into 2 L of water for a total alkalinity of 545 mg/L as HCO_3^- (8.9 mM of [HCO_3^-] or 446 mg/L - $CaCO_3$). After the bicarbonate addition, the pH was raised to 8.6.

The combined ozone plus hydrogen peroxide (i.e., peroxone) process was found to be very effective for MTBE destruction and even more effective in bicarbonate spiked water. For example, 99% of 0.7 mM MTBE can be destroyed with 12.0 mg/L-min of ozone and 4.0 mg/L-min of hydrogen peroxide after 30 min. During the course of the

reaction, the pH changes from 8.6 to 7.6, while the corresponding pH change in bicarbonate-free water was from 6.0 to 4.7. The higher rate of reaction in the peroxone runs at higher bicarbonate levels suggests that the carbonate radical is highly reactive toward MTBE, and that it functions as an effective ·OH radical trap that is able to engage in further oxidation reactions electron transfer with MTBE.

The principal reaction intermediates that were observed in these reactions were t-butyl alcohol, methyl acetate, acetone, and t-butyl-formate (TBF). Of these reaction intermediates, the tertiary-butyl formate yield was the highest as shown in Figure 3 (e.g., maximum observed yield of TBF is 24%) but, at the same time, it also reacts with hydroxyl radical and is, therefore, completely destroyed after 15 min of treatment.

It is clear from our experiments that the rate of MTBE degradation in the JFK-2 groundwater is much higher than the corresponding rate of degradation in Milli-Q water. For example, the MTBE degradation rate in the treated JFK-2 water is seven times greater than the rate in Milli-Q water for the same MTBE concentration (i.e., 0.7 mM). The results of these experiments are summarized in Table 9.

The relative enhancements in rate of degradation of MTBE by the combined use of hydrogen peroxide and ozone ranged from 7.2 to 9.8 compared to the rate obtained with ozone alone. The optimum hydrogen peroxide dose for MTBE removal from the JFK water was relatively low (i.e., < 0.16 w/w {peroxide/ozone-mass ratio}). A typical peroxide-to-ozone for optimal treatment is usually around 0.5. The lower ratio observed in this study (0.16) is the evidence for the presence of other ozone-consuming constituents, such as bicarbonate, in addition to hydrogen peroxide in JFK water.

Discussion

The relative enhancement of organic compound degradation during sonolytic processing by the addition of ozone has been reported previously (*14,27,28*). Barbier and Petrier showed that the combined ozone-ultrasound process was capable of complete mineralization of 4-nitrophenol (*29*). In the bulk aqueous phase, ozone can be decomposed by hydroxide ion, OH^-, or the conjugate base of H_2O_2 (HO_2^-) to yield $HO_2\cdot$ and $\cdot OH$ as follows:

$$O_3 + OH^- \rightarrow HO_2^- + O_2 \quad (7)$$

$$HO_2^- + H^+ \rightarrow H_2O_2 \quad (8)$$

$$O_3 + HO_2^- \rightarrow \cdot OH + O_2^- + O_2 \quad (9)$$

$$O_2^- + H^+ \rightarrow HO_2\cdot \quad (10)$$

$$O_3 + \cdot OH \rightarrow HO_2\cdot + O_2 \quad (11)$$

$$O_3 + O_2^- \rightarrow O_3^- + O_2 \quad (12)$$

$$O_3 + H_2O \rightarrow \cdot OH + OH^- + O_2 \quad (13)$$

In addition to the above sequence of reactions, the peroxone process involves the coupled reaction of ozone and hydrogen peroxide as follows:

$$O_3 + H_2O_2 \rightarrow \cdot OH + HO_2\cdot + O_2 \quad (14)$$

$$O_3 + HO_2\cdot \rightarrow \cdot OH + 2\,O_2 \quad (15)$$

The above series of elementary reactions constitute a free radical chain reaction leading to the degradation ozone and the formation of hydroxyl radical and hydroperoxyl radical as

reactive intermediates. The chain termination steps are as follows:

$$HO_2\cdot + \cdot OH \rightarrow H_2O + O_2 \quad (16)$$

$$\cdot OH + \cdot OH \rightarrow H_2O_2 \quad (17)$$

In related experiments we reported on the production of hydrogen peroxide due the termination reaction (eq. 17) and due to the self-reaction of two hydroperoxyl radicals (*15*). Since a high concentration of iron (II and III) was measured in the groundwater (Table 2), MTBE could also be eliminated via Fenton's reactions as hydrogen peroxide was added or formed. The classical Fenton's reaction

$$Fe^{2+} + H_2O_2 \rightarrow Fe^{3+} + \cdot OH + OH^- \quad (18)$$

becomes another alternate source of ·OH in the groundwater as hydrogen peroxide was added or formed. As mentioned by Joseph et al. (*30*), the enhancement on the degradation of azo dyes from Fenton's reaction would be decreased as a high concentration of Fe^{2+} was added due to the direct reduction of ·OH radicals by the following reaction:

$$Fe^{2+} + \cdot OH \rightarrow Fe^{3+} + OH^- \quad (19)$$

Without adding enough O_3 or H_2O_2, the ·OH radicals produced during sonication with low ozone dose were terminated via eq. 19. This may explain the lower elimination rate constants observed at JFK-2 water than at Milli-Q water as ultrasound was present and O_3 dose was lower 7.4 mg/L-min (Table 8).

During acoustic cavitation, water is pyrolytically decomposed leading to the formation of hydroxyl radical as follows:

$$H_2O \xrightarrow{)))\,\Delta} H\cdot + \cdot OH \quad (20)$$

$$O_2 + H\cdot \rightarrow HO_2\cdot \quad (21)$$

Ozone can react in aqueous solution either directly with target substrates or indirectly with the decomposition products. In the ozone-ultrasound process, however, ozone most likely decomposes in the gas phase of the cavitation bubbles by a thermal process that yields oxygen atoms and oxygen.

$$O_3 \xrightarrow{)))\,\Delta} O_2 + O(^3P) \quad (22)$$

$$O(^3P) + H_2O \rightarrow 2\cdot OH \quad (23)$$

In addition, a wide variety of reactions may also be expected to occur directly in the gas phase of cavitation bubbles. This is a likely pathway for MTBE degradation in the sonolytic systems. The most likely reaction pathways for the degradation of MTBE involve its pyrolytic breakdown, its reaction directly with hydroxyl radical, and its direct reaction with ozone.

The positive effects of the bicarbonate radical formation on MTBE oxidation are due to the following sequence of reactions involving the formation of carbonate radical, which in turn abstracts a hydrogen atom from MTBE leading to the formation of an unstable carbon center radical intermediate.

$$\cdot OH + HCO_3^- \rightarrow CO_3^{-}\cdot + H_2O \quad (24)$$

$$\cdot OH + CO_3^{2-} \rightarrow CO_3^{-}\cdot + OH^- \quad (25)$$

$$CO_3^{-}\cdot + (CH_3)_3COCH_3 \rightarrow HCO_3^- + (CH_3)_3COCH_2\cdot \quad (26)$$

The combination of ozonation coupled with ultrasonic irradiation is effective for the total elimination of MTBE from JFK groundwater. For example, the half-life for the sonochemical degradation of MTBE (0.72 mM) in JFK-2 groundwater, using 20 kHz Radial Tube Resonator Reactor operated at an ozone dose rate of 11.9 mg L^{-1} min^{-1}, is 9 minutes. The corresponding time for 95% removal of MTBE is 38 minutes.

The sonochemical reactors can be ordered in terms of their efficiency with respect to the degradation of MTBE in the following way, AST (358 kHz) > RTR > NAP. MTBE is eliminated more rapidly from actual contaminated groundwater than from Milli-Q water with the same initial concentration of MTBE. This is most likely due to the fact that ozone is more effectively converted to hydroxyl radical in high alkalinity groundwater; and that the carbonate radical, which is formed from the oxidation of bicarbonate by hydroxyl radical, reacts further with MTBE by a hydrogen-atom abstraction pathway. MTBE can also be rapidly eliminated from JFK groundwater by the direct chemical oxidation by the mixture of hydrogen peroxide and ozone. For example, the half-life for MTBE destruction in JFK groundwater with peroxone in a 2 L reactor with an ozone dose rate of 11.9 mg L^{-1} min^{-1} and a hydrogen peroxide dose rate of 6 mg L^{-1} min^{-1} is only 3 minutes and the corresponding time for 95% destruction was 13 minutes. In all cases, the intermediate reaction intermediates are converted further to yield more stable reaction products that include acetic acid, formic acid, methanol, formaldehyde, and carbon dioxide.

Acknowledgments

Support for this research has been provided by DARPA, ONR and DOE.

References

1. Begley, R.; Rotman, D. *Chem. Week.* **1993**, *152*, 7.
2. Shelly, S.; Fouhy, K. *Chem. Eng.* **1994**, *Jan*, 61-63.
3. Mackay, D.; Shiu, W.-Y.; Ma, K.-C. *Illustrated Handbook of Physical-Chemical Properties and Environmental Fate for Organic Chemicals*; Lewis Publishers: Michigan, 1993; Vol. III.
4. Book, S. *MTBE in Public Drinking Water*; Book, S., Ed., 1997.
5. Suflita, J. M.; Mormile, M. R. *Environ. Sci. Technol.* **1993**, *27*, 976-978.
6. Steffan, R. J.; McClay, K.; Vainberg, S.; Condee, C. W.; Zhang, D. L. *Appl. Environ. Microbiol.* **1997**, *63*, 4216-4222.
7. Hardison, L. K.; Curry, S. S.; Ciuffetti, L. M.; Hyman, M. R. *Appl. Environ. Microbiol.* **1997**, *63*, 3059-3067.
8. Borden, R. C.; Daniel, R. A.; Lebrun, L. E.; Davis, C. W. *Water Resources Research* **1997**, *33*, 1105-1115.
9. Mo, K.; Lora, C. O.; Wanken, A. E.; Javanmardian, M.; Yang, X.; Kulpa, C. F. *Appl. Microbiol. Biot.* **1997**, *47*, 69-72.
10. Velleitner, N. K.; Papailhou, A. L.; Croue, J. P.; Peyrot, J.; Dore, M. *Ozone. Sci. Eng.* **1994**, *16*, 41-54.
11. Barreto, R. D.; Gray, K. A.; Anders, K. *Water Res.* **1995**, *29*, 1243-1248.
12. Hua, I.; Hochemer, R. H.; Hoffmann, M. R. *Environ. Sci. Technol.* **1995**, *29*, 2790-2796.
13. Hua, I.; Hochemer, R. H.; Hoffmann, M. R. *J. Phy. Chem.* **1995**, *99*, 2335-2342.

14. Hua, I.; Hoffmann, M. R. *Environ. Sci. Technol.* **1996**, *30*, 864-871.

15. Hua, I.; Hoffmann, M. R. *Environ. Sci. Technol.* **1997**, *31*, 2237-2243.

16. Mason, T. J.; Lorimer, J. P. *Sonochemistry: Theory, Application and Uses of Ultrasound in Chemistry*; John Wiley & Sons: New York, 1988.

17. Flint, E. B.; Suslick, K. S. *Science* **1991**, *253*, 1397-1399.

18. Kang, J. W.; Hoffmann, M. R. *Environ. Sci. Technol.* **1998**, *32*, 3194-3199.

19. Kang, J. W.; Hung, H.-M.; Lin, A.; Hoffmann, M. R. *Environ. Sci. Technol.* **1999**, *33*, 3199-3205.

20. Glaze, W. H.; Kang, J. W.; Chapin, D. H. *Ozone. Sci. Eng.* **1987**, *9*, 335-352.

21. Lazrus, A. L.; Kok, G. L.; Gitlin, S. N.; Lind, J. A.; McLaren, S. E. *Anal. Chem.* **1985**, *57*, 917-922.

22. Glaze, W. H.; Kang, J. W. *J. Am. Water Works Ass.* **1988**, *80*, 57-63.

23. Lilie, J.; Henglein, A.; Hanrahan, R. J. *RCDC* **1978**, 40p.

24. Chen, S.; Hoffman, M. Z.; Parson, G. H. J. *J. Phys. Chem.* **1975**, *79*, 1911-1915.

25. Weeks, J. L.; Rabani, J. *J. Phys. Chem.* **1966**, *70*, 2100.

26. Atkinson, R. *Chem. Rev.* **1986**, *86*, 69-201.

27. Hart, E. J.; Henglein, A. *J. Phy. Chem.* **1986**, *90*, 3061-3062.

28. Olson, T. M.; Barbier, P. F. *Water Res.* **1994**, *28*, 1383-1391.

29. Barbier, P. F.; Petrier, C. *Adv. Oxid. Technol.* **1996**, *1*, 154-159.

30. Joseph, J. M.; Destaillats, H.; Hung, H.-M.; Hoffmann, M. R. *J. Phy. Chem. A* **1999**.

Table 1. The physical parameters for the three ultrasonic systems.

System	AST, 358 kHz	NAP, 20 & 16 kHz	RTR, 20 kHz
Transducer Area, cm^2	25	1262	376
Reactor Vol., L	0.5	9	2
Output Power, W	50 or 123	700-1800	533
Gas (O_2 + O_3) flow rate, mL/min	120	480	240

Table 2.The sample characteristics used in this study.

Sample	MTBE + D. I. Water	JFK Groundwaters*
MTBE, mM	0.01-0.5	0.3 (JFK-1) 0.75 (JFK-2)
pH	5.8	6.8
Calcium, mg/L	-	130 - 200
Iron, mg/L	-	50 - 200
Magnesium, mg/L	-	28 - 86
Alkalinity, mg/L	-	530 - 670
Carbonate, mg/L	-	<1
Bicarbonate, mg/L	-	530 - 1200
TDS, mg/L	-	1400 - 1600
Sulfate, mg/L	-	<25
Sulfide, mg/L	-	<0.2
Nitrate, mg/L	-	0 - 0.44
Chloride, mg/L	-	67 - 500
TOC, mg/L	0.6 - 30	40 (JFK -1) 68 (JFK-2)

* Data from Dames & Moore group company.

Table 3. Summary of measured first-order rate constants (s^{-1}) for MTBE degradation in the JFK-2 groundwater in the AST reactor at 358 kHz and at 15 °C. Effects of ultrasonic power and ozone where $[O_3]_o = 12$ mg L^{-1}.

Conditions	Power	k_o (s^{-1})	$t_{1/2}$ (min)
US - no O_3	50 W	0.77×10^{-4}	150
US - no O_3	123 W	4.30×10^{-4}	26.8
US + O_3	50 W	4.10×10^{-4}	28.2
US + O_3	123 W	13.1×10^{-4}	8.8
O_2 + no US	-	0.58×10^{-4}	199
O_3 + no US	-	4.50×10^{-4}	25.7

Table 4. Summary of measured first-order rate constants (s^{-1}) for MTBE degradation in the JFK-2 groundwater in the AST reactor at 15 °C. Effects of ozone dosage at a fixed power of 123 W.

Conditions	O_3 Dosage	k_o (s^{-1})	$t_{1/2}$ (min)
O_2 + US	0 mg/L-min	9.7×10^{-4}	11.9
O_3 + US	7.24 mg/L-min	13.5×10^{-4}	8.6
O_3 + US	12.4 mg/L-min	19.8×10^{-4}	5.8
O_3 + US	20.2 mg/L-min	20.2×10^{-4}	5.7

Table 5. Summary of measured first-order rate constants, k_o, (s^{-1}) for MTBE degradation in the NAP reactor at 15 °C as a function of $[MTBE]_o$ (O_3 dose: 5.3 mg/L-min).

Conditions	Power	k_o (s^{-1}) 0.05 mM	k_o (s^{-1}) 0.1 mM	k_o (s^{-1}) 0.5 mM	k_o (s^{-1}) JFK-1
US - no O_3	1200 W	0.3×10^{-4}	0.18×10^{-4}	0.3×10^{-4}	-
US - no O_3	1800 W	-	-	0.3×10^{-4}	0.30×10^{-4}
US + O_3	700 W	4.15×10^{-4}	2.35×10^{-4}	1.40×10^{-4}	-
US + O_3	1200 W	4.22×10^{-4}	-	1.48×10^{-4}	-
US + O_3	1800 W	-	-	2.40×10^{-4}	4.12×10^{-4}

Table 6. Summary of measured first-order rate constants (s^{-1}) for MTBE degradation in the JFK-2 groundwater sample treated in the NAP Reactor at 15 °C as a function of applied power and ozone dosage rate.

O_3 Dose ($mg\ L^{-1}\ min^{-1}$)	O_3 Alone k_o (s^{-1})	US + O_3 k_o (s^{-1}) NAP 700 W	US + O_3 k_o (s^{-1}) NAP 1200 W	US + O_3 k_o (s^{-1}) NAP 1800 W
0	0	-	0.37×10^{-4}	0.09×10^{-4}
1.94	0.85×10^{-4}	-	1.73×10^{-4}	2.08×10^{-4}
3.86	-	-	2.55×10^{-4}	3.00×10^{-4}
5.33	1.77×10^{-4}	2.28×10^{-4}	3.22×10^{-4}	3.45×10^{-4}

Table 7. First-order rate constants and half-lives for MTBE degradation in distilled water as function of ozone dosage rate in the RTR reactor system at 15 °C.

O_3 Dose (mg L^{-1} min^{-1})	k_o (s^{-1})	$t_{1/2}$ (min)
0	1.95×10^{-4}	59.2
4.3	7.72×10^{-4}	15.0
7.3	9.78×10^{-4}	11.8
11.9	8.58×10^{-4}	13.5

Table 8. First-order rate constants and half-lives for MTBE degradation in distilled water and JFK groundwater as function of the oxidant and the ozone dosage rate in the RTR reactor system (20 kHz, 267 W L^{-1}) at 15 °C.

Oxidant	Ultrasound	DW k_o, (s^{-1})	JFK-2 k_o, (s^{-1})	$t_{1/2}$ (min)
O_2	no	~ 0	-	> 200
O_3 (4.3 mg/L-min)	no	-	1.97×10^{-4}	59
O_3 (11.9 mg/L-min)	no	0.57×10^{-4}	4.08×10^{-4}	28
O_2	yes	1.95×10^{-4}	0.82×10^{-4}	140
O_3 (4.3 mg/L-min)	yes	7.72×10^{-4}	1.80×10^{-4}	64
O_3 (7.4 mg/L-min)	yes	9.78×10^{-4}	12.30×10^{-4}	9.4
O_3 (11.9 mg/L-min)	yes	8.58×10^{-4}	13.00×10^{-4}	8.9

Table 9. First-order rate constants and half-lives for MTBE degradation in distilled water and JFK groundwater as function of the hydrogen peroxide and the ozone dosage rates at 15 °C.

Oxidant	HCO_3^-	DW k_o, (s^{-1})	JFK-2 k_o, (s^{-1})	$t_{1/2}$ (min)
O_3 (11.9 mg/L-min)	no	0.57×10^{-4}	-	203
$O_3 + H_2O_2$ (11.9 mg /L-min O_3) (5 mg /L-min H_2O_2)	no	26.7×10^{-4}	-	4.3
$O_3 + H_2O_2$ (11.9 mg /L-min O_3) (5 mg /L-min H_2O_2)	yes 8.9 mM	57.5×10^{-4}	-	2.0
O_3 (4.3 mg /L-min)	yes	-	1.97×10^{-4}	59
O_3 (11.9 mg/L-min)	yes	-	4.08×10^{-4}	28
$O_3 + H_2O_2$ (11.9 mg /L-min O_3) (2 mg /L-min H_2O_2)	yes	-	34.7×10^{-4}	3.3
$O_3 + H_2O_2$ (11.9 mg /L-min O_3) (4 mg /L-min H_2O_2)	yes	-	29.3×10^{-4}	3.9
$O_3 + H_2O_2$ (11.9 mg /L-min O_3) (6 mg /L-min H_2O_2)	yes	-	39.8×10^{-4}	2.9

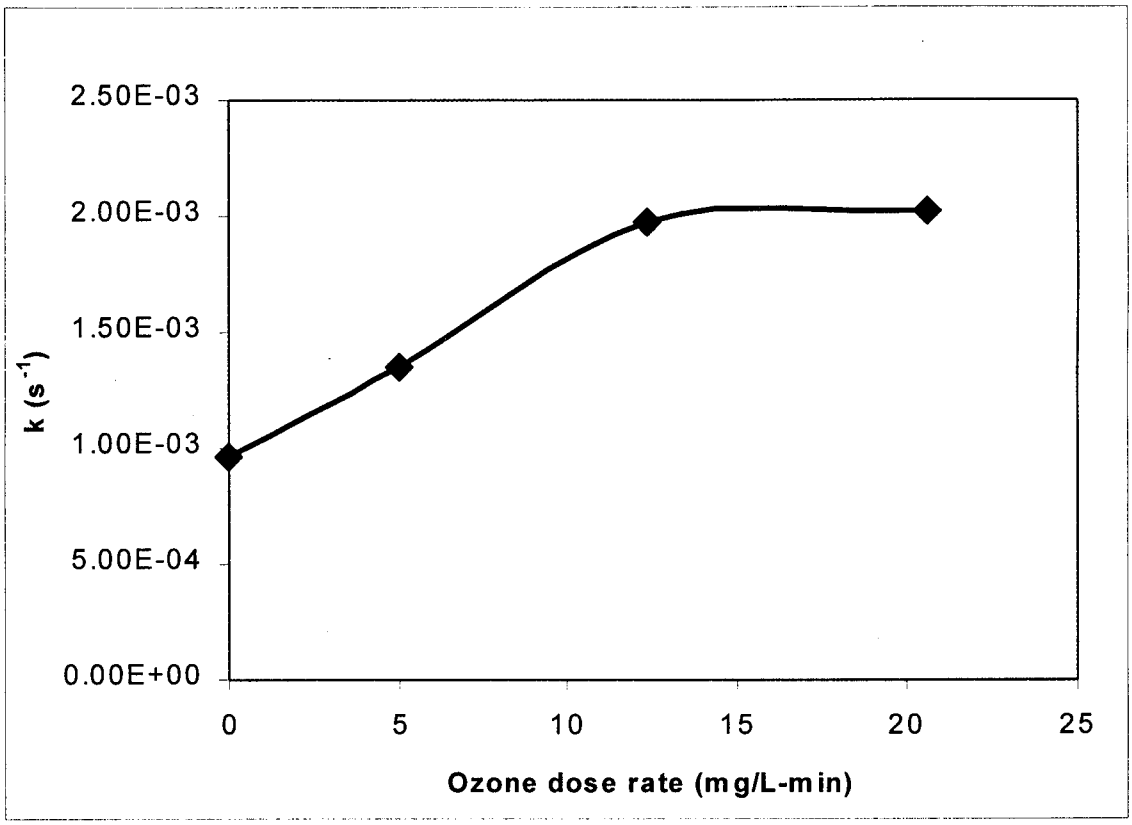

Figure 1. Measured first-order rate constants, k_0 (s^{-1}) for MTBE degradation as a function of ozone dose rate at AST system (246 WL^{-1}).

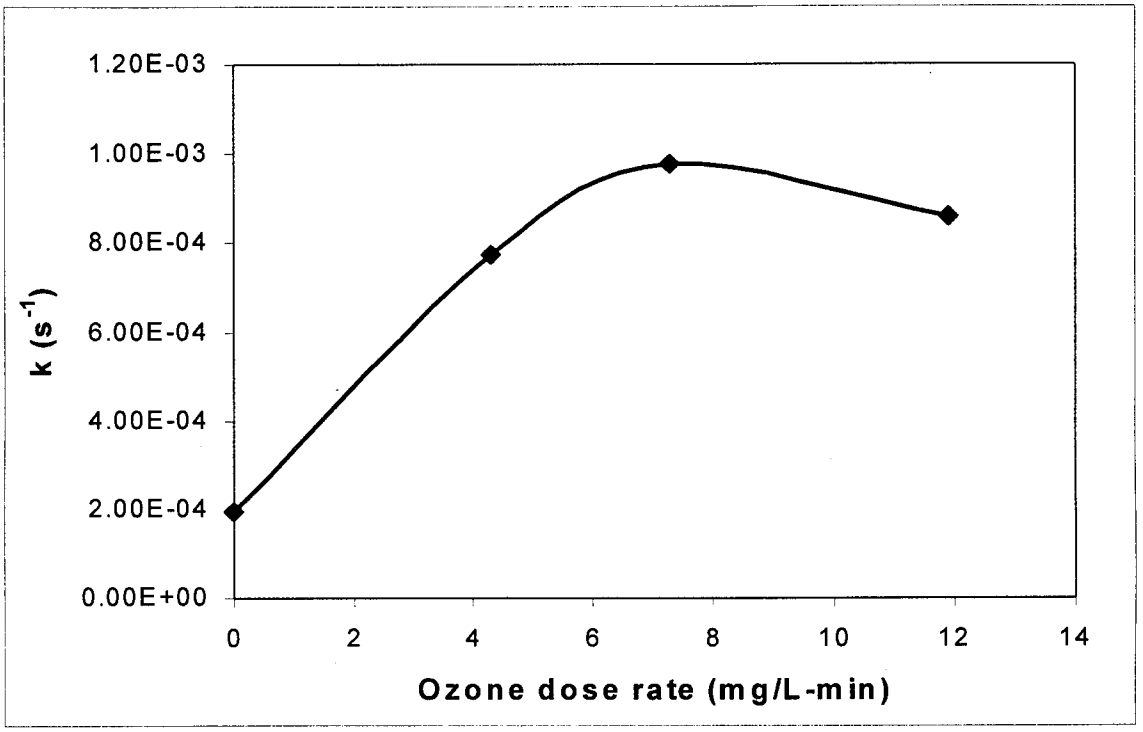

Figure 2. Variation of the observed first-order rate constant for MTBE degradation in the RTR reactor (267 WL^{-1}) with ozone dose rate.

Figure 3(a)

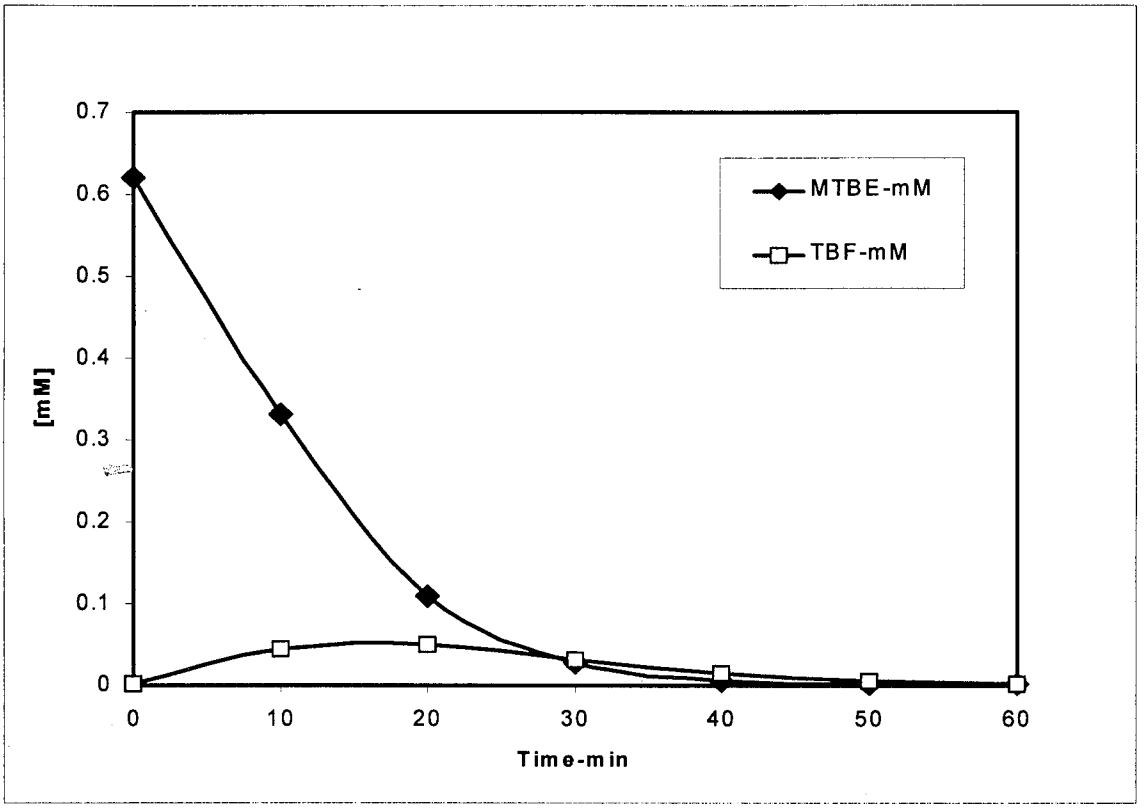

Figure 3(b)

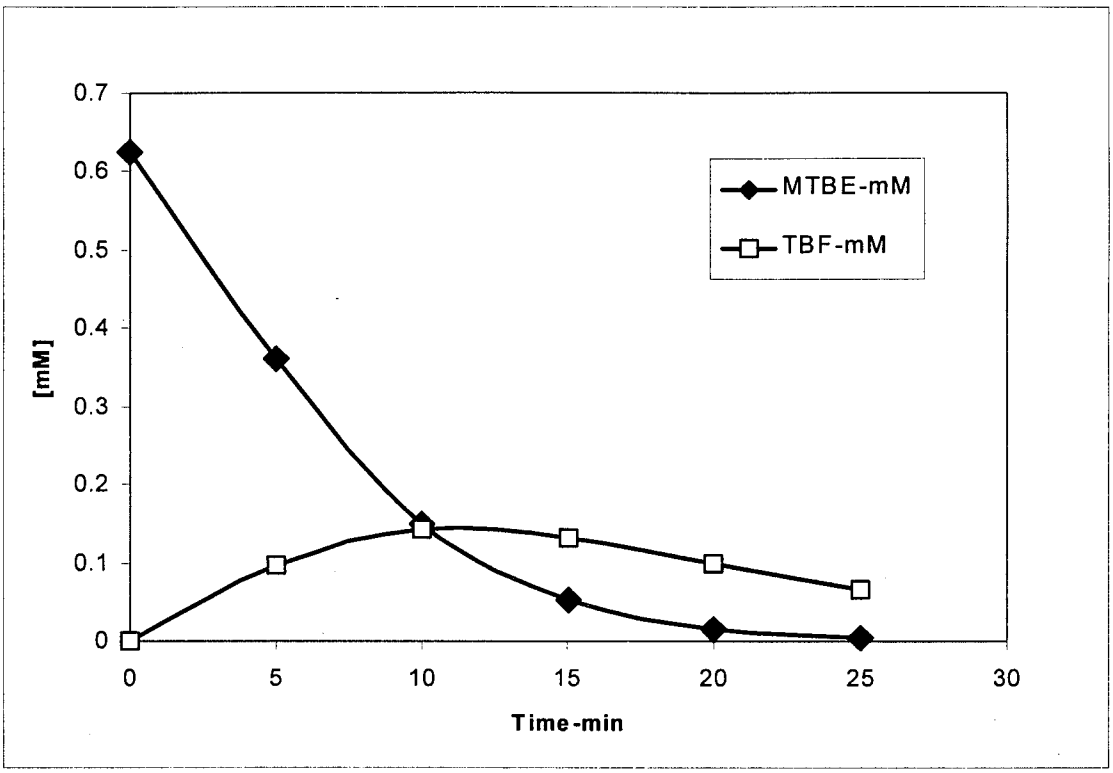

Figure 3. Production of t-butyl formate (TBF) as an intermediate during the oxidative degradation of MTBE; (a) in AST system (246 WL^{-1} and O_3 dose: 10.3 mg/L-min), (b) O_3 (12 mg/L-min) + H_2O_2 (4 mg/L-min).

Chapter 9

Conclusions

Ultrasonic irradiation has been shown to enhance a variety of different chemical reactions in aqueous solution. The existence of high temperatures inside of collapsing cavitation bubbles is significant for the application of sonolysis for environmental remediation. We have shown that rates of degradation of selected chlorinated methanes, ethanes and ethenes are consistent with: 1) complete decomposition of the solute contained in collapsing bubbles, 2) about 15% ultrasound power efficiency for transient cavitation and, 3) a rather flat $N(R_o) \propto R_o^n$, $n \simeq 0$, initial radius bubble distribution under continuous sonication.

The non-linear dependence of first-order degradation rate constants, k_X vs. H_X, Henry's law constant, directly reveals that rate constants are not solely determined by equilibrium parameters. Rectified diffusion contributes significantly to the composition of the bubble vapor prior to collapse, particularly for the less volatile substrates. The solute content of collapsing bubbles is composed of the equilibrated vapor at R_o, plus the amount incorporated by diffusion from the surrounding solution during the acoustically driven expansion from R_o to R_{max}, the maximum radius attained prior to collapse. The finding that k_X's decline above 600 kHz is ascribed to the fact that increasingly smaller bubbles collapse at rates reaching a limiting value at sufficiently high frequencies.

The kinetics of sonolytic oxidation of iodide was used to quantify the •OH radical. With an estimated 15% ultrasound power efficiency and 7% reaction efficiency for •OH inside the bubble to react with iodide near the interfacial region of bubbles, a temperature of ~ 4000 K was predicted for 205 and 358 kHz from the power dependence data. The optimal production rate of •OH depends on frequency and ultrasonic power intensity, e.g., the optimal frequencies at power intensity = 83 and 33 W/L are 358 and 205 kHz

respectively. This suggests that the optimal conditions for sonochemical reaction have to be determined by optimization of multiple parameters.

In chapter 4, the rates of sonolytic degradation of CCl_4 and the primary intermediate in the sonication of CCl_4 and C_2Cl_6 were shown to increase with ultrasonic frequency with optimal degradation rates at 500 kHz. At 205 kHz, the sonolytic degradation rate constants for the chlorinated methanes were found to increase with a corresponding increase in their respective Henry's Law Constants (i.e., $K_{H,CCl_4} > K_{H,CHCl_3} > K_{H,CH_2Cl_2}$) in the order $k_{CCl_4} > k_{CHCl_3} > k_{CH_2Cl_2}$. This relative order is consistent with the argument that the driving force for diffusion into the bubbles is increased as the value of K_H is increased.

Since acoustic cavitation can increase the surface area of the reactive solids by causing particles to rupture, the combination of ultrasound and Fe^0 were applied to the degradation of CCl_4 and some aromatic compounds. The combination of ultrasound and Fe^0 is a heterogeneous reaction system involving solid/liquid, gas/solid, and gas/liquid interfaces. In the coupled ultrasound and iron system, the contribution to the overall degradation rate by direct reaction with Fe^0 results in an overall rate enhancement by a factor of 40 for the degradation of CCl_4. The rates of mass transport of nitrobenzene, nitrosobenzene and aniline to and from the Fe^0 surface are enhanced by hydrodynamic cavitation. Oxidation of surface inhibiting intermediates during sonication also contributes to the observed overall rate enhancements of the target substrates. The relative concentrations of the principal reaction intermediates in US/Fe^0 systems, nitrosobenzene and aniline appear to be influenced significantly by total available surface area of Fe^0. In conclusion, the combination of ultrasound and Fe^0 appears to have a positive synergistic

effect on the reduction of nitro aromatic compounds. These enhancements are attributed 1) to the continuous cleaning and chemical activation of the Fe^0 surface by the combined chemical and physical effects of acoustic cavitation, and 2) to accelerated mass transport rates of reactants to the Fe^0 surfaces. Additional kinetic enhancements are attributed to the production of H^+ during the course of the reaction.

Ultrasonic irradiation in the presence of ozone was used to efficiently degrade methyl tert-butyl ether (MTBE) from aqueous solution and from real groundwater (collected at JFK International Airport). For sonolysis alone or for sonolysis in the presence of ozone, higher overall reaction rates were observed at 358 and 618 kHz than at 205 and 1078 kHz. These observations are consistent with results reported for the frequency-dependent sonolysis of chlorinated hydrocarbons and iodide (chapters 2-4). A linear dependence of the first-order rate constant for the simultaneous degradation of O_3 on power density was also observed. In addition, naturally-occurring organic matter (NOM), which might affect the oxidation rate of advanced oxidation process (AOP) that depend on hydroxyl radical production, has a negligible affect on the rates of degradation of MTBE.

The sonolytic degradation of MTBE from groundwater has been investigated in three different reactor configurations and frequencies: Allied Signal ELAC (AST, 358 kHz), Near Field Acoustical Processor (NAP, 20 & 16 kHz) and Radial Tube Resonator (RTR, 20 kHz). The sonochemical reactors can be ordered in terms of their efficiency with respect to the degradation of MTBE in the following way, AST (358 kHz) > RTR > NAP. The higher elimination of MTBE at groundwaters by ultrasound/O_3 systems is most likely due to the fact that ozone is more effectively converted to hydroxyl radical in high alkalinity groundwater; and that the carbonate radical, which formed from the oxidation of

bicarbonate by hydroxyl radial, reacts further with MTBE by a hydrogen-atom abstraction pathway. MTBE can also be rapidly eliminated from JFK groundwater by the direct chemical oxidation by the mixture of hydrogen peroxide and ozone.

Even though a wide variety of organic compounds have been demonstrated to be completely degraded by ultrasound or the combination of ultrasound with other methods, our understanding of complicated sonochemical mechanisms are often speculative and inconclusive. The complexity of sonolysis mainly arises from the highly variable physics of cavitation bubbles. Many critical questions such as the detailed nature of bubble collapse, the temperatures and pressures inside the cavitation bubbles, and the diffusion between the bubble and the solution remain unanswered. Future research should focus on probing the temperature inside the bubble more accurately. Sonoluminescence may be used to probe the temperature based on specific emission spectra (*Nature* **1999**, *398*, 402).

Another goal of future research in sonochemistry will be the optimization of sonochemical efficiency through a change in the acoustic field design. Umemura *et al.* (*J. Acoust. Soc. Am.* **1997**, *101(1)*, 569) have employed a second-harmonic superimposition technique to *in vitro* and *in vivo* systems. Significant synergistic effects between the fundamental and the second harmonic were observed in both *in vitro* and *in vivo* experiments using a progressive wave field. Ultrasonic irradiation based on this approach may be more efficient for the specific conditions needed for water treatment. Further theoretical study of this technique involving the combination of various frequencies of ultrasound as a function of their phase differences is necessary.